The Influence of Self-Motion on Electrosensory Acquisition in Weakly Electric Fish

A Computational and Behavioural Approach

Mary Upshall

Thesis submitted to the University of Ottawa in partial fulfillment of the requirements for the Ph.D. degree in Biology.

Ottawa-Carleton Institute of Biology
Department of Biology
Faculty of Science
University of Ottawa
Ottawa, Canada

Acknowledgements

Thank you to the Ontario Graduate Scholarship (OGS) for funding two years of my Ph.D. research (2020, 2021).

This dissertation would have never been possible without the endless patience and guidance of Dr. John Lewis. I have been truly blessed to have such a wonderful mentor to introduce me to the world of academia and research. Not only is he a brilliant man but his support is unmatched. I am forever grateful for everything he has taught me and am honoured to call him my supervisor and friend. Thank you, John.

I would also like to acknowledge Dr. Aaron Shifman for patiently teaching me everything I know about programming. I was lucky enough to have a year before COVID with Aaron to show me the ropes. His friendship (and coffee) was instrumental to the work presented here.

There are two that I would especially like to thank. Without Maddison Reed, and Stephanie Gaudreau I surely would have given up years ago. Not everyone gets to say they got to go to work with their best friends every day. Having these two with me each step of the way made every hurdle easier, and I cherish the time we had together.

Of course, the input of my committee improved my work in every way. Their expertise in neural, motor, and behavioural physiology helped guide my ideas and ensure I stayed on track. Thank you, Dr. Emily Standen and Dr. Tuan Bui for being my supervisors-away-from-home. Em, our No Forks and coffee chats always made me feel more confident both in and out of academia. Tuan, I don't think I'll meet a funnier PI. You made my first international conference so much more enjoyable. Lastly, Dr. Jayne Yack, your evolutionary and hypothesis testing insight made my fundamental understanding much stronger. Thank you for always trekking out to uOttawa for our meetings.

Outside of academia I was lucky to have the unwavering support of family and friends. My partner, Brandon Hunter, has been my rock. Not only has he encouraged and cheered me on the whole way, but he's also picked up my slack all while going to school himself. His dedication and discipline inspired me to go into everyday giving it my all. He is a superstar. Thank you for everything you are.

Finally, to my mother and brother, Marion Upshall and Mike Raffaghello, for taking my endless phone calls of rants and breakdowns. Your support has meant the world to me.

Table of Contents

List of Figures

List of Tables

General Abstract

Weakly electric fish have an electric organ which generates an electric field surrounding their body. Electroreceptors embedded in the skin of these fish encode the field perturbations produced by environmental objects forming the basis for electric sensing. Interestingly, the spatial properties of the electric field change significantly with body pose, but how this affects sensing is not clear. Using novel computational and statistical techniques, this thesis addresses the impact of body-pose on electric sensing in the wave-type electric fish, *Apteronotus albifrons*. We developed an unsupervised behavioural identification pipeline to classify the movements which make-up the behavioural repertoire in freely-swimming fish. We then investigate the impact of different environments on the underlying statistics of the behavioural repertoire. We found that certain movements were context specific: scanning (quick back-and-forth swimming) is more prevalent in static environments, while tail-bending is more frequent in temporally varying environments. Finally, we simulate the fish's electric field under the same conditions to estimate the available electrosensory information. These results suggest that body-pose may improve information acquisition in some contexts. Overall, this thesis combines behavioural and computational approaches to suggest that self-motion improves electrosensory acquisition in wave-type weakly electric fish.

Les poissons faiblement électriques possèdent un organe électrique qui génère un champ électrique autour de leur corps. Les objets dans l'environnement de ces poissons causent des perturbations dans leur champ électrique. Ces perturbations sont encodées par des électrorécepteurs intégrés partout sur leur peau, ce qui constitue ainsi la base de la perception électrique. De plus, les propriétés spatiales du champ électrique varient considérablement en fonction de la posture corporelle. Cependant, l'impact de ces variations sur la perception électrique reste incertain. À l'aide de techniques informatiques et statistiques novatrices, cette thèse étudie l'influence de la posture corporelle sur la perception électrique chez le poisson électrique de type ondulatoire *Apteronotus albifrons*. Nous avons développé une méthode d'identification comportementale non supervisée, permettant de classifier les mouvements qui composent le répertoire comportemental des poissons en nage libre. Ensuite, nous avons examiné l'effet de différents environnements sur les statistiques sous-jacentes de ce répertoire. Nous avons découvert que certains mouvements sont propres à des contextes spécifiques. Par exemple, le balayage (nage rapide d'avant en arrière) est plus fréquent dans les environnements statiques, tandis que les flexions de la queue sont plus fréquentes dans les environnements temporellement dynamiques. Finalement, nous avons simulé le champ électrique du poisson dans ces conditions afin d'estimer l'information électrosensorielle disponible. Ces résultats suggèrent que la posture corporelle pourrait améliorer l'acquisition d'informations dans certains contextes. Dans l'ensemble, cette thèse combine des approches comportementales et informatiques pour proposer que leurs mouvements corporels améliorent l'acquisition électrosensorielle chez les poissons faiblement électriques de type ondulatoire.

Chapter 1: Introduction – Weakly Electric Fishes

1.1 Abstract

Weakly electric fishes generate a 3-D electric field to sense their environment. Electroreceptors distributed over the length of their bodies form a 2-D sensing array which detect perturbations in their self-generated field. This review will focus on a particular subset of weakly electric fish, the wave-type knifefishes. Their knife-like shape, owing to their narrow bodies, lack of dorsal fin, and the modified anal fin permits unique swimming capabilities. They swim as easily backwards as they do forwards and can hover in place. Generally, they have excellent locomotory control in all directions. In other words, their proficient omnidirectional locomotor strategy is suitably accompanied by an omnidirectional sensing system. This paired sensory-motor interaction has led to hypotheses suggesting that these fish use stereotyped movements and body shapes, called active sensing movements, to increase sensory acquisition. Active sensing movements such as tail bending and scanning (quick back-and-forth swimming) appear to be generated in a task-specific manner. Other studies have demonstrated that the sensory consequences of these movements can be canceled out via long-term synaptic plasticity in upstream brain regions. Moreover, others suggest a combination of these two theories proposing that active sensing movements enhance ecologically relevant signals, such as those due to prey, while canceling out repetitive background signals. In

any case, the exact role these movements play in shaping the incoming sensory information is unclear. This article will first review the background relating to the sensory and motor systems separately, then follow with a focus on the sensory-motor interaction. We will go into the evolution of research pertaining to active sensing movements, the different hypotheses, and finally, where the field is headed.

1.2 Introduction

1.2.1 Electric sensing

Electric sensing, while foreign to us, is an effective sensing strategy employed by a variety of aquatic and semi-aquatic animals including some fishes, amphibians, and even the platypus (Jørgensen, 2005). While the platypus has its own unique mechanism for electric sensing, fishes and amphibians have independently developed a passive sensing mechanism that allows them to detect external bio-electric or low frequency fields via the ampullary receptors (Benda, 2020; Jørgensen, 2005). These receptors formed the passive electric sense by adapting some of the mechanisms employed by the lateral line system for mechanosensation (Caputi, 2017). The passive electric sense was first classified in sharks and rays who use passive sensing for prey capture, as well as orientation and navigation via electric fields (Carlson et al., 2019; Kalmijn, 1971). Some electroreceptive teleosts have taken passive electric sensing one step further and have evolved an active electric sense. This additional electric sense is termed “active” because the fish expend energy to generate an electric field to gain sensory information (Nelson & MacIver, 2006). In other words, they are electrogenic as well as electroreceptive. The idea of generating an electric field is perhaps most familiar in

electric eels who use an electric organ (EO) located in their tail to generate a voltage of up to 860 V (de Santana et al., 2019) to stun prey. In a similar fashion, weakly electric fish also produce their own electric fields via their EO, though it is far too weak to stun prey. Instead, they sense the field perturbations produced by the environment to navigate, hunt, and communicate (Benda, 2020; Caputi, 2017; Lewis, 2014).

1.2.2 Weakly electric fish and the wave-type knifefishes

Interestingly, there are phylogenetically independent orders of weakly electric fish. Though the explanation for this convergent evolution is debated, the two different orders (Osteoglossiformes and Gymnotiformes) are nocturnal predators and tend to live in murky waters (Benda, 2020; Stoddard, 2009). The two families, Gymnarchidae and Mormyridae belonging to the Osteoglossiformes order are native to Africa, while the phylogenetically independent Gymnotiformes order are native to South America. Both exclusively live in low-conductivity fresh water tropical habitats (Benda, 2020; W. G. R. Crampton & Albert, 2006). All weakly electric fish have an electric organ (EO) which varies in length and location within the body depending on the species. Generally, the EO consists of generating cells that are modified muscle fibers (myogenic). The exception to this is the ghost knifefishes (Apteronotidae belonging to the Gymnotiformes) whose generating cells are modified neural fibers and are therefore neurogenic. In both cases, these generating cells are referred to as electrocytes (Bennett, 1970, 1971). Much like a battery, electrocytes are stacked in series and in parallel. Their collective sum of membrane potentials, referred to as the electric organ discharge (EOD), generates the electric field that surrounds the body of the fish in all

directions (Bennett, 1971; Stoddard, 2009). Weakly electric fish have EOD ranges from a few to tens of millivolts to a few volts (Benda, 2020; Stoddard, 2009) which are emitted in either a pulse-type or a wave-type manner, depending on the species. In the hindbrain of pulse-type and wave-type fish lies the medullary command center or the pacemaker nucleus, which drives electrocyte activity (Markham, 2019). The production of an EOD in pulse-type fish is more irregular and often larger in amplitude (few volts) relative to the wave-type fish whose EOD is quasi-sinusoidal
and has an amplitude on the order of a few to tens of millivolts (Benda, 2020). Variations in EOD rate are often species specific and even sex specific thereby offering important social information (Markham, 2019). This article will primarily focus on wave-type Gymnotiformes and the fascinating interplay of their sensory and motor capacities. References regarding pulse-type species will be provided throughout for those interested in more information. Additionally, there will be a brief section (see the Quantitative behavioral analysis in pulse-type fish section) discussing recent advances in pulse-type fish as it pertains to this article. Wave-type knifefishes include the Sternopygidae (glass knifefishes) and the Apteronotidae (ghost knifefishes) families which inhabit fresh waters throughout the neotropics (Kramer, 2019). While both families are species diverse, the Apteronotids are the most species diverse among the Gymnotiformes (W. G. R. Crampton & Albert, 2006; Peixoto et al., 2021; Turner et al., 2007). Despite this diversity, approximately 70% of Apteronotids inhabit large deep river channels, which are typically fast flowing (Bernt et al., 2019; W. Crampton et al., 2007). As a result, it is hypothesized that these rapidly changing habitats promoted an

adaptation that led to the high electrosensory sampling rates (EOD frequencies) seen in Apteronotids. In some members, the EOD frequency
has an upper bound of 1800 Hz, owing to the neurogenic nature of their electric organ (Kramer, 2019). In contrast, Sternopygidae myogenically produce their electric organ discharge in a quasi-sinusoidal manner with frequencies up to 800 Hz (Bennett, 1971; Kramer, 2019). Eigenmannia (genus belonging to Sternopygidae) for example, are more widely spread, residing in floodplains, caves, streams, and river channels (Peixoto & Ohara, 2019). For more information on the diversity and phylogeny of Gymnotiformes, see (W. G. R. Crampton & Albert, 2006), bearing in mind that the taxonomy of several species of neotropical fish is yet to be studied (Peixoto et al., 2015; Peixoto & Ohara, 2019).

1.2.3 Sensory inputs: Electric images and electroreception

When an object with electrical properties differing from that of the surrounding water enters the near field sensory range it perturbs the fish's basal electric field (Benda, 2020; Lissmann & Machin, 1958). The so-called field perturbation is given by the difference between the basal field (no object) and the perturbed field (with object). The transdermal potential associated with the field perturbation is commonly referred to as the electric image (see Figure 1.1 A and B). As demonstrated in Figure 1.1, the electric image displays voltage on the y axis and rostro-caudal (body) location on the x axis. The object perturbs the field causing a 2-D Gaussian shape with its peak at the object's location relative to the rostro-caudal axis of the fish. Field perturbations depend on whether the object is more or less conductive than water which results in more or

less current, respectively, flowing toward the object. If the electrical properties of the object were equivalent to those of water, then it would be “invisible” to the electric sense (Heiligenberg, 1973; Lewis, 2014). A conductor will produce an electric image with a positive peak while a resistor will produce a negative peak (Benda, 2020; Lewis, 2014) features of the electric image will depend on object distance, size, and shape. For example, larger objects will produce a larger image amplitude. Closer objects will also produce larger image amplitudes but will also be narrower. Thus, combinations of image features may be used to resolve size-distance ambiguity among other physical properties (Lewis, 2014; Rasnow, 1996; Sim & Kim, 2011; von der Emde et al., 1998). However, object information is also not necessarily limited to image features. Moving away from the classic electric image, a recent study instead looked at the information provided by single receptors. Interestingly, the information provided by four sensory receptors was sufficient to determine object location (Pourziaei et al., 2022).

In any case, perturbations are detected by electroreceptive organs distributed over the length of the fish’s body with a higher density located in the peri-oral region, thought to be significant for prey-capture (Caputi, 2017). Due to the physics associated with electric fields (see Benda, 2020 for a brilliantly comprehensive review), the sensory range of the EOD falls off at an exponential rate, meaning the detection of small objects such as prey are only detectable in the near field (estimated to be less than 1 body length; Babineau et al., 2007; Benda, 2020; Nelson & Maciver, 1999). Additionally, electroreceptors only respond to the transdermal voltage measured at the body surface, thus they form a 2-D array comparable to the retina (Benda, 2020; Bennett, 1971). Of the two types of electroreceptor classes, the ampullary receptors are tuned to low

frequency electric fields, while tuberous receptors are dedicated to detecting perturbations in the self-generated electric field and are thus tuned to the EOD frequency (Zakon, 1986). There are far more tuberous receptors (approximately 14,000) than ampullary receptors (approximately 700) (Carr et al., 1982; Krahe & Maler, 2014; Sim & Kim, 2011).

They are sensitive to perturbations in the range of 0.1 – 1 $\mu V\ cm^{-1}$ (Bennett, 1971; Nelson & Maciver, 1999a; Sim & Kim, 2011). Tuberous receptors are grouped into P-type receptors (or P-units) and T-type receptors (or T-units). T-units, with powerful temporal resolution, encode the local phase of each EOD cycle and are important for measuring phase-modulations (Caputi, 2017). P-type receptors detect phase and amplitude changes in the EOD and are important for electrolocation (Chacron et al., 2001). They fire at a fixed phase of the EOD cycle but skip an uncertain number of cycles between firings, that is until a stimulus such as an object, causes the units to increase their probability of firing as a function of peak-to-peak amplitude (Caputi, 2017). They adapt quickly and consequently respond mostly to changes in the environment (Nelson et al., 1997).

1.2.4 Neural coding of electorsensory inputs

Both T-type and P-type receptors are tuned to the EOD frequency of the fish. For example, *Apteronotus albifrons* has an EOD frequency around 1000 Hz and so the P- and T-type receptors would be receptive in this high frequency range. However, the perturbations elicited by a prey, for example, will cause amplitude modulations to the

fish's own EOD (see Figure 1.1 C). The frequency of these amplitude modulations will be much lower than the fish's EOD frequency (~25 Hz; Nelson & Maciver, 1999). Interestingly, there is evidence that information pertaining to these behaviorally relevant frequencies, occurring in a much lower range (0 – 100 Hz), can indeed still be encoded by P-type receptors (Chacron et al., 2005).

The electroreceptive sensory cells (tuberous and ampullary) transduce information by experiencing a change in ionic conductance of their plasma membranes upon a change in transdermal voltage elicited by an external stimulus (Caputi, 2017). The sensory cells then synapse on primary afferent fibers which ascend and topographically map onto the electrosensory lateral line lobe (ELL) in the hindbrain (Clarke & Maler, 2017). Within the brain there is a significant amount of feedback and interplay between brain regions that are involved in electrosensation. The ELL contains ON- and OFF- pyramidal cells which increase their firing rate (bursts) in response to their preferred stimuli. For a conductive object, this preferred stimulus would be a looming motion for the superficial ON cells, and a receding motion for the OFF cells. The opposite would be true for resistive objects (Clarke et al., 2014, 2015; Clarke & Maler, 2017). In short, there are other brain regions and feedback loops that communicate with the ELL to help filter and integrate sensory information in a spatiotemporal manner and enable the fish's ability to electrolocate. For further details on the specifics of these pathways see the detailed works of Clarke & Maler (2017), Caputi (2017), and (Krahe & Maler, 2014). A few key aspects of the results of these

neural interactions will be important and their implications will be discussed further in the Sensory-motor interaction section.

Motor outputs: Locomotion in wave-type knifefish

In addition to the extensive body of research dedicated to understanding the sensory capabilities of knifefishes and other weakly electric fish, there has also been a considerable interest relating to their unique locomotory capabilities. As with any fish, there are forces acting on it as it swims. In the vertical direction, forces to consider include weight, buoyancy, and hydrodynamic lift. In the horizontal direction, thrust and drag play the largest roles. The magnitude of these force components is determined by the shape of the fish and the propulsion mechanism (Sfakiotakis et al., 1999). Consequently, the knife-like shape of gymnotiforms is fundamental to their omnidirectional swimming abilities. They lack dorsal, adipose, and pelvic fins and instead have a modified anal fin, called the ribbon fin (Shirgaonkar et al., 2008). Extending down the ventral midline of the fish, the ribbon fin undulates and produces thrust granting high maneuverability, thought to be the reason for its evolution (Blake, 1983; Ruiz-Torres et al., 2013). It is the counter propagating waves of the ribbon fin toward a nodal point that permits hovering in place, and their ability to swim backwards as easily as forwards (Lannoo & Lannoo, 1993; Ruiz-Torres et al., 2013). With a midline nodal point position, the fish hovers, and as the nodal point shifts rostrally with fewer undulations, forward swimming speed increases (Curet et al., 2011; Ruiz-Torres et al., 2013; Sefati et al., 2012). However, depending on the flow perturbation of their environments, knifefish use different gaits. In more turbulent conditions the fish will increasingly use a combination of their ribbon fin, pectoral fins, and body bends to

maintain position compared to laminar flow conditions which is dominated by ribbon fin undulations with a rigid body (Ortega-Jiménez & Sanford, 2021). Beyond their biomechanical and hydrodynamic implications, the precise and flexible maneuverability of knifefish at low velocities makes them ideal models for autonomous aquatic robots, with applications such as exploration and search and rescue used to interact and work in cluttered environments (MacIver et al., 2004). Recent focus has turned to making robots more realistic, such as using soft materials in combination with a computational algorithm to generate undulating patterns that share similarities with actual knifefishes (Veenstra et al., 2018). Modeling robots after knifefishes is also motivated by the interactions between sensory acquisition and motor ability: these fish pair omnidirectional swimming with an omnidirectional sensory system which enables them to effortlessly tackle complex habitats (MacIver et al., 2004).

1.3 Sensory-motor interaction

1.3.1 Prey-capture

Prey-capture behaviors of knifefishes provide an interesting test case for sensory-motor coordination. The motor system must execute the necessary maneuvers to pursue the prey while orienting the sensory array (the electroreceptors) to optimize sensing (Nelson & Maciver, 1999a; Ruiz-Torres et al., 2013). The short sensory range and high speeds add to this challenge. There are two levels to this. First, the prey needs to be within sensory range to be detectable; and second, there are behaviors that the fish performs to execute the prey-capture event. Using orientation angles (roll, pitch, and yaw), Nelson & Maciver (1999a) described the motion of the black ghost knifefish

during prey capture. They found that the fish would lead with the dorsum in most cases. For example, if the fish was swimming forward the nose would be pitched (tilted) downwards, whereas if the fish was swimming backward the nose would be pitched upward. Finally, if the fish was swimming laterally it would lead with the dorsum by rolling orthogonal to the vertical axis (side swimming). This behavior was also observed in shallow environments where fish would perform side swimming leading with their dorsum (Lannoo & Lannoo, 1993). These observations suggested that the modified adipose fin covered with electroreceptors, called the dorsal filament (Franchina & Hopkins, 1996) plays a role in prey capture (Nelson & Maciver, 1999a). The prey detection event itself occurs rostrally or in the midbody region of the fish. Upon detection the fish brings the prey to the mouth region by performing a rapid reversal (~100 ms; otherwise known as a scan) (Lannoo & Lannoo, 1993; Nelson & Maciver, 1999a; Postlethwaite et al., 2008). This behavior was often accompanied by the tendency of the tail to bend in the direction of the prey (Lannoo & Lannoo, 1993). Heiligenberg (1975) proposed that perhaps these scans may be a strategy to compensate for the lack of focus mechanism (comparable to lacking a lens in vision) of the electroreceptor array. Specifically, scanning allows the prey to pass over a large number of receptors which may be a compensation for decreased image quality (Lannoo & Lannoo, 1993; Nelson & Maciver, 1999a). MacIver et al. (2001) then followed up using black and brown ghost knifefishes to investigate the impact of different water conductivities (ranging from 35 to 600 mS cm^{-1}) on prey-capture. Increasing water conductivity causes the EOD to be short circuited causing a smaller electric field amplitude (Benda, 2020). As such, both detection distance and success of prey-capture

were affected. The lower the conductivity, the larger the detection distance (2.8 cm on average) and the higher the rate of capture. In the same study, MacIver et al. (2001) also found that these previously identified dorsal orienting and scanning behaviors associated with prey capture were adaptive rather than ballistic. This means that if the prey were to change direction, the fish would adapt its behavior accordingly to compensate. Further studies simplified the fish to an ellipsoid model and revealed that the prey-capture behaviors are performed in such a way where they require minimal mechanical effort (Postlethwaite et al., 2008). These prey-capture studies elegantly demonstrate the importance of a coordinated sensory-motor interaction. That is, the omnidirectional sensing system is paired with an omnidirectional swimming strategy. Thus, the positioning of the electrosensory array is presumably optimized for better sensing. The fish controlling its locomotion will in turn be influencing the spatiotemporal inputs from the electrosensory world (Nelson & Maciver, 1999a). These behaviors, such as leading with the dorsum, scanning, and tail bending, are all known as “active sensing movements” that are hypothesized to optimize electrosensory input.

1.3.2 Can active sensing movements improve sensory acquisition?

1.3.2.1 General active sensing

The term active sensing refers to the production of energy for the purposes of gathering sensory information (Nelson & MacIver, 2006). For example, bats generate sound waves and use the reflected signals to make sense of their environment, known as echolocation. In the presence of novel objects bats increase the rate and bandwidth of their echolocating calls to increase the resolution of incoming sensory information

(Geva-Sagiv et al., 2015). Similarly, rats use their whiskers to actively extract sensory information by increasing the frequency of whisking in the presence of novel objects (Mitchinson et al., 2007). Perhaps a more relatable example
would be the human haptic system. When investigating an unfamiliar object, we actively move our fingers to feel textures and explore (Schroeder et al., 2010). In this last example we use motion to disambiguate object features. Analogously, weakly electric fish have been shown to increase stereotypic or active sensing movements which have been hypothesized to increase sensory acquisition. We know that normal movement greatly affects the electrosensory scene (electric images) but presumably there are behavioral strategies such as these active sensing movements used to improve the available electrosensory information (Assad et al., 1999a).

1.3.3 Active sensing movements in weakly electric fish

1.3.3.1 Scanning

A commonly proposed active sensing movement is scanning or a rapid reversal, previously mentioned in the Prey-capture section. Both terms refer to the quick backward swimming of the fish, usually with a rigid body. Early studies performed by Hagiwara et al. (1965) found that the location of an object along the rostro-caudal axis of the fish would influence whether the electric image was positive or negative, regardless of its conductivity. They then proposed that scanning, or the act of bringing the object across the length of the body to activate a whole array of receptors would be preferred (Hagiwara et al., 1965; Heiligenberg, 1975; Scheich & Bullock, 1974). However, Heiligenberg (1975) computationally modeled these experimental conditions

and found that while this effect was present, it was in actuality much smaller, and this biphasic nature was confounded by experimental conditions. Heiligenberg did, however, agree that the image quality could be improved by passing the object over spatially separated receptors on the basis that the electrosensory array lacks a focusing mechanism. This hypothesis was later elaborated on with evidence showing scanning was theoretically able to improve “electroacuity” or the ability to distinguish two objects (Babineau et al., 2007). In computational results from Babineau and colleagues (2007) it was shown that prey-like objects could in principle be distinguished from the background using scanning behaviors due to higher electroacuity ability near the midbody, on account of the fish’s geometry and electric field.

1.3.3.2 Whole body oscillations

Whole-body oscillations are defined as broad-spectrum (up to 1 Hz) volitional movement which have been noted in a refuge tracking performance task in Eigenmannia sp. (Stamper et al., 2012). This task involves Eigenmannia maintaining their position within a rostro-caudally moving refuge, which they are known to be good at. In the light (primarily visual and electrosensory cues) the fish tracked the refuge nearly perfectly, while in the dark (primarily electrosensory cues), the whole-body oscillations emerged. Stamper et al. (2012) suggest that this increase in energy expenditure is a form of active sensing used to shape the spatiotemporal dynamics of electrosensory feedback. Follow-up work demonstrated that the fish use active sensing movements to maintain a sensory slip, defined as a dynamic difference between fish

and refuge position, predicted to prevent perceptual fading Biswas et al. (2018) which is further supported by some recent mathematical evidence Sontag et al. (2022).

1.3.3.3 Tail bending

Tail bending is another commonly observed active sensing movement, seen when the animal explores novel objects (Benda, 2020). This sweeping motion of the tail back and forth, creates an asymmetry between the left and right side of the fish. It also increases the electric image amplitude when the tail is closer to the object, proposed to enhance the electric image (Heiligenberg, 1975). Conversely, large amplitudes due to postural changes could instead swamp out the much smaller prey-related signals. Consequently, other studies suggest that tail bending must be canceled out (Bastian, 1975, 1995, 1999). Evidence has demonstrated that simple, repetitive postural changes at a fixed frequency are filtered out in the electrosensory lateral line lobe (ELL). In short, this cancellation is mediated by the descending pathways to the ELL whereby the correlation in pre- and postsynaptic activity leads to a plastic decrease in excitatory input (anti-hebbian plasticity; Bastian 1995, 1996). That said, other feedback mechanisms have been shown to improve pyramidal cell responses to behaviorally relevant stimuli, such as prey signals (Bastian, 1999; Bratton & Bastian, 1990). Additionally, there is also a body of computational evidence demonstrating an added benefit of tail bending. One example includes providing distance cues of objects irrespective of their size and conductivity (Sim & Kim, 2011). More broadly, it was also predicted that bending the tail toward an object while maintaining a rigid body stabilizes the receptor array and allows easier interpretation by the electrosensory system by reducing the amount of reafferent modulations (Assad et al., 1999a). This would indicate

that tail bending could allow the fish to also disambiguate object features by stabilizing the image pattern on the receptor array while tail bending to modulate the amplitude of the object (Assad et al., 1999a). Some studies offer a hybrid hypothesis suggesting that the amount of descending feedback that the different pyramidal cell types in the ELL receive could allow for different degrees of cancellation (Bastian et al., 2004; Chacron et al., 2003; Krahe et al., 2008; Stamper et al., 2012). As such, the authors suggest that the tail bending itself is canceled out but that unpredictable signals related to external stimuli (environmental motion) are enhanced (Stamper et al., 2012).

1.4 Where the field is headed

Knifefishes and many other weakly electric fishes are an effective model system used to understand the effects of sensory-motor interaction. The tight coupling of the sensory and motor systems as seen by the matching of their sensory range with their locomotory abilities indicates that these behaviors generate and shape sensory flow (Hofmann et al., 2014a; Snyder et al., 2007). While tail bending and scanning have been robustly documented and discussed for at least 50 years, the swimming behaviors of freely moving fish aren't as clear cut and simple. Given the omnidirectional locomotory and sensory pairing, it is probable that there are many other behaviors that influence the electric image in different contexts. More work is needed to identify the influence of motion on sensory input and in turn, the influence on electric sensing in more natural contexts.

1.4.1 Quantitative behavioral identification

The subjectivity involved in identifying putative sensing movements (active sensing movements and behavior in general), may misrepresent the true complexity of behavioral repertoires (Wiltschko et al., 2015). More recently, methods that enable the unbiased quantification of behavior are becoming more accessible. Unbiased behavioral identification aims to reduce or remove the subjectivity of labeling animal behavior by instead using data-driven techniques. There are a multitude of techniques emerging in the field of behavioral quantification falling under the umbrella of either unsupervised or supervised approaches.

Unsupervised approaches use various machine learning techniques to uncover patterns in the data and usually involve a dimensionality reduction and some form of feature extraction and clustering (Valletta et al., 2017). Stephens et al. (2008) for example, showed that the complex behavior of C. elegans from a high dimensional dataset could be elegantly described using just four dimensions while still accounting for 95% of the variance in the data. The next step in the unsupervised method is to cluster the reduced dataset. Clustering finds groups that share features while also maximizing the difference between other groups (Valletta et al., 2017). This step can be done several different ways depending on the goal. Supervised approaches are also popular strategies for quantitative behavioral identification. In this case however, machine learning is used to fit the data to previously determined behavioral features (Valletta et al., 2017). For more information on behavioral identification methods and examples of their uses in the field, see reviews by Valletta et al. (2017) and (Datta et al., 2019).

1.4.2 Quantitative behavioral analysis in pulse-type fish

Within the field there have been some implementations of quantitative behavioral identification approaches. While these studies have yet to be performed in wave-type knifefishes, there has been some advancement in the pulse-type species. Notably, Hofmann et al. (2014a) took a kinematic approach to identifying behaviors specific to novel object exploration. Using cluster analysis applied to the velocities with respect to thrust, yaw, and slip the authors identified prototypical movements (PMs) in single frame, multi frame homogenous (sequence of same PMs) and heterogenous sequences (transitions between PMs), as well as more complex combinations of PM transitions (chains of 5 PM transitions). They found that motor patterns were related to the inspection of objects. For example, in trials where a novel object was present, the fish performed more approach sequences, followed by stationary behaviors and backward swimming behaviors (comparable to object scans) which was significantly different from trials without the object. They found that overall, in trials with novel objects, there was a decrease in the diversity of the more complex behavior sequences perhaps due to the presence of novel objects triggering directed and stereotyped motor patterns.

1.5 Neural recordings in freely swimming fish

Historically, physiological studies were hard to perform in freely moving fish (Assad et al., 1999a) leading to unanswered questions regarding the variety in descending feedback and cancellation in behaviorally relevant contexts. However, recent works by Fotowat et al. (2019) and Wallach & Sawtell (2022) use exciting techniques to record neural activity in freely swimming pulse-type fish. Wallach &

Sawtell (2022) observed freely behaving pulse-type mormyrids, *Gnathonemus petersii*, in a simple environment. They monitored the fish's EOD rate, real-time tracking of the fish's heading, and the physiological data from the implanted electrodes in the granular layer of the ELL. Using a computational model of the ELL they found that the ELL can combine motor-related signals with spatially distributed (environmental) electrosensory input to achieve reafference cancellation. The authors suggest that future studies should focus on what happens in the ELL and other regions when the environment is systematically changed. Other recent studies in mormyrid pulse-type fish provide evidence to support the importance of motor control in active sensory learning (Pedraja et al., 2020). Fotowat et al. (2019) used Gymnotus sp. to wirelessly record neural activity from the pallium thought to be involved in spatial learning. These fish increase their EOD rate near objects and food (Jun et al., 2016) to increase electrosensory sampling providing a convenient read-out of attention. They also perform active sensing scans similar to knifefishes to bring objects to the electrosensory dense head region (Fotowat et al., 2019). Fotowat et al. (2019) found that the neural firing of most units occurred only when the fish was swimming and especially during backward swimming (scans) and when the sensory sampling (EOD rate) was increased. They also propose that active sensing movements in general are important for spatial learning. Compellingly, the neural anatomy of Gymnotus is nearly identical to Apteronotus (Fotowat et al., 2019; Lannoo & Maler, 1990) providing good reason to assume that these findings would be extendable to wave-type knifefishes as well, though this has yet to be done.

1.6 Conclusion

So far, we have discussed several behavioral and computational studies suggesting an important contribution of sensorimotor interaction in the perception of the electrosensory world. Active sensing movements such as tail bending and scanning are two of the most prevalent. Conversely, we have demonstrated that there is also a body of evidence indicating that these behaviors are canceled out, especially repetitive tail-bending behaviors. The evolution of these conflicting hypotheses led to a combination of the two suggesting the possibility of preferentially encoding objects of interest, such as prey, via active sensing movements while concurrently canceling out the larger image components due to the background (Babineau et al., 2007). This was supported by findings suggesting that the interplay between brain regions and feedback loops generates a neural code for spatially localized motion even in the presence of a noisy background (Clarke & Maler, 2017). Further studies also demonstrate that active sensing elicits an amplification of the sensory input that is necessary for spatial learning and navigation. For a detailed review on the neural mechanisms underlying these processes see (Engelmann et al., 2021a). Moving forward, further work involving neural recordings from freely behaving fish in physiologically relevant environments is needed. This, in combination with computational modeling of the electric images and behavioral quantification techniques, will provide the tools necessary to assess the true sensory input to the system. These will be essential in determining exactly how active motion is impacting electric sensing and if it is indeed maximizing sensory related input as suggested (Assad et al., 1999a; Hofmann et al., 2014a). Recent advances in all these categories of research should bring us closer to deciphering the reason these active

sensing behaviors are so apparent. In turn, sensorimotor interaction in electric sensing will provide insight to the many other animals that use active sensing strategies to improve the saliency of their sensory world.

1.7 Figures

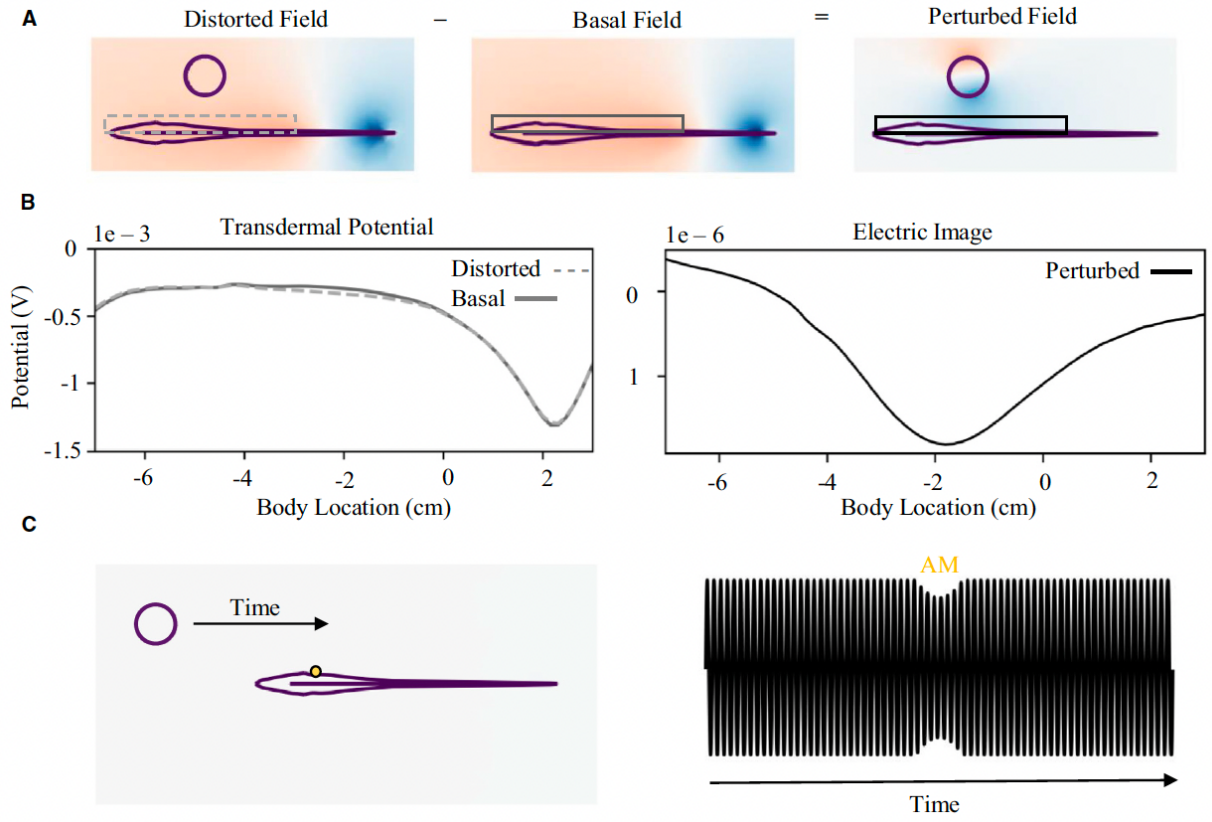

Figure 1.1 Electroreception in Apteronotus albifrons.

A) Left: The distorted field of the fish due to the object (purple circle). Middle: The basal field is the fish's own electric organ discharge alone. Right: If you subtract these two fields you are left with the perturbed field, meaning the electric fi(A) Left: The distorted field of the fish due to the object (purple circle). Middle: The basal field is the fish's own electric organ discharge alone. Right: If you subtract these two fields you are left with the perturbed field, meaning the electric field due to the object alone. In both the distorted field and the perturbed field, the object is 1 cm^2, located 1 cm from the fish and 1/3^{rd} of the fish's body length from the nose. (B) Left: The transdermal potential (the potential difference across the fish's skin) due to the distorted field (grey dashed line) and the basal field (solid dark grey line). Both line types (dashed and solid) also correspond to their respective boxes enclosing the first 2/3^{rds} of the fish in (A). The x-axis shows the body location enclosed in A with the object (purple circle) being located at 2 cm (1/3^{rd} of the fish's body length from the nose). Right: The electric image resulting from the perturbed field which is the difference between the transdermal potentials between the distorted field and the basal field (dashed line minus solid line in the left panel). Notice the different scale in the y-axis. Here the x-axis also corresponds to the box enclosing the first 2/3rds of the fish in the right-hand image in (A). (C) Left: Schematic of the object (purple circle) moving rightward, lateral to the fish's right side. The yellow circle on the fish's body denotes a single electroreceptor. Right: The electric organ discharge oscillating in time. To the left of the amplitude modulation (AM) would be before the object passes over the receptor, at the AM would be exactly when the object passes over the receptor, and to the right of the AM would be after the object passes the receptor. Note: part C is a schematic, and the amplitudes/frequencies are not to scale.

Chapter 2: General Thesis Overview

The following chapters address the role of motion on electrosensory acquisition in weakly electric fish using behavioural and computational approaches. Overall, I aim to address so-called active sensing behaviours with a particular focus on scanning.

Historically, some aspects of active sensing behaviours such as tail bending and scanning in wave-type weakly electric fish have been quantified in task-specific experiments (Biswas et al., 2018; MacIver et al., 2001; Nelson & Maciver, 1999b; Pedraja et al., 2020; Stamper et al., 2012). Additionally, research has made strides in the theoretical implications of simplified movements as a means of improving electrosensory properties, such as contrast (Assad et al., 1999b; Babineau et al., 2007; Heiligenberg, 1975; Rasnow, 1996; Sim & Kim, 2011). However, research in freely-swimming weakly electric fish is lacking. We address this gap by studying freely-swimming *Apteronotus albifrons* and the implications of body-shape on electric sensing. One advantage to using *A. albifrons* is that their physiology is well characterized (Bastian, 1999; Bernt et al., 2019; W. Crampton et al., 2007; W. G. R. Crampton, 2019; W. G. R. Crampton & Albert, 2006; Engelmann et al., 2021b; Moller, 1995; Rasnow, 1996; Stoddard, 2009; Turner et al., 2007; Upshall, 2024), and certain aspects of active sensing have been addressed in prey-capture studies (Nelson & Maciver, 1999b). Furthermore, active sensing research in freely-swimming fish has been mostly limited to pulse-type fish (Hofmann et al., 2014b; Wallach & Sawtell, 2023). Using *A. albifrons*, a wave-type fish, we address how continuous electric sampling of their environment may influence electric sensing as well as the potential role of body-shape.

In Chapter 3 I introduce a custom-made behavioural identification pipeline. I developed this pipeline throughout my studies as the behavioural experiments evolved and the analysis requirements became more complex. My first goal is to demonstrate the value of the pipeline in standardizing and mass-analyzing components of behaviour. This is especially beneficial to behavioural characterization in weakly electric fish where the behaviours are quantitatively poorly described. Furthermore, given the suggested importance of such behaviours in electrosensation, having accessible methodology to analyze their body-shape dynamics over time provides a novel perspective for investigating active sensing behaviours.

In Chapter 3 I analyzed behavioural data with freely-swimming fish in a neutral and novel environment. I used these data to first characterize the baseline behavioural repertoire of weakly electric fish in the neutral environment. I then show that two of the six identified behavioural components correspond with descriptions of scanning behaviours and that they increase in the presence of novel objects.

Chapter 4 expands on the findings in Chapter 3. I aimed to use the computational techniques developed in Chapter 3 to address the effects of more complex environmental settings. I had recognized that more natural environments would display spatial and temporal changes. The flexibility of the behavioural apparatus allowed me to introduce spatially novel objects without any movement, as well as with object movement, without disturbing the fish between trials. We know from Chapter 3 that a static novel object increased scanning events. As a resulted, I predicted that increasing

the environmental complexity would increase uncertainty such that the fish would benefit from increased sensory acquisition. I posited that the introduction of temporal dynamics would induce different active sensing behaviours such as tail-bending and nose-poking. I further observed the behaviour of the fish with repeated trials to induce habituation. Here I expected that as familiarity increased, we would see a shift in the behavioural strategy. By comparison across time, I aimed to improve the understanding of the fish's evolution of behaviour throughout the experiment where we expected active sensing behaviours to be most prevalent amongst uncertainty.

In Chapter 5 I turned to the implications of movement on the electrosensory inputs available to the fish. The behavioural evidence thus far is only correlative without physiological evidence. I aim to show that active sensing behaviours provide more sensory information by modifying the electrosensory input to the electroreceptors. I used a novel custom-made software which computes the effects of the electric field and the environmental surroundings. I then simulated the effects of scanning, from simple scenarios building up to using the real data obtained in Chapter 4.

Together, these three data chapters build a stronger foundation for the implications of active sensing employed by weakly electric fish. I provide open-source software for implementing these computational approaches in behavioural identification. I implement novel methodology to build and support previous hypotheses, and finally, provide future directions for the development of experiments to concretely address sensory-motor interaction and their associated behaviours.

Chapter 3: Quantitative Behavioural Identification Indicates Increased Scanning in Novel Environments in Weakly Electric Fish

3.1 Abstract

Weakly electric fish detect perturbations in a self-generated electric field to navigate their surroundings and capture prey. Perturbations depend on the relative positions of objects and the geometry of the electric field, which changes with body pose. Self-motion thus greatly impacts electrosensory inputs. Indeed, some specific movements, such as back-and-forth scanning, are thought to provide a basis for active sensing that enhances electrosensory perception. Other animals have also been shown to increase active sensing movements in novel environments. Here, we subjected 9 fish to novel conditions and quantified the effects on behaviours, including scanning. We used a data-driven behavioural identification analysis to determine the building blocks of behaviour, known as behavioural syllables. We found that behavioural syllables associated with quick straight back-and-forth swimming, increased in the novel

environment, consistent with a role of scanning in active sensing. This high-throughput analysis pipeline provides a statistically motivated baseline with which to standardize and investigate electrosensory behaviours and helps overcome some of the challenges associated with high behavioural variability in general.

Keywords: Weakly electric fish, scanning, electrosensation, *Apteronotus albifrons,* animal behaviour, behavioural classification.

3.2 Introduction

Sensory systems have evolved a variety of strategies to encode information about the environment (Davis, 2019). In some cases, these strategies involve the coordinated movement of sensory structures. Determining how these movements enhance information acquisition requires a detailed understanding of both sensory and motor dynamics (Schroeder et al., 2010).

The nonlinearities inherent to sensory and motor systems, in addition to the highly variable nature of animal behaviour, present significant challenges (Kappeler, Peter, and Kraus, 2010).

Recently, high-throughput computational pipelines have been developed to efficiently analyse the large datasets required to characterize behavioural variability (Hsu & Yttri, 2021; Todd et al., 2017; Weinreb et al., 2024). Here, we use a similar approach to evaluate active sensing in weakly electric fish. These fish use an electrosensory system to gather spatial and object related information within a body-length of their surroundings. The self-generated electric organ discharge results in an

omnidirectional electric field. This coupled with skin-embedded electroreceptors along the body used to detect field perturbations, is the basis of the electric sense. Additionally, these anguilliform fish can swim omnidirectionally with impressive motor control presumably to support tight sensorimotor feedback.

Scanning is a forward-to-backward quick swimming movement thought to be an active sensing strategy that allows for enhanced sensory sampling (Assad et al., 1999a). As the fish swims by a novel object, the field perturbation due to the object forms an electric image on their skin that moves along the length of its body; in the next phase of a scan, the fish doubles-back by reversing with the image passing along its body again (Benda, 2020; Nelson & Maciver, 1999a; Upshall, 2024). Given the dispersal of receptors over the body, scanning could thus improve object distinction by involving more receptors (Assad et al., 1999a). Additionally, said receptors are known to habituate quickly, thus motivating the need for increased movement (Hopkins, 1976).

Descriptions and quantification of these electrosensory scanning behaviours vary across the literature. They have been referred to as B-scans (bidirectional scans), fore-aft movements, va-et-vient movements, scanning, and probing (Engelmann et al., 2021a; Gómez-Sena et al., 2014; Nelson & Maciver, 1999a; Stamper et al., 2012; Uyanik et al., 2020). Studies have noted increased scanning in various spatial learning-related tasks, and prey-capture – suggesting a physiological role in task-specific environments (Engelmann et al., 2021b; Jun et al., 2016; Jung & Engelmann, 2019;

MacIver et al., 2001). The overall significance of scanning across studies is additionally convoluted by species variability as well as inter- and intra- variability amongst fish.

If we are to understand the physiological relevance of scanning in novel environments, then it is necessary to quantitatively motivate and standardize its behavioural description. This statistical approach has been effective in convergently related species demonstrating scanning-like behaviours and increased electric organ discharge rate near novel objects (Hofmann et al., 2014a; Pedraja et al., 2020). More recently, with new computational techniques, the classification of animal behaviour has been in favour of statistically driven behaviour identification models (Datta et al., 2019). These models use a series of steps starting with user-defined locomotive statistics to identify components of behaviour which are most different from each other. Wiltschko et al. (2015) defines these components as behavioural “syllables” using spoken language as their analogy, with syllable combinations being analogous to words (Berman et al., 2014; Weinreb et al., 2024; Wiltschko et al., 2015). Taking advantage of this computational approach, we developed a behaviour identification software pipeline which identified six behavioural syllables. We found that two of the six identified syllables form the basis for scanning, and these were produced more in novel environments. This supports previous hypotheses that scanning may be used to extract more information in novel conditions (Jun et al., 2016). We also provide a standardized baseline of behavioural syllables which can be used to assess changes in the overall behavioural repertoire while accounting for environmental context and movement dynamics.

3.3 Methods

3.3.1 Animals

Apteronotus albifrons were obtained from Big Al's (Ottawa, ON). Fish were housed individually in 5L tanks with a 12h:12h light:dark cycle. Tank water was maintained at a temperature of ~26-28ºC and at a conductivity of ~160-220 µS. Fish were fed bloodworms three times weekly. All experimental protocols were approved by the Animal Care and Committee of the University of Ottawa (Protocol BLe-3678).

3.3.2 Experimental Design

Individual fish (n=9) were placed in an experimental tank with a water heater (~26-28 ºC) and O_2 bubbler with a pre-set conductivity of 180 µS $\pm$ 20 µS. The fish was placed in a rectangular (36 cm x 14 cm x 5.5 cm) plexiglass refuge and allowed to acclimate prior to data collection for 20-24 hours. The 61-L tank (60.96 cm x 30.48 cm x 30.48 cm) containing the refuge was filled with water until just before the top of the refuge was reached. The entire apparatus was set atop a custom-made infrared light array (850 nm) apparatus illuminating the tank from the bottom. The video camera was attached above the tank (Titri Raspberry Pi 4 Night Vision 5MP Adjustable-Focus OV5647 Sensor Video Camera with 30CM FFC) and connected to a Raspberry Pi 1 (model A+). Recordings were taken in the dark at 30fps and 1080p.

Artificial objects were produced using 6 independent shunting circuits with a resistance of 75 kΩ. These circuits shunt the current from the fish's electric field between the inside and outside of the refuge, mimicking the effect of real objects on the

fish's electric field (Lomovtsev et al., in prep). The ends of each circuit comprised a 2mm diameter carbon rod 1cm in length, (non-polarizing; STAEDTLER Mars carbon 200-4B) connected by modified 0.062" power connector female pins, encased in silicone tubing (VWR International 0.063"ID 0.189"OD) and silicone adhesive (LePage 1366092). The inside ends were embedded in the plexiglass on the lower half of the longitudinal walls, three to a side and separated by 3.5cm (see Figure 3.1).

The fish were acclimated to the refuge with the shunting circuit set to "open" such that no path for current was available between inside and outside. This same open circuit is used for the first trial (control-11, see Figure 3.1). For the second trial (novel), all 6 shunting circuits are connected, so that the electric field current is shunted through a 75 kΩ resistor to outside the refuge. For the final trial (control-2), the shunting circuit was returned to the "open" state, as in control-1. Each trial was 10 minutes in duration, with video recording performed in 5-minute pieces, for the duration of the 30-minute experiment. All analyses were limited to the first 5 min of each trial.

3.3.3 Behavioural Analysis Pipeline

3.3.3.1 Positional Labelling

All videos were analyzed using DeepLabCut (DLC), an open-source machine-learning based software for labelling positional data (Mathis et al., 2018). We trained the model with 1500 labelled frames to 215,000 iterations with a loss rate value of 0.0046. The resulting datasets comprised a frame-by-frame record of fish position and shape (six points along the body in x,y, pairs; see Figure 3.1B). We then used linear

interpolation to fill in values where the DLC model likelihood was less than 90% (pandas.pydata.org). The maximum interpolation window for each x, y body point coordinate in time was 60 frames. The resulting data were then smoothed in time using a gaussian filter function (length = 11 frames, width = 2 frames; scipy.org). All parameters used in the preprocessing step are available in the params.yaml on GitHub (https://github.com/maryupshall/pyUCAB).

3.3.3.2 Behaviour Identification and Classification

To analyse fish position and shape over time, we adopt an approach inspired by previous work (Hsu & Yttri, 2021; Todd et al., 2017; Wiltschko et al., 2015) but customized for our data i.e. with specific adaptations to improve the classification of behaviours across various time scales and allow more flexibility in parameter manipulation (see GitHub https://github.com/maryupshall/pyUCAB for details). In the following, we describe our general workflow that involves five steps: feature selection, dimensionality reduction, clustering, classification, and prediction.

3.3.3.2.1 Feature Selection and Extraction

To characterize the baseline behaviour of weakly electric fish, we must first choose relevant features of the data that best describe the behaviours of interest. We were interested in the fish's shape dynamics as well as how it moves translationally in space and time (see features_utils.py for custom functions used in feature extraction on GitHub). Unless otherwise stated the following were performed on each of the six points along the midline of the fish from nose to tail. To capture body shape in each time point

(frame), we used the instantaneous angles between body points. We then applied principal component analysis (PCA) to these body angles and used the loadings for the first three components (collectively accounting for ~98% of the variance from the original angle space) as our angle features. To capture dynamics of swimming, we used the heading direction and velocity vector of the nose point, as well as the magnitudes from a wavelet analysis in time for the nose and tail points. The wavelet analysis was performed using the PyWavelet package (Lee et al., 2019) taken over two frequencies (0.5, 1; equivalent to *scales*sampling_period*) for both the x- and y- component separately. We used the continuous wavelet transform function (*cwt*) and implemented the Morlet wavelet object with the default widths (range 33ms – 1 second). This methodological addition allowed us to capture movements of nose and tail over time periods of 0.5 and 1 seconds (Cazelles et al., 2008; Hossain et al., 2022; Lee et al., 2019; Todd et al., 2017; Lilly, 2017) and greatly improved classification. In summary, we obtained a total of 13 features for each time point of our trials: 3 body angle features, 2 features for heading direction and velocity, and 8 wavelet features (2-time scales each for the x and y coordinates of the head and tail).

3.3.3.2.2 Dimensionality Reduction

As the number of features increases, it is more computationally expensive and increasingly challenging to develop a reasonable classification model. To mitigate this “curse of dimensionality”, dimensionality reduction is recommended (Keogh & Mueen, 2017). As in previous work (Hsu & Yttri, 2021) we used uniform manifold approximation and projection (UMAP; McInnes & Healy, 2018) to reduce our feature space from 13 to

7 dimensions. UMAP is a non-linear method of dimensionality reduction that has easy-to-use and readily available functions pre-developed in a reputable python library (umap; https://umap-learn.readthedocs.io; McInnes & Healy, 2018). The UMAP function requires an input parameter for the output dimensionality. Here we used PCA to identify the number of dimensions required to explain 90% of our data (7 dimensions), though others have successfully used values closer to 70% (Hsu & Yttri, 2021; Todd et al., 2017). After this step in the process, we are left with 7 composite features for each time point.

3.3.3.2.3 Clustering

To identify the "behavioural syllables" (basis movements) from the reduced features, the data were then clustered using hierarchical density-based clustering for applications with noise (Campello Ricardo J. G. B. and Moulavi, 2013). This is an adaptation of the density-based clustering technique but is much less sensitive to noise – meaning it can still identify a group of points as a cluster even if there are a lot of sparser points in the surrounding space. Though there are also other options for clustering (k-means, for example), this algorithm is well-suited to the high variability associated with behavioural data (Campello Ricardo J. G. B. and Moulavi, 2013). For further information and implementation tips see https://hdbscan.readthedocs.io. See Table 3.1 for parameter summary. The output clusters identified in this step form a basis for the individual behavioural syllables i.e. each cluster is a distinct syllable.

3.3.3.2.4 Classification

The classification step involves mapping the reduced features onto the clusters identified in the clustering step; this will then allow us to identify a behavioural syllable (i.e. cluster) from feature data at each time point. We used a random forest classifier to fit several decision trees to our dataset where 80% was dedicated to training and 20% for testing (see scikit-learn docs for sklearn.ensemble.RandomForestClassifier). We took an unsupervised approach here, training the classifier with data-driven behavioural identification rather than training using predetermined behaviours (labelled data). We identified the best hyperparameters using the randomized search cross validation function from the model selection package in sklearn. See Table 3.1 for parameter summary.

3.3.3.2.5 Prediction

The last step in the process involves applying the resulting classifier to the remainder of our dataset such that the most probable syllable (cluster) is assigned to the feature data at each time point. At this point, each time point is associated with a distinct behavioural syllable.

3.3.3.3 Post-identification Analysis

We assumed that our frame rate resolution of ~33ms (30fps) was shorter than the duration of any distinct behavioural syllable; specifically, we set a minimum bout length for any syllable to be 3 frames (100ms). Thus, we replaced syllable labels for all bout lengths less than 3 frames with null values. If the null frame sequence was less

than 3 frames, we interpolated them using the pandas library function and set them equal to the closest previous and valid labelling bout. Any null sequence longer than 3 frames was left as is. Across all trials, null values made up 0-10% of time points and had an average bout length of 3.1 frames. Post-interpolation the null values made up less than 1% of the data.

3.3.3.4 Transition Probabilities

Ethograms involving the transition probabilities between syllables were generated using the pandas library crosstab function (*pd.crosstab()*). Bootstrapping transition probabilities was performed as follows: random data were generated by shuffling the original data and generating 10,000 corresponding transition matrices per fish per condition. For each behavioural transition we generated a distribution of transition probabilities based on this shuffled data; from this distribution we found the p-value associated with the observed (true) transition probability. The ethograms (Figure 3.4 A-C) were generated using plotting functions in the python package NetworkX in combination with the matplotlib.pyplot library. The transitions were plotted if the p-value was <0.005. For all other associated p-values and transition probabilities see the supplemental materials. All other figures were created using functions provided in matplotlib or seaborn libraries.

3.4 Results

To characterize scanning across contexts, we tracked freely-swimming fish in two different environments: a baseline condition and a “novel” condition in which six

electrosensory objects were added (see Methods; Figure 3.1). We used fish trajectories, heading direction, velocity and body shape, as locomotory features. Similar to previous work, we identified these features using an unsupervised clustering algorithm which identified 6 basic behavioural syllables (Weinreb et al., 2024; Wiltschko et al., 2015). (Figure 3.4.1; see Methods for details). Figure 3.1 shows the resulting color-coded clusters that we then named based on visual inspection as: forward straight swimming (FS), backward straight swimming (BS), stationary wiggle (SW), pivot (PV), forward C-shaped swimming (FC), and backward C-shaped swimming (BC). See Figure 3.1C for pictographs of each behaviour and the Supplemental section for video examples.
FS and BS are characterized by forward and backward swimming respectively, with an average peak velocity of ~ -12 ± 3.5cm/sec which was lower than previously observed peak scanning velocities -19.1± 5.2cm/sec (MacIver et al., 2001), possibly due to our relatively smaller sized fish and smaller testing arena. PV and SW also displayed directionality in their velocity statistics, this was over smaller displacements and velocities compared to FS and BS (PV: 7.15 ± 2.4cm/sec; SW: 4.2 ± 1.7cm/sec). The PV syllable involved a brief backward movement with a fixed head position, whereas, the SW involved a stationary wiggle, with occasional slight forward displacements. The C-shaped (FC and BC) syllables involved swimming speeds similar to those of FS and BS but differed in the degree of body curvature (nose-midpoint-tail angle <160 degrees).

3.4.1 Some behavioural syllables are expressed more often than others in the baseline condition

We quantified the expression of each syllable by its bout length (consecutive repetition of a given syllable) and the number of times these bout lengths occurred for

each syllable which we call bout counts. In the baseline condition (control-1), the straight behavioural syllables (FS and BS) were both the most frequent and had the longest bout lengths, representing over 50% (FS 27.6 ± 5.4%; BS 23.2 ± 9.7%) of the total behavioural repertoire (collection of syllables).

The least common syllables were the pivot (PV) and wiggle (SW) (see Figure 3.1 C), respectively occurring 10.1 ± 4.6% and 4.1 ± 3.4% of the time on average. The FC and BC syllables comprised the remaining time, occurring moderately frequently (15.4 ± 5.5% and 19.6 ± 4.6%, respectively).

In addition, we found that the production of each syllable was consistent over the duration of the trial (see Supplemental Figure 3.1) indicating that the fish had no preference for any one syllable at different time points.

3.4.1.1 Expression of behavioural syllables changes with novelty

In the novel condition, all fish changed their behavioural repertoire, as described by overall changes in the distribution of syllable expression (chi-square p-value < 0.01×10^{-10}). When looking at isolated syllables however, these changes are subtle, with only a few syllables showing detectable changes (Figure 3.2). The frequency of FS increased slightly in 7/9 fish (+2.4± 2.5%) (Wilcoxon statistic=5.0, p-value=0.04). However, this was accompanied by a significant decrease in FS bout length (Figure 3.2) which suggested that the fish performed faster switching between syllables and shorter bout durations of FS. Interestingly, BS was modified differently than FS across conditions. BS showed an increase in bout frequency compared to both control-1 and

control-2. This was accompanied by a negligible difference in bout length which suggested that most fish were increasing backward straight swimming without increasing velocity.

Increased expression of FS was accompanied by decreases in three other syllables, while BS and SW remained unchanged. PV, decreased in frequency for all 9 fish in the novel condition (Wilcoxon statistic=0.0, p-value=0.004). This decrease was accompanied by a decreased expression of FC and BC as well.

Interestingly, when we reintroduced the fish to control conditions (control-2), we also observed a significant difference in the distribution of behaviours when compared to control-1 for all fish (p-value $<0.01 \times 10^{-50}$).

The control-2 condition had the opposite effect on FS with a minimal decrease in frequency by $2.3 \pm 2.0\%$ (Wilcoxon statistic=2.0, p-value=0.01), however the bout length remained the same as in control-1 which indicated a small decrease of FS. Control-2 instead showed more frequent instances of BC compared to control-1 (Wilcoxon statistic=1.0, p-value=0.008), which was not present in the novel comparison indicating that the decline in FS was possibly being allocated to BC in control-2.

3.4.1.2 Scanning is described by a syllable sequence and is more prominent in novel conditions

We described scanning using repeating sequences of FS-BS syllables aligning with their bidirectional swimming (b-scans) identifier. We quantified repeating sequences by computing the syllable transitions across conditions (i.e. FS-BS and BS-

FS). To focus on syllable switching, we removed self-to-self transitions such as FS-FS or BS-BS (Figure 3.3, Hofmann et al., 2014) as is common when looking at transition states.

In Figure 3.3 we plot the syllable-to-syllable transition probabilities (%) which describes the probability that one syllable will follow another. The base of the arrow leaving the syllable has a probability (%) labelled at its centre denoting the next likely state. Coloured arrows show statistically significant transitions from low (dark blue) to high (light blue green) probability. Significance was determined by generating 10,000 shuffled syllable sequences observed in control-1 which resulted in 10,000 transition matrices. With these we produced probability distributions for each transition pair, representing the probability of observing a given transition by chance. We then compared the true probability observations from each condition and generated p-values. For comparison we plotted insignificant transitions using grey arrows if they were otherwise significant in at least one condition (control-1, novel, or control-2). Transitions that were insignificant (p-value>0.005) across all conditions were omitted for clarity (see Supplemental 3.2 for all transition probabilities and p-values).

In the novel condition the fish had the highest transition probability for BS-FS (50%, p-value=2.17e-13) followed by FS-BS (47%, p-value=0.0015) both of which were more likely than chance. In both control-1 and -2 the FS-BS transition probabilities (32%, p-value=0.885 and 28%, p-value=0.834, respectively) were found to be equivalent to observations due to chance.

Of the remaining 3 transition pairs, BS-BC, FS-FC, and FC-BC, the BS-BC transition was different from chance in all three conditions. The latter two were found to

be more likely than chance in either control-1 or -2 but were found to be no different from random in the novel condition (FS-FC, p-value=0.0081; FC-BC, p-value=0.022).

These indicated that the fish trended toward straight swimming behaviours and favoured both BS and FS overall in the novel condition. The bidirectionality of both FS-BS and BS-FS which was absent in the control conditions, provided further evidence for scanning-like behaviours in novel conditions.

We further investigated this by looking at the transitions between 3 consecutive syllables, namely sequences of FS-BS-FS and BS-FS-BS (see Figure3.3E). These sequences occurred most frequently in the novel condition ($12.4 \pm 6.0\%$) which was significantly higher than control-1 (Wilcoxon statistic=3.0, p-value=0.020) and control-2 (Wilcoxon statistic=1.0, p-value=0.008).

3.5 Discussion

Electric sensing is a dynamic sensory process that depends on the fish's self-motion, and the dynamic properties of their environment. Given their short sensory range and the fast adaptation of their electrosensory receptors, movement is essential to electrosensory perception (Upshall, 2024). Certain movements have been hypothesized to be involved in or even enhance the quality of incoming electrosensory information (Biswas et al., 2018; Fotowat et al., 2019; Hofmann et al., 2014b; Jun et al., 2016; Stamper et al., 2012; Uyanik et al., 2020). Here, we showed that scanning, classically described as a forward-to-backward swim with a rigid (straight) body,

increases in novel environments. This is consistent with the idea that weakly electric fish may use scanning to extract electrosensory-based information.

Previous work suggests that scanning does a few things to possibly improve electrosensory acquisition. First, it increases the spatial sampling area by passing an object over more receptors than it would if it remained static (Assad et al., 1999a). It may also improve the signal to noise ratio by sampling an object multiple times during a back-and-forth scan, taking advantage of electroreceptor properties which favour increased velocity (W. G. R. Crampton, 2019; Nelson & Maciver, 1999a). It can also aid spatial learning attributed to upstream hindbrain feedback circuits which have been shown to be selective toward the sensory input arising from these movements (Engelmann et al., 2021). Electrophysiological studies show that the change in direction from forward to backward swimming and vice versa elicits a bursting firing pattern in the electrosensory lateral line lobe (ELL), and other centres involved in higher order electrosensory feedback loops (Clarke & Maler, 2017). While some centres do encode continuous smooth motion, it is evident that there are more dedicated to reversals in direction, as elicited in scanning, which may facilitate spatial learning by the creation of ‘time stamps’ (Engelmann et al, 2021). While these electrophysiological studies were performed on immobilized fish, our results demonstrating increased scanning in the novelty condition of freely swimming fish support these findings. Recently, work using convergently related species have been successful in recording from the ELL in a freely swimming fish with and without an object of interest (Wallach & Sawtell, 2023). Similar methodology to investigate scanning specifically will provide the necessary neurophysiological evidence for confirmation of its proposed roles.

Our experiments were performed over a relatively short time (5-minutes) and a relatively sparse and static environment. It will be important for future experiments to determine if the overall baseline behaviours we describe extrapolate to environments involving more spatial and temporal complexity. For example, do the fish respond differently to a moving stimulus compared to a stationary stimulus of the same type? If movement is to prevent adaptation of the electroreceptors, then it is possible that the fish would be able to conserve energy and simply observe the movement of the object instead. Alternatively, if the quality of the moving stimulus is of low resolution, then perhaps the fish will need to move more to gain spatial and temporal information, a strategy observed in other animals that use motion for sensory acquisition (Mitchinson et al., 2007; Schroeder et al., 2010).

Further to improving understanding of behaviour in different environments, our computational approach to behavioural identification provides a standardized baseline with which to investigate other frequent combinations of syllables and their possible role in active sensing. This in combination with varying environmental complexity will facilitate identification of context dependent behaviour. Furthermore, future work obtaining electrosensory inputs to the receptors will allow us to understand the information due to the environment in combination with the fish's movement and determine if self-motion is helping or hindering electrosensation.

3.6 Figures

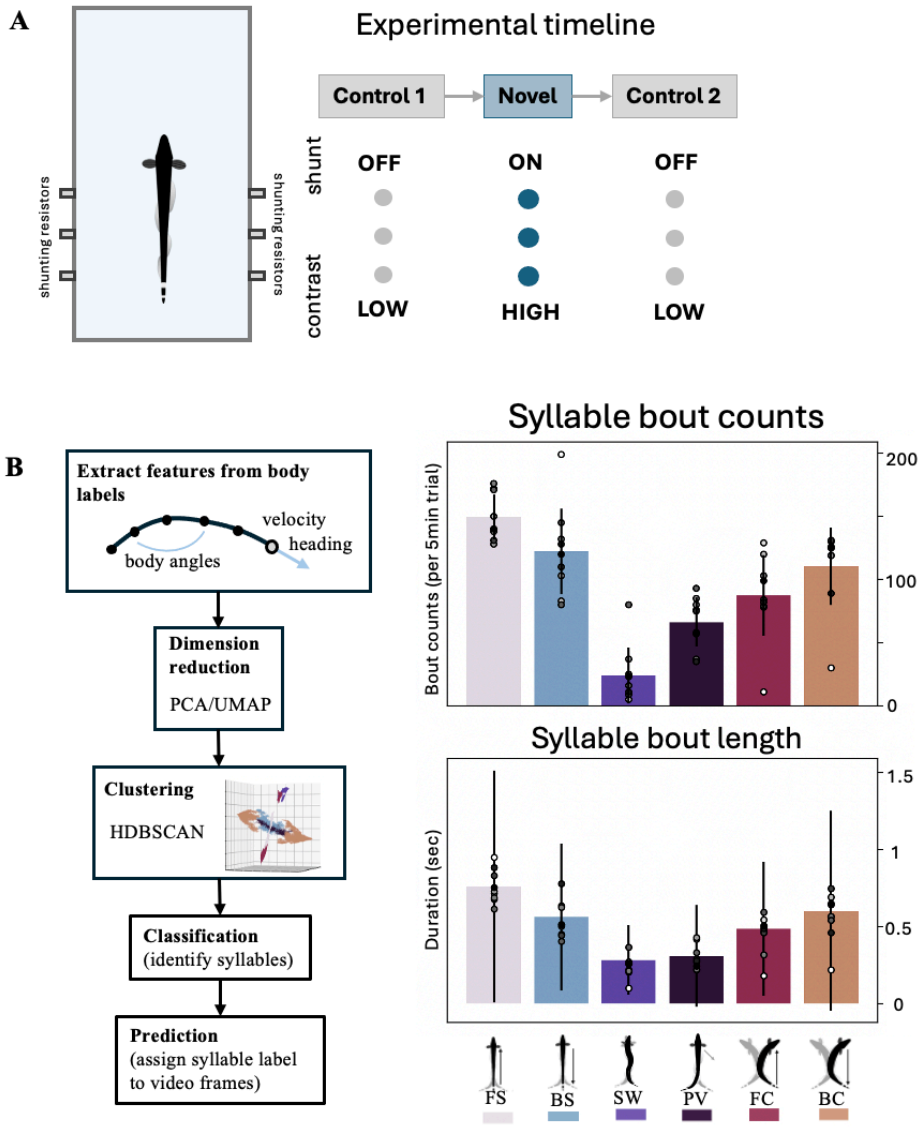

Figure 3.1 Computational characterization results in 6 behavioural syllables.

A) Schematic of Apteronotus albifrons in experimental refuge with 6 total shunting resistors – 3 per side. Experimental timeline showing order of events. Control-1: The shunt is off, contrast is low. 3 grey circles depict side view of resistors. Novel: The shunt is on, contrast is high. 3 blue circles depict side view of resistors. Control-2: Same as control-1. B) Left: Order of methodological events for behavioural characterization. Right: Syllable bout counts and syllable bout lengths for each syllable. Fish icons (x-axis) correspond to abbreviations and bar colour. Small circles = raw data. Black bars = standard deviation. FS = forward straight; BS = backward straight; SW = slight wiggle; PV = pivot; FC = forward C-shaped; BC = backward C-shaped.

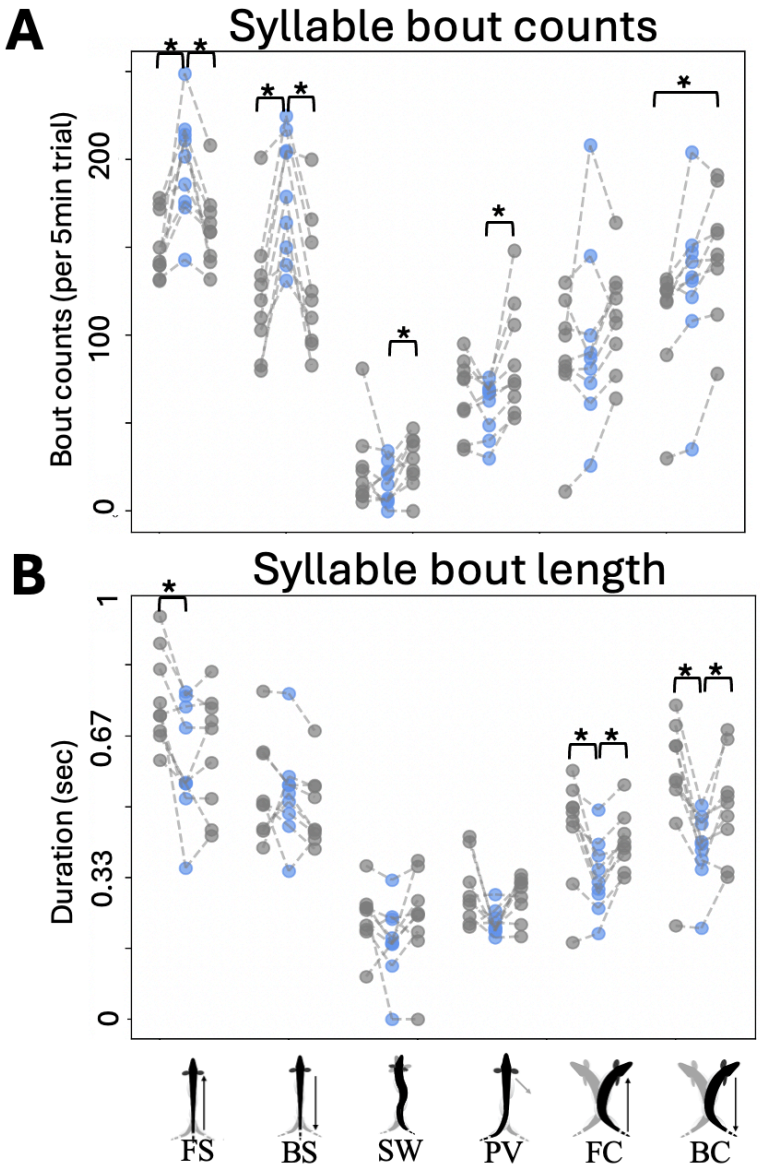

Figure 3.2 Syllable bout statistics show select differences between environmental conditions.

*A) Syllable counts for each individual fish. Dashed lines connect control-1 to novel to control-2 (left to right; grey, blue, grey) for a given individual. * = p-value < 0.05. B) Syllable bout length. Same format as A). Fish icons (x-axis) and corresponding abbreviation denotes behavioural syllable. FS = forward straight; BS = backward straight; SW = slight wiggle; PV = pivot; FC = forward C-shaped; BC = backward C-shaped.*

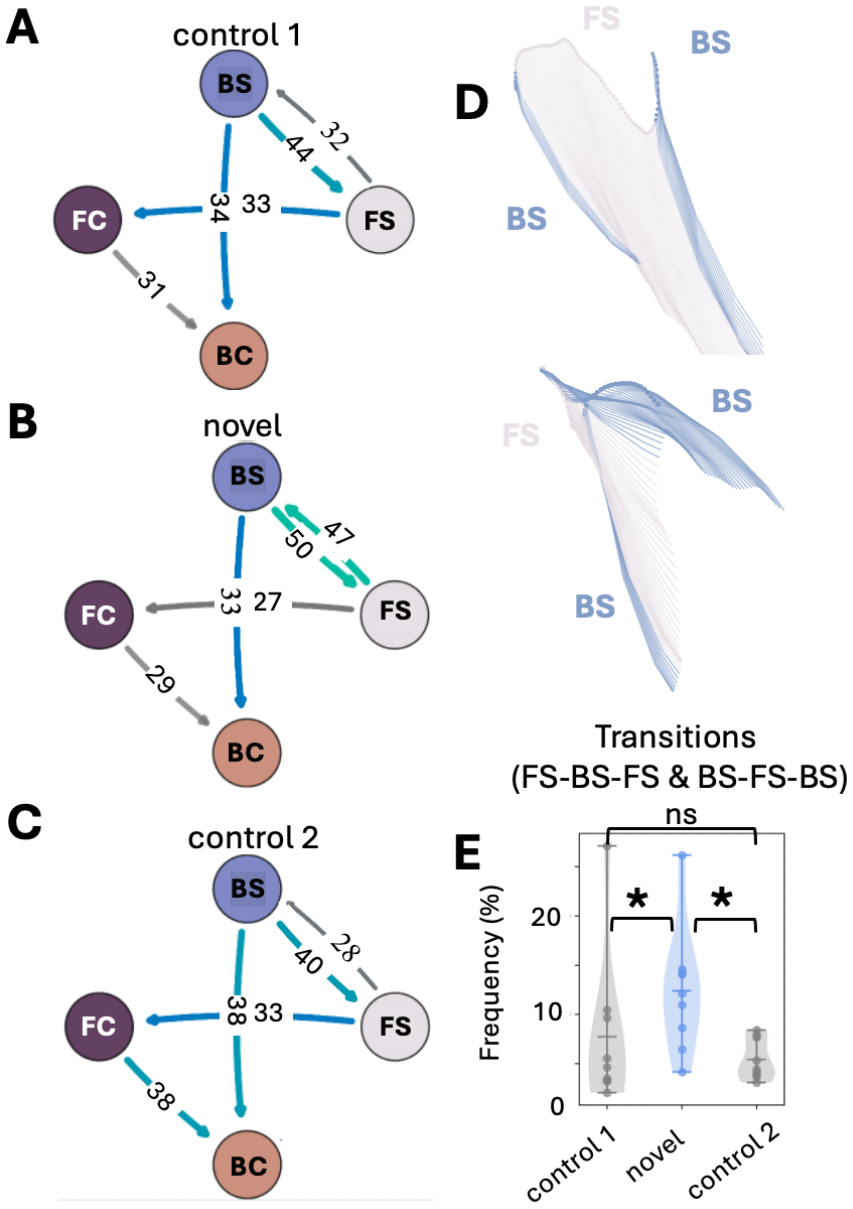

Figure 3.3 Syllable transition probabilities suggest increased scanning in novel environments.

*A-C) Control-1, novel, and control-2 ethograms with transition probabilities (%) between behavioural syllables. Grey arrows = insignificant. D) Raw data snippet of fish performing two different scan events. Fish splined from head to tail. Colours correspond to syllable at that time-point. Small circles at the end of each line denotes head position. E) Frequency (%) of events containing three consecutive syllables indicative of a scan (FS-BS-FS; BS-FS-BS). * = p-value<0.05. Raw data shown with small circles. Mid-line horizontal bar = mean.*

3.7 Tables

Table 3.1 Parameter descriptions for functions used in behavioural identification methods.

Pipeline Step	Parameter	Description	Value
Clustering (HDBSCAN)	min_cluster_size	Minimum cluster size required to be considered a cluster. Smaller values result in more clusters.	0.5% of training set (training set = 30% of total set; 600,000 frames)
Clustering (HDBSCAN)	min_sample_size	Low values result in decreased conservativeness.	1 (Hsu & Yttri, 2021)
Clustering (HDBSCAN)	cluster_selection_method	Leaf cluster selection method produces more fine-grained clusters compared to excess of mass (eom).	Leaf
Classification (Random Forest)	max_depth	Depth the nodes can expand. Higher max depth results in overfitting (poor generalization).	19
Classification (Random Forest)	n_estimators	Number of trees in the forest to improve model performance but increase computational cost.	298

3.8 Supplemental

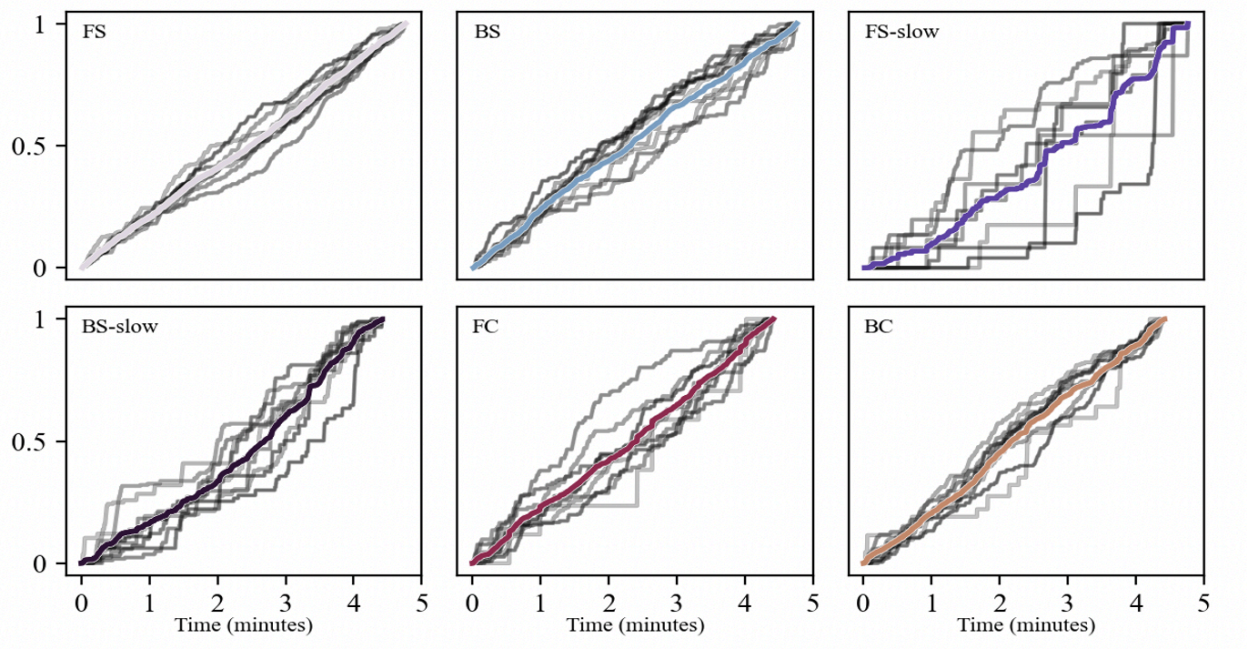

Supplemental Figure 3.1 Cumulative sum of each syllable over the 5-minute trial in control-1 is consistent over time.

3.8.1 Ethogram and Statistics

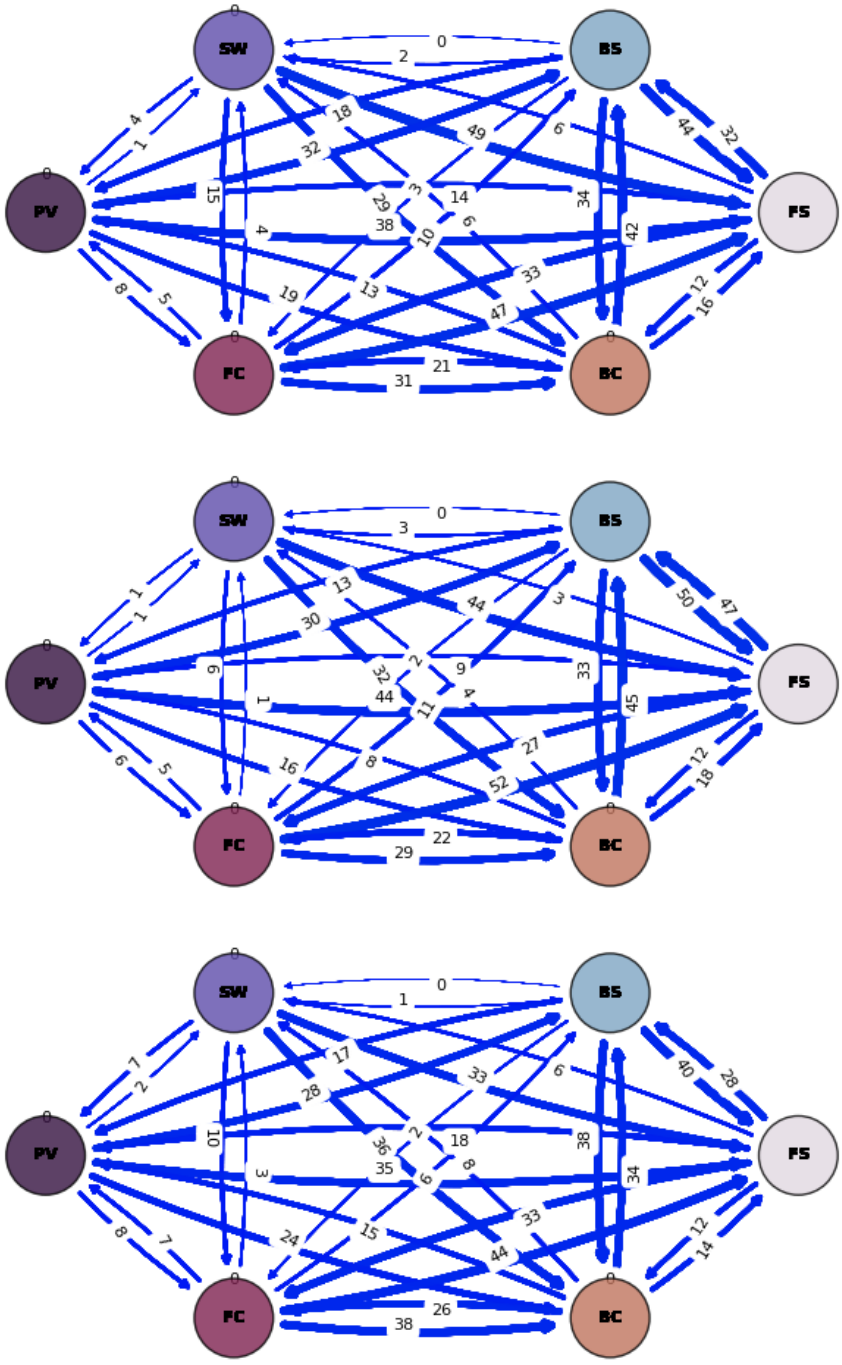

Supplemental Figure 3.2 Full version of ethograms in Figure 3 including all transition probabilities.

3.8.1.1 Control-1 Transition Matrix Statistics

{'start_state': 'FS', 'end_state': 'FS', 'probability': 0.0, 'pvalue': 0.0}

{'start_state': 'FS', 'end_state': 'BS', 'probability': 0.325526130333935, 'pvalue': 0.8853999999998579}

{'start_state': 'FS', 'end_state': 'SW', 'probability': 0.06583465487211841, 'pvalue': 0.8224444444444393}

{'start_state': 'FS', 'end_state': 'PV', 'probability': 0.1413767275118789, 'pvalue': 0.7099333333333129}

{'start_state': 'FS', 'end_state': 'FC', 'probability': 0.3381709724881202, 'pvalue': 1.1468603844377867e-13}

{'start_state': 'FS', 'end_state': 'BC', 'probability': 0.12909151479394737, 'pvalue': 0.11498888888889858}

{'start_state': 'BS', 'end_state': 'FS', 'probability': 0.4417297517966474, 'pvalue': 7.77777779942257e-05}

{'start_state': 'BS', 'end_state': 'BS', 'probability': 0.0, 'pvalue': 0.0}

{'start_state': 'BS', 'end_state': 'SW', 'probability': 0.002272394901735795, 'pvalue': 0.04248888888888888}

{'start_state': 'BS', 'end_state': 'PV', 'probability': 0.18546379184441786, 'pvalue': 0.0470444444445175}

{'start_state': 'BS', 'end_state': 'FC', 'probability': 0.03037121422003363, 'pvalue': 0.10025555555555953}

{'start_state': 'BS', 'end_state': 'BC', 'probability': 0.3401628472371653, 'pvalue': 0.0009555555556406414}

{'start_state': 'SW', 'end_state': 'FS', 'probability': 0.49537217718377136, 'pvalue': 0.9467444444443065}

{'start_state': 'SW', 'end_state': 'BS', 'probability': 0.02244668911335578, 'pvalue': 0.041199999999999994}

{'start_state': 'SW', 'end_state': 'SW', 'probability': 0.0, 'pvalue': 0.5519666666666667}

{'start_state': 'SW', 'end_state': 'PV', 'probability': 0.04023240631936284, 'pvalue': 0.2279999999999969}

{'start_state': 'SW', 'end_state': 'FC', 'probability': 0.15096556701629166, 'pvalue': 0.5203666666666101}

{'start_state': 'SW', 'end_state': 'BC', 'probability': 0.29098316036721833, 'pvalue': 0.8214111111110037}

{'start_state': 'PV', 'end_state': 'FS', 'probability': 0.3849522225014344, 'pvalue': 0.9418999999998978}

{'start_state': 'PV', 'end_state': 'BS', 'probability': 0.3250099929547596, 'pvalue': 0.8601666666665087}

{'start_state': 'PV', 'end_state': 'SW', 'probability': 0.016306389815844768, 'pvalue': 0.31318888888889285}

{'start_state': 'PV', 'end_state': 'PV', 'probability': 0.0, 'pvalue': 0.017222222222222222}

{'start_state': 'PV', 'end_state': 'FC', 'probability': 0.08035241319476986, 'pvalue': 0.141444444444444}

{'start_state': 'PV', 'end_state': 'BC', 'probability': 0.1933789815331914, 'pvalue': 0.43706666666652333}

{'start_state': 'FC', 'end_state': 'FS', 'probability': 0.47374695823131674, 'pvalue': 0.01642222222235279}

{'start_state': 'FC', 'end_state': 'BS', 'probability': 0.10143144441936638, 'pvalue': 0.04328888888888848}

{'start_state': 'FC', 'end_state': 'SW', 'probability': 0.045524209056210505, 'pvalue': 0.6623666666666658}

{'start_state': 'FC', 'end_state': 'PV', 'probability': 0.059505534615868855, 'pvalue': 0.10242222222222049}

{'start_state': 'FC', 'end_state': 'FC', 'probability': 0.0, 'pvalue': 0.08832222222222222}

{'start_state': 'FC', 'end_state': 'BC', 'probability': 0.3197918536772375, 'pvalue': 0.007533333333307413}

{'start_state': 'BC', 'end_state': 'FS', 'probability': 0.16261742005798377, 'pvalue': 0.008922222222219483}

{'start_state': 'BC', 'end_state': 'BS', 'probability': 0.4211675483242385, 'pvalue': 0.04964444444467331}

{'start_state': 'BC', 'end_state': 'SW', 'probability': 0.06406008930461726, 'pvalue': 0.824033333333281}

{'start_state': 'BC', 'end_state': 'PV', 'probability': 0.13848895819729876, 'pvalue': 0.7103111111110941}

{'start_state': 'BC', 'end_state': 'FC', 'probability': 0.21366598411586168, 'pvalue': 0.8431111111110936}

{'start_state': 'BC', 'end_state': 'BC', 'probability': 0.0, 'pvalue': 0.01658888888888889}

3.8.1.2 Novel Transition Matrix Statistics

{'start_state': 'FS', 'end_state': 'FS', 'probability': 0.0, 'pvalue': 0.0}

{'start_state': 'FS', 'end_state': 'BS', 'probability': 0.4718768296360997, 'pvalue': 0.0014555555557315136}

{'start_state': 'FS', 'end_state': 'SW', 'probability': 0.03715476763116156, 'pvalue': 0.6103222222222316}

{'start_state': 'FS', 'end_state': 'PV', 'probability': 0.09279082114098723, 'pvalue': 0.27417777777776825}

{'start_state': 'FS', 'end_state': 'FC', 'probability': 0.2754667474203247, 'pvalue': 0.008111111111227975}

{'start_state': 'FS', 'end_state': 'BC', 'probability': 0.1227108341714268, 'pvalue': 0.11332222222223023}

{'start_state': 'BS', 'end_state': 'FS', 'probability': 0.501047932494542, 'pvalue': 2.1660451210436804e-13}

{'start_state': 'BS', 'end_state': 'BS', 'probability': 0.0, 'pvalue': 0.0}

{'start_state': 'BS', 'end_state': 'SW', 'probability': 0.004523744297259654, 'pvalue': 0.04248888888888888}

{'start_state': 'BS', 'end_state': 'PV', 'probability': 0.13367114602963848, 'pvalue': 0.6199111111110686}

{'start_state': 'BS', 'end_state': 'FC', 'probability': 0.02648538211897491, 'pvalue': 0.08368888888889217}

{'start_state': 'BS', 'end_state': 'BC', 'probability': 0.3342717950595849, 'pvalue': 0.0012777777778633093}

{'start_state': 'SW', 'end_state': 'FS', 'probability': 0.44091440825720746, 'pvalue': 0.9081333333330304}

{'start_state': 'SW', 'end_state': 'BS', 'probability': 0.035591206179441476, 'pvalue': 0.04375555555555566}

{'start_state': 'SW', 'end_state': 'SW', 'probability': 0.0, 'pvalue': 0.5519666666666667}

{'start_state': 'SW', 'end_state': 'PV', 'probability': 0.018685844243653573, 'pvalue': 0.2147888888888889}

{'start_state': 'SW', 'end_state': 'FC', 'probability': 0.06721713415425384, 'pvalue': 0.20427777777774506}

{'start_state': 'SW', 'end_state': 'BC', 'probability': 0.32648029605433254, 'pvalue': 0.876755555555415}

{'start_state': 'PV', 'end_state': 'FS', 'probability': 0.4427464058223761, 'pvalue': 0.009133333333417482}

{'start_state': 'PV', 'end_state': 'BS', 'probability': 0.30778307399417476, 'pvalue': 0.8286888888887084}

{'start_state': 'PV', 'end_state': 'SW', 'probability': 0.014375633388073109, 'pvalue': 0.31318888888889285}

{'start_state': 'PV', 'end_state': 'PV', 'probability': 0.0, 'pvalue': 0.017222222222222222}

{'start_state': 'PV', 'end_state': 'FC', 'probability': 0.06840937970078811, 'pvalue': 0.13304444444444602}

{'start_state': 'PV', 'end_state': 'BC', 'probability': 0.16668550709458782, 'pvalue': 0.2777444444444097}

{'start_state': 'FC', 'end_state': 'FS', 'probability': 0.5218103528668634, 'pvalue': 0.015988888889021946}

{'start_state': 'FC', 'end_state': 'BS', 'probability': 0.1179072319983647, 'pvalue': 0.0773555555555655}

{'start_state': 'FC', 'end_state': 'SW', 'probability': 0.010249751667376189, 'pvalue': 0.22604444444444222}

{'start_state': 'FC', 'end_state': 'PV', 'probability': 0.05320366720027811, 'pvalue': 0.10033333333333092}

{'start_state': 'FC', 'end_state': 'FC', 'probability': 0.0, 'pvalue': 0.08832222222222222}

{'start_state': 'FC', 'end_state': 'BC', 'probability': 0.29682899626711756, 'pvalue': 0.022211111111072546}

{'start_state': 'BC', 'end_state': 'FS', 'probability': 0.18510194038300995, 'pvalue': 0.0344222222220773}

{'start_state': 'BC', 'end_state': 'BS', 'probability': 0.4534149645507743, 'pvalue': 0.03358888888912881}

{'start_state': 'BC', 'end_state': 'SW', 'probability': 0.0465460427465849, 'pvalue': 0.6892111111110755}

{'start_state': 'BC', 'end_state': 'PV', 'probability': 0.08954800495881152, 'pvalue': 0.2775777777777378}

{'start_state': 'BC', 'end_state': 'FC', 'probability': 0.2253890473608194, 'pvalue': 0.891533333333311}

{'start_state': 'BC', 'end_state': 'BC', 'probability': 0.0, 'pvalue': 0.01658888888888889}

3.8.1.3 Control-2 Transition Matrix Statistics

{'start_state': 'FS', 'end_state': 'FS', 'probability': 0.0, 'pvalue': 0.0}

{'start_state': 'FS', 'end_state': 'BS', 'probability': 0.28140080246873184, 'pvalue': 0.8345999999998971}

{'start_state': 'FS', 'end_state': 'SW', 'probability': 0.06496323813802528, 'pvalue': 0.8224444444444393}

{'start_state': 'FS', 'end_state': 'PV', 'probability': 0.18687221096787404, 'pvalue': 0.023399999999993426}

{'start_state': 'FS', 'end_state': 'FC', 'probability': 0.339076643728996, 'pvalue': 1.1468603844377867e-13}

{'start_state': 'FS', 'end_state': 'BC', 'probability': 0.1276871046963729, 'pvalue': 0.11403333333334148}

{'start_state': 'BS', 'end_state': 'FS', 'probability': 0.40954670354773676, 'pvalue': 0.0016222222224391292}

{'start_state': 'BS', 'end_state': 'BS', 'probability': 0.0, 'pvalue': 0.0}

{'start_state': 'BS', 'end_state': 'SW', 'probability': 0.000925925925925926, 'pvalue': 0.04248888888888888}

{'start_state': 'BS', 'end_state': 'PV', 'probability': 0.17981806699972394, 'pvalue': 0.9333999999999119}

{'start_state': 'BS', 'end_state': 'FC', 'probability': 0.027682559466281884, 'pvalue': 0.08368888888889217}

{'start_state': 'BS', 'end_state': 'BC', 'probability': 0.3820267440603315, 'pvalue': 3.333333341903888e-05}

{'start_state': 'SW', 'end_state': 'FS', 'probability': 0.3331772176784511, 'pvalue': 0.7155666666665119}

{'start_state': 'SW', 'end_state': 'BS', 'probability': 0.01064814814814814, 'pvalue': 0.04118888888888888}

{'start_state': 'SW', 'end_state': 'SW', 'probability': 0.0, 'pvalue': 0.5519666666666667}

{'start_state': 'SW', 'end_state': 'PV', 'probability': 0.07677029646271089, 'pvalue': 0.30531111111106035}

{'start_state': 'SW', 'end_state': 'FC', 'probability': 0.10396662245259222, 'pvalue': 0.2972222222221915}

{'start_state': 'SW', 'end_state': 'BC', 'probability': 0.36432660414698653, 'pvalue': 0.9458999999998007}

{'start_state': 'PV', 'end_state': 'FS', 'probability': 0.3500386224736704, 'pvalue': 0.8751333333331629}

{'start_state': 'PV', 'end_state': 'BS', 'probability': 0.28625767129638874, 'pvalue': 0.7980555555553878}

{'start_state': 'PV', 'end_state': 'SW', 'probability': 0.025425422113745086, 'pvalue': 0.4164444444444384}

{'start_state': 'PV', 'end_state': 'PV', 'probability': 0.0, 'pvalue': 0.017222222222222222}

{'start_state': 'PV', 'end_state': 'FC', 'probability': 0.08878434417994198, 'pvalue': 0.17546666666667732}

{'start_state': 'PV', 'end_state': 'BC', 'probability': 0.2494939399362538, 'pvalue': 0.7946666666664605}

{'start_state': 'FC', 'end_state': 'FS', 'probability': 0.44387350786048013, 'pvalue': 0.03697777777800049}

{'start_state': 'FC', 'end_state': 'BS', 'probability': 0.06368033716635164, 'pvalue': 0.004322222222221876}

{'start_state': 'FC', 'end_state': 'SW', 'probability': 0.03309519205869336, 'pvalue': 0.5402666666666643}

{'start_state': 'FC', 'end_state': 'PV', 'probability': 0.07580539718627922, 'pvalue': 0.19281111111110752}

{'start_state': 'FC', 'end_state': 'FC', 'probability': 0.0, 'pvalue': 0.08832222222222222}

{'start_state': 'FC', 'end_state': 'BC', 'probability': 0.38354556572819565, 'pvalue': 0.00011111111109152194}

{'start_state': 'BC', 'end_state': 'FS', 'probability': 0.14624643191421005, 'pvalue': 0.0027111111111117773}

{'start_state': 'BC', 'end_state': 'BS', 'probability': 0.3457786041568207, 'pvalue': 0.9157888888886921}

{'start_state': 'BC', 'end_state': 'SW', 'probability': 0.08650235635989284, 'pvalue': 0.8815666666666151}

{'start_state': 'BC', 'end_state': 'PV', 'probability': 0.15325920531501971, 'pvalue': 0.8076111111110846}

{'start_state': 'BC', 'end_state': 'FC', 'probability': 0.2682134022540567, 'pvalue': 0.02023333333336219}

{'start_state': 'BC', 'end_state': 'BC', 'probability': 0.0, 'pvalue': 0.01658888888888889}

Chapter 4: Unsupervised characterization of behavioural syllables during object exploration

4.1 Introduction

The tendency for object exploration is largely based upon familiarity where animals are observed to decrease exploration with increased habituation (Heyser & Chemero, 2012). On a general level this holds true, however the motivation and execution of object investigation induces behaviours that derive from several factors. These may include the internal state driven by individual personality or context and history. Therefore, the perception and subsequent behavioural output are a result of the internal process. This means that across and even within individuals the same behaviours may serve different functions and conversely, different behaviours may serve a single function (Noer et al., 2015). These are the principles that make behavioural identification in weakly electric fish especially challenging given their coupled electrosensory and motor systems. These fish are well recognized for their complex swimming abilities. Being anguilliform fish they have significantly more

locomotor-control for finer-tuned swimming movements compared to most fish of other body-types (Blake, 1983; Ruiz-Torres et al., 2013; Upshall, 2024). Embedded in their skin are electroreceptors that detect perturbations within their short range (1-2 body lengths) self-generated electric field. Given this sensory-motor pairing, many have studied how these fish adjust their body-shape in response to environmental factors to separate possible behaviours involved in electrosensation from ordinary locomotion (Snyder et al., 2007). In the present study, we take advantage of the inherent tendency to explore objects and subject the fish to an environment with simple, stationary objects, compared to a more complex and temporally varying environment. By changing the environmental context, we aim to elicit a change in behaviour. We repeat the exposure to the same environments to increase habituation and statistically address behaviours previously hypothesized to improve electrosensation which we expect would be more prevalent when the environment is most unfamiliar.

Previous studies demonstrate that weakly electric fish indeed have the necessary information to discriminate between objects with different properties. For example, they can distinguish objects of different sizes, shapes, and materials (Benda, 2020; Lewis, 2014; Upshall, 2024; von der Emde, 1990, 1999). Theoretical and electrophysiological evidence further show that they can gather more sensory information with deliberate body movements, also called active sensing movements (Babineau et al., 2006; Engelmann et al., 2021b; Sim & Kim, 2011).

Though we expect others exist, scanning, tail-bending, and probing stand out as likely active sensing candidates (Assad, 1997; Caputi, 2017; Heiligenberg, 1975; Hofmann et

al., 2014a; Jung & Engelmann, 2019). Here we refer to scanning as quick back-and-forth swimming with a straight body-pose and tail-bending is the lateral sweeping back-and-forth of the tail. Probing we define as the fish using its nose to poke at objects which we often call nose-probing, similar to behaviours observed in convergently related species (Hofmann et al., 2014a).

To date, our understanding of the potential role of active sensing is limited to simple objects and environments. Aside from studies specific to prey-capture (Nelson & Maciver, 1999a) and refuge tracking (Biswas et al., 2018; Pedraja et al., 2020; Stamper et al., 2012; Uyanik et al., 2020), we know little of the fish's behaviour in general exploration and novel environments.

We are interested in elaborating on our previous findings of scanning and whether its output increases in contexts other than those with a non-moving novel object. We postulated that increasing environmental diversity by adding temporal variation and observing the fish over longer periods of time would allow more opportunities to observe tail-bending, scanning, and probing. We further aimed to assess their possible contextual dependence suggesting either an electrosensory role or otherwise locomotory byproduct.

Our results suggest increased scanning to be specific to the introduction of a novelty producing spatially focused exploration and possibly involved in risk assessment. We found that tail-bending-like behaviours (C-bending) and nose-probing increase as the fish habituates and with a higher specificity for temporally complex environments. Our evidence supports the possibility of increased sensory acquisition

using active sensing behaviours and provides further insight to their contextual roles which we show are more time-dependent than stimulus-dependent.

4.2 Methods

4.2.1 Animals

Apteronotus albifrons were ordered from Big Al's (Ottawa, ON). Fish were housed individually in 5L tanks with a 12h:12h light:dark cycle. Tank water was maintained at a temperature of ~26-28ºC and at a conductivity of ~160-220 µS. Fish were fed bloodworms three times weekly. All experimental protocols were approved by the Animal Care Committee of the University of Ottawa (Protocol BLe-3678).

4.2.2 Experimental Design

Fish were acclimated to the experimental refuge (14 cm x 35.5 cm x 5.5 cm) within a heated tank (26-28 ºC depending on their home tank) with bubbled O_2 for 12-24 hours. Embedded in both longitudinal walls of the refuge were three cylindrical resistors (0.5 cm radius) spaced 3.5 cm apart (see Figure 4.1). During the acclimation period the carbon (non-polarizing) resistors were left in open circuit to mimic three circular and opaque windows on both walls. See Chapter 3 for details.

The resistors were controlled with a custom software used to modify the resistance and create different environmental electrosensory scenes. In the static environment the resistors were set to 75 kΩ (low-contrast relative to plexiglass) and

were held temporally constant. This was our simplest environment and can be thought of as making the windows less opaque compared to the acclimated baseline. Each fish experienced this environment first to minimize any potential startle effect. Test trials suggested that in many cases, the introduction of higher contrast stimuli without gradually ramping the intensity would cause panic (defecation and high velocity swimming).

We used two different temporally varying environments. Both used the same background where we gradually ramped over 5-seconds to a moderate contrast with an average amplitude of 25 k$\Omega \pm$ 10 kΩ. The resistors were temporally varied at frequencies ranging from 0.1-1Hz with three resistors on one wall synchronized and in anti-phase to the resistors on the opposite wall. This was designed to simulate natural plant-like swaying movements. To one of the temporally varying environments, we added an additional transient looming stimulus (contrast amplitude 7.5 k$\Omega \pm$ 2.5 kΩ; frequency variation 2-5 Hz for 3-seconds) with a 1-second ramp on either side to avoid abrupt changes. These stimuli totalled 25% of the total trial duration. Likely due to the frequency of events we found both temporally varying environments to be statistically indistinguishable and we consequently analyzed the two separately but categorized them as the same temporal condition.

Using a group of 18 fish each fish experienced each trial for 5-minutes broken up by 5-minute breaks. Round 1: 1) Static environment; break; 2) Temporal environment; break; 3) Temporal environment + stimulus; break; 4) Static environment. This was then

repeated after a 1–2-hour rest. Round 2: 1) Static environment; break; 2) Temporal environment + stimulus; break; 3) Temporal environment; break; 4) Static environment. 9 fish experience Round 1 followed by Round 2 while the remaining 9 experience Round 2 followed by Round 1. The breaks occurred with the fish in the static environment.

Fish were filmed top-down at 30 fps to obtain video used to extract positional data. For detailed data acquisition see Chapter 3.

4.2.3 Analysis

Positional data were acquired using DeepLabCut (Mathis et al., 2018) which labelled 6 points down the midline of the fish (see Chapter 3 for model result details). We preprocessed the data by interpolating labels where the likelihood was below 90%. All data were smoothed with a gaussian moving average (length=11, width=2). The data were then analyzed using a custom modelling pipeline (https://github.com/maryupshall/pyUCAB; described in detail in Chapter 3) to quantitatively acquire the behavioural syllables. As in our previous work, 4 of the 10 resulting syllables were combined to merge left and right components of the same type, resulting in 6 behaviour syllables total. This merge was used to simplify the results by reducing the overall number of syllables for subsequent statistical analysis.

Quantitative analysis of syllable bouts was performed in Python using the scikit-learn module as well as custom code to compute kinematic and statistical results.

Linear mixed models (see equation 1) were done in R using $lmer()$ (lme4 package) fit by restricted maximum likelihood (REML). The resulting statistics were output using *summary()* (lmerTest package; Kuznetsova et al., 2017) which used the Satterthwaite's method t-test to generate t-values and p-values. We also used *anova()* to repeat the statistics to compute the F-value and confirm the p-values.

$$model <- lmer(y \sim time + condition\ (time|individual) \qquad (1)$$

Equation (1) where y = total distance travelled, total area covered, and time spent near the resistors, for a total of 3 LMMs. Further summary statistics and graphs are provided in the Supplementary section. The syntax above uses $<-$ which assigns the righthand function to the $model$ object. The dependent variable y is calculated using $time$ and $condition$ as fixed effects. The variable $individual$ is the random effect with which $time$ is allowed to vary with the slope and the intercept (not shown) is allowed to vary randomly as indicated by the vertical bar in $(time|individual)$. The $\sim$ is used to set the righthand equation to y and this entire function $y \sim time + condition\ (time|individual)$ is passed to the $lmer$ () function.

4.3 Results

In the present study, we use broad statistical measures characterizing exploration and body-shape to describe the fish's behaviour in different environments. As is commonly done in novelty tests, we used locomotor and proximity measures as indications of exploration to evaluate the fish's overall interest in the objects (dos Santos

et al., 2023; Martins et al., 2012). We assumed exploration (willingness to engage) would increase with novelty (Martins et al., 2012). As in previous work (Angiulli et al., 2020) we used total distance travelled, percentage of area covered, and time-spent near the electrosensory objects as our global exploratory metrics. For the body-shape metrics, we used behavioural identification techniques to identify 6 components or "syllables" of behaviour, capturing quantitative data to explore behavioural statistics more closely. These syllables included two syllables describing straight body-pose swimming in the forward (FS) and backward (BS) direction. Bent-shaped body-poses were also directionally separated which we call the forward C-shaped bend (FC) and the backward C-shaped bend (BC). The last two syllables described movements of smaller displacement which were the stationary wiggle (SW) and the pivot (PV) syllables. In combining classic behavioural measures with behavioural identification techniques, we describe how the fish behaves over time and across conditions of increased spatiotemporal complexity.

4.3.1 Global and Body-Shape Statistics Vary in First Exposures to Different Environments

Post-acclimation we exposed the fish to two types of environments. The first was the "static" environment where we simulated simple, non-moving objects. Still, we assumed the objects in this environment would be perceived as most novel given no prior exposure. The second, "temporally dynamic" environment, we simulated the objects to move in a pseudorandom, slow (0.1-1Hz) manner. We assumed the addition of object motion would also be perceived as a novelty. With trial repetition we expected

habituation to both environmental contexts. See Figure 4.1A and the methods section for more detail.

In Figure 4.1 we focus on the first time the fish was introduced to the static environment compared to the first time the fish was introduced to the temporally dynamic environment. In the static environment we found that the fish travelled a farther total distance yet covered less area compared to the temporally dynamic environment (see Figure 4.1B). We had originally thought that increased travel would inherently result in increased area coverage. We then posited that to cover less area with more translational movement the behaviour of the fish must be spatially repetitive. Alternatively, to cover more area with less distance travelled the fish would need to position its body to increase spatial coverage.

In either case, the change in global metrics from the static to the temporally dynamic environment indicated that the fish changed their exploratory strategy. To begin to resolve these questions we next looked at the level of the behavioural syllables.

Continuing with the first exposure to each environment we assessed the frequency counts of each syllable. The fish in the static environment exhibited increased forward and backward swimming and decreased the remaining 4 syllables (see Figure 4.2). These were consistent with previous findings where higher frequency counts of FS and BS indicated increased scanning (see Chapter 3). Increased scanning would also coincide with spatial repetitiveness.

In the temporally dynamic environment, fish increased PV and FC counts. Increased C-shaped swimming or tail-bending would allow the fish to sweep over more area with less translational movement.

We next investigated if the response was due to the environmental conditions or a non-specific effect of the ordering of the exposures. Therefore, we introduced the conditions in alternation and observed their behaviour over time. We also include where the fish spent the most time and assess a possible spatial preference relative to the resistors.

4.3.2 Both Time and Environmental Condition Shape Fish Behaviour

We found the first static and first temporally dynamic trials mentioned above to exhibit the largest difference between consecutive trials (see Figure 4.3A). We used a linear mixed model (LMM) to assess the influence of the experimental factors (time, environmental condition, and individual; see Methods for model details). The repetition unveiled a strong influence of time (F-value=34.53, p-value=1.57e-5) resulting in decreased total distance travelled of the fish (see Figure 4.3). Overall, the time effect was stronger than the effect of the environmental condition, though condition still played a role (F-value=7.00, p-value=0.01).

When looking at the fraction of area covered our LMM showed slight evidence of environmental condition involvement (F-value=7.04, p-value=0.01; see Figure 4.3B). However, the extent of this effect is likely stunted given the relatively small refuge

resulting in most fish covering >70%. Nonetheless, the data showed that area coverage was not positively correlated to distance travelled. Instead, we found a slight negative correlation for all trials across time for distance and area ($R<-0.62$, $p\text{-value}<0.001$).

We investigated the time spent near the resistors and confirmed a spatial preference (Figure 4.3C) for the resistor half of the tank that faded with time ($p\text{-value}=0.01$) and was more associated with the static environment ($p\text{-value}=0.02$).

These results suggested that the fish were switching from a resistor-focused exploration to a general exploration state as novelty wore off with time. To further understand the movements involved in this shift we again looked at the syllables.

We observed that time influenced all syllables except for BC (see Figure 4.4C). BS decreased with time while PV increased with time, and both showed evidence of a condition effect (see Figure 4.4A & B). PV was often associated with the refuge perimeter (walls, doors, and resistors). In this context the fish would decrease displacement leading with its snout near the wall (see Supplemental Figure 4.1) and do what we termed a nose-probing behaviour.

FC and FS were unaffected by condition but showed a slight increase and decrease, respectively, over time (not shown). Lastly, SW exhibited frequencies less than 5% and while we recognize that they possibly serve a more specific purpose, we excluded them for the purposes of this manuscript.

4.3.3 Syllable Count Correlations Show Increased Bending in TD Conditions

Overall, the change in the syllables described less straight swimming (FS, BS), more nose-poking (PV), and possibly more bending over time (FC, BC). We had assumed that an increase in bending with the fish laterally sweeping its tail, could further account for increased area coverage with less distance travelled. If this is correct, then we should see increased C-bending (FC and BC) over time and decreased straight swimming (FS and BS). Additionally, if the fish increased bending overall, then we would expect a positive correlation between forward and backward C-shaped swimming.

To test this, we considered the correlative nature of the dataset. As with most behavioural data the complexity and possible interacting variables requires caution. The mutual exclusivity of each syllable meant that the syllables were at least in some way influenced by each other since the fish cannot perform two syllables at once. We address the relationships between these states shown in Figure 4.5A (see Correlation Matrices Over Time).

To investigate the possible role of C-shaped syllables in the observed increased area coverage we focused on the correlation between the forward and backward component of C-shaped swimming. The FC-BC R-value associated with Figure 4.5A, showed the pair to have the largest correlation difference amongst the syllable pairs between environmental conditions. Using a new LMM we modelled the effects of time,

environmental condition, and C-shaped behaviours (FC and BC) on area coverage. We found both FC frequency count (p= 0.034) and environmental condition (p= 0.016) had a small impact on the percentage of area covered.

We further compared the count frequency of forward C-shaped swimming to backward C-shaped swimming (see Figure 4.5B). Given the time effect we first addressed each trial separately and fit a linear regression model to each FC-BC comparison. Within each trial we evaluated the R-value and found mixed results over time (see FC-BC Linear Regression by trial). However, we looked at round 2 alone and found that both static trial-1 (R=-0.29; p=0.25) and static trial-4 (R=-0.20, p=0.44) had no linear relationship, whereas both temporally dynamic trials (trial 2 and 3) had a positively correlated FC-BC relationship (R=0.63, p=0.005; R=0.52, p=0.028). Having addressed the individual trial statistics, we then looked at the condition effect across all trials. Again, we found no linear FC-BC correlation for fish in the static condition (R=0.15, p=0.21), but found a moderate positive relationship for fish in temporally dynamic conditions (R=0.45, p=8.9e-5).

4.4 Discussion

Separating active sensing from ordinary locomotion has been a challenge in weakly electric fish research. Our paradigm set to invoke different behavioural states using different spatiotemporal sensory scenes which we could observe over time. Our global findings indicated that the fish travelled a farther distance but covered less area in the static environment compared to the temporal environment. Though we also found

a strong time effect, we saw evidence of two strategies. The first was increased spatial repetitiveness via scanning near the resistors during the first introduction to the static environment. The second was increased C-shaped bending to induce the opposite effect, by increasing area coverage over distance travelled. The latter was also accompanied with increased nose-probing.

Trial repetition allowed us to observe the evolution of the fish's behaviour as familiarity increased. Recent work assessing the cost-benefit of energy production for increased retrieval of sensory information suggests that animals adjust their expenditure according to signal strength or noise. Similarly, boldness studies also show adjustment based on risk-assessment (Magnhagen et al., 2012). The former comparative study provides evidence supporting increased relative exploration or energy expenditure as the sensory signal is weakened or includes high levels of uncertainty (Chen et al., 2020). In our experimental design, the highest level of uncertainty arises when we first introduce the static stimulus. We assume this to be due to the use of virtual objects whereby the fish receives no prior indications that their environment will change. Compared to introducing a true object which would include water displacement (mechanical information), possible olfactory and acoustic signals. As such, though the change was small, we expected it to elicit the largest novelty response. With the introduction of unexpected novelty, we also assume the highest levels of uncertainty from the perspective of the fish. Therefore, we propose that increased backward swimming resulting in scanning behaviours is the beginning phase to this cost-benefit analysis. Given the evidence supporting increased sensory information gain specific to

the backward motion of a scan (Jun et al., 2016) as well as the impressive regenerative capacities of the tail-end of weakly electric fish (Sîrbulescu et al., 2009), we propose that increased scanning would pose the least risk in novelty assessment.

As the fish became more familiar with the new environmental condition we saw increased nose-probing and C-shaped swimming. Probing is largely discussed in the context of a convergently related species of weakly electric fish. These fish use a sensory appendage with increased electrosensitivity located on their snout to probe novel objects (Hofmann et al., 2014a). Though *Apteronotus albifrons* do not possess the chin appendage, they do have a higher density of receptors on the head, especially near the perioral region. This is sometimes referred to as an electrosensory fovea (Caputi, 2017). Perhaps as the fish becomes more familiar with the environment and their perceived risk decreases, they are more willing to investigate via nose-probing behaviours.

We assume C-bending to be similar to tail-bending which has been proposed to provide sensory cues as outlined in previous work (Babineau et al., 2007; Heiligenberg, 1975; Sim & Kim, 2011). However, the sensory signals of environmental objects are miniscule compared to the effects of tail-bending. When the fish bends its tail 20-50 degrees the induced amplitude modulations are 50-150 μV compared to detection levels which can be as low as 0.1-1 μV (Assad, 1997; Nelson & Maciver, 1999a).
Recent work using a convergently related species implanted an electrode into the brain of a freely-swimming fish (Wallach & Sawtell, 2023). Wallach & Sawtell (2023) found

that with environmental information and top-down information from higher brain centres, the fish was able to predict and effectively cancel out the effects of tail-bending. However, this also required a familiarity with their surroundings, therefore cancellation would only be partially effective in novel environments. We propose that as the perceived risk of exploration decreases with increasing familiarity, the fish increases tail-bending which allows for a larger survey of the surrounding area. Perhaps this contributes to spatial learning until full cancellation is achieved.

We found evidence of condition effects due to the spatiotemporal nature of the stimuli indicating a possible role of bending and nose-probing. Though we controlled for the time effect, this would benefit from further investigation. Other possibilities of a relatively small condition effect include that the behavioural information relative to the stimulus condition was not available on the syllable level but instead required further investigation at the transition level or combination of syllables. However, preliminary exploration of first order transitions showed no clear evidence that this was the case (not shown). Additionally, our understanding of the significance of the stimulus inputs is limited to modelled evidence using simulated fish, however we cannot know how the fish will truly perceive them. To confirm the sensory information available to the fish during the performance of the behavioural syllables, further experimental analysis is required. The incoming sensory input requires investigation to support the proposed function of active sensing movements.

Given the complexity of the possible motivations for behaviour production, understanding the effects of time, space, variability, personality, and novelty are all

important precursors. In these simple conditions, our study suggests that active sensing movements evolve over time, with a role of increased bending in temporally varying environments compared to scanning in novel conditions. We also provided a possible context and time-dependence with which probing and bending behaviours emerge, motivating the need for future work investigating sensory input analyses.

4.5 Figures

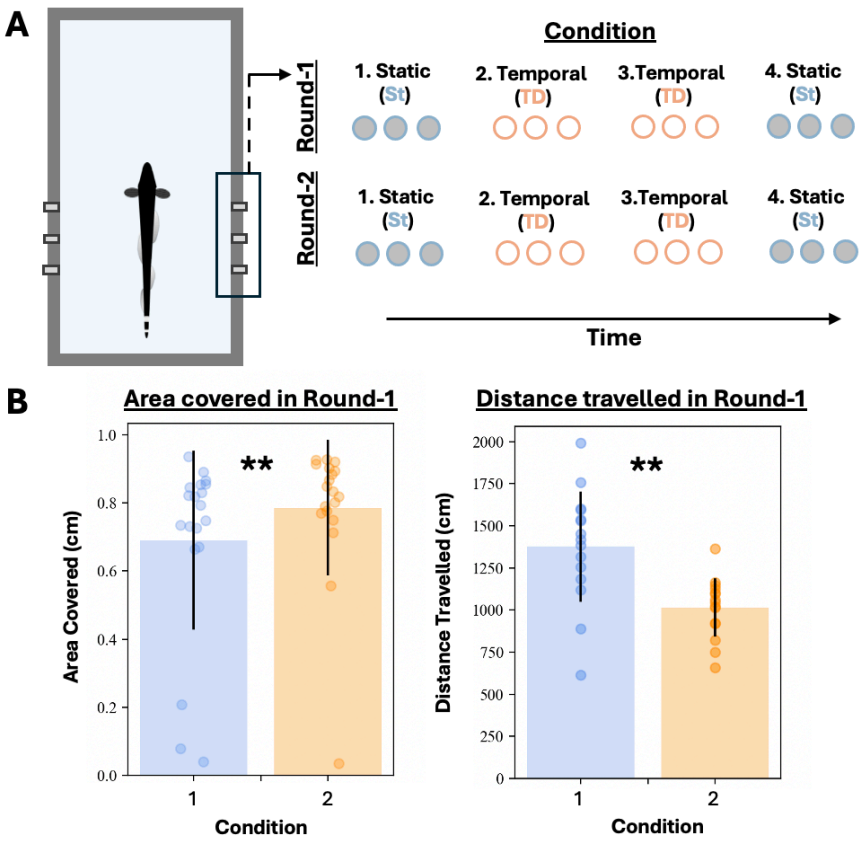

Figure 4.1 Fish cover more area but travel less distance in temporally dynamic vs static environment.

A) Schematic of fish in refuge with resistors represented by small grey rectangles. Experimental sequence depicted on the right. The low contrast, static environmental condition is shown with light grey circles outlined in blue. The high contrast, temporally dynamic (TD) environment is shown with white circles outlined in orange. The sequence 1-4 is repeated (round-2). B) Left: Ratio of total area covered. Blue bar is the average area covered for the static condition fish for trial 1, round 1. Orange bar is the same for the temporally dynamic condition. Right: Total distance travelled (cm) for static (blue) and TD (orange) in the first trial of round 1. Small, coloured circles show raw data points. Black bars show standard deviation. Area covered Wilcoxon statistic = 16.0, Bonferroni corrected p=0.00129; Distance travelled Wilcoxon statistic = 14.0, Bonferroni corrected p=0.00083.

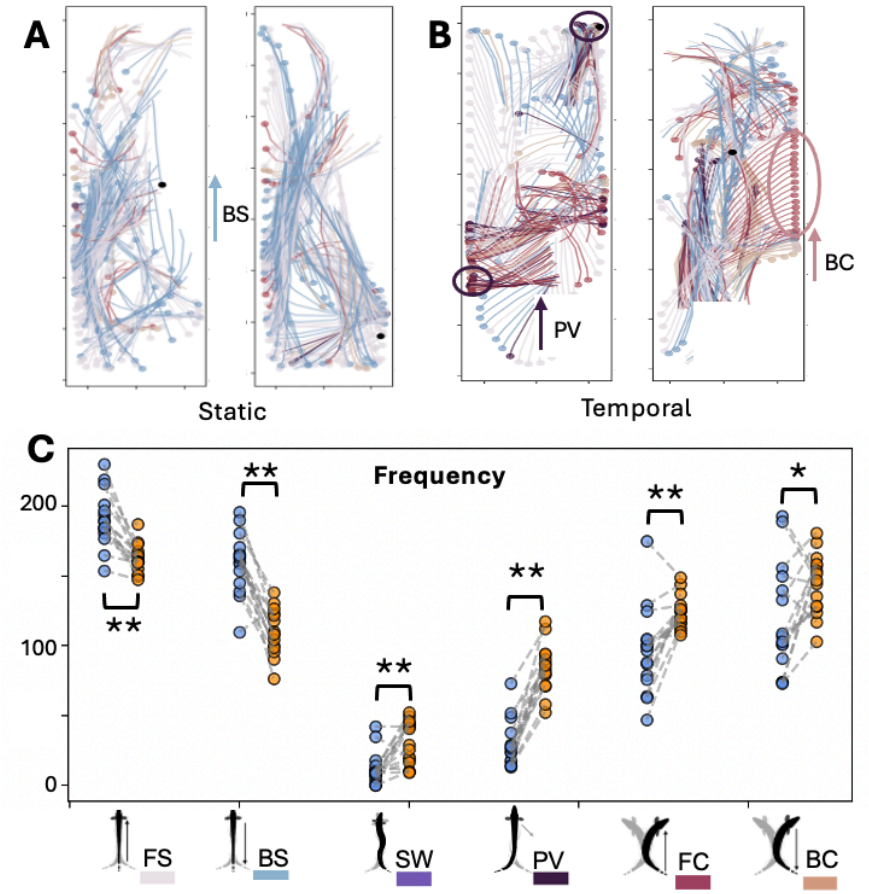

Figure 4.2 Syllable frequencies are different between static and temporally dynamic condition.

*A) Fish line drawing from raw data during static condition example. Colour corresponds to syllable label at that time point (see legend below C). Blue arrow indicating increased BS in static condition. B) Same as A) but for temporally dynamic condition. Left example: circles show PV syllable time points. Right example: Orange circle shows example of BC syllable time points. C) Syllable frequency count for forward straight (FS), backward straight (BS), stationary wiggle (SW), pivot (PV), forward C-shaped (FC), and backward C-shaped (BC). Blue circles show raw data for fish in static condition. Grey dashed line connects within an individual. Orange circles show frequency count during TD condition. Wilcoxon, Bonferonni corrected ** = $p < 0.01$, * = $p<0.05$.*

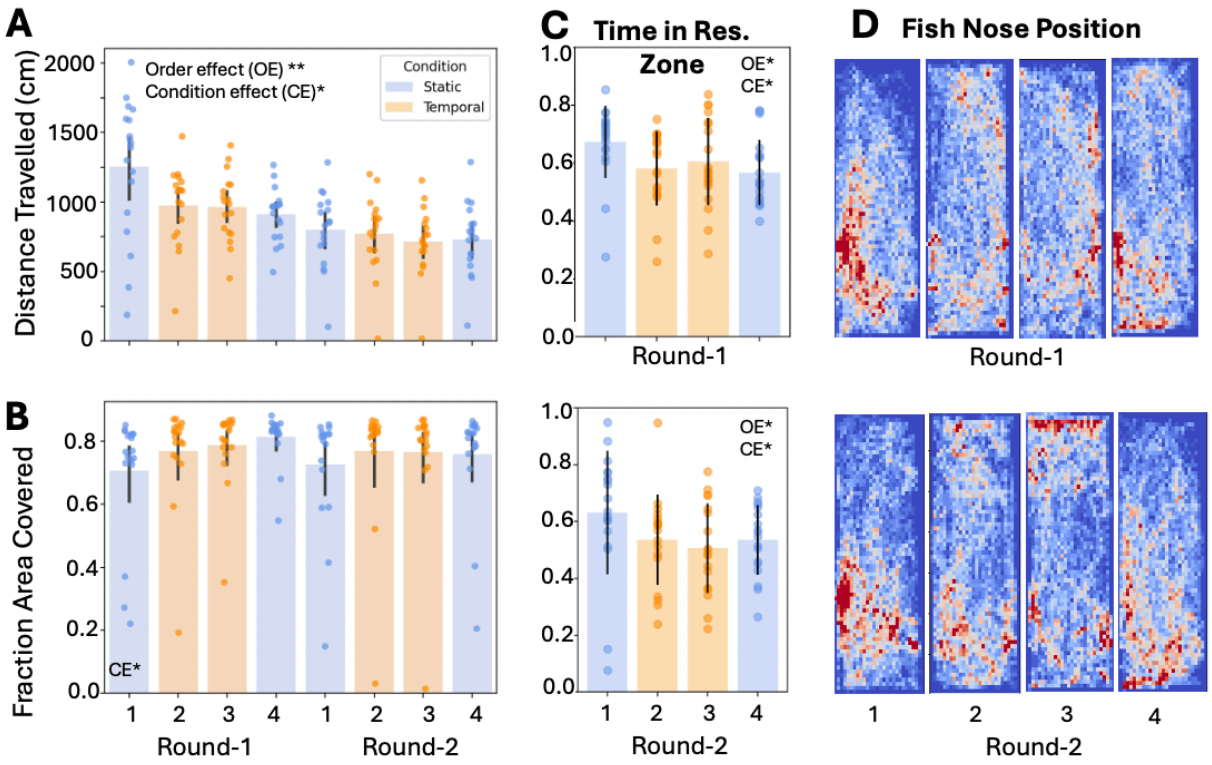

Figure 4.3 Distance travelled and area covered vary across time.

A) Total distance travelled (cm) over time for trials 1-4 in round 1 and 2. Order effect p=1.57x10-5; condition effect p=0.01. B) Fraction of area covered. Condition effect = 0.01. C) Time spent near the resistors (resistor zone). Time effect = 0.01; condition effect = 0.02. D) Position density heat maps of the nose point of 1 example fish for both round 1 (top) and round 2 (bottom). The same individual is presented in all heat maps.

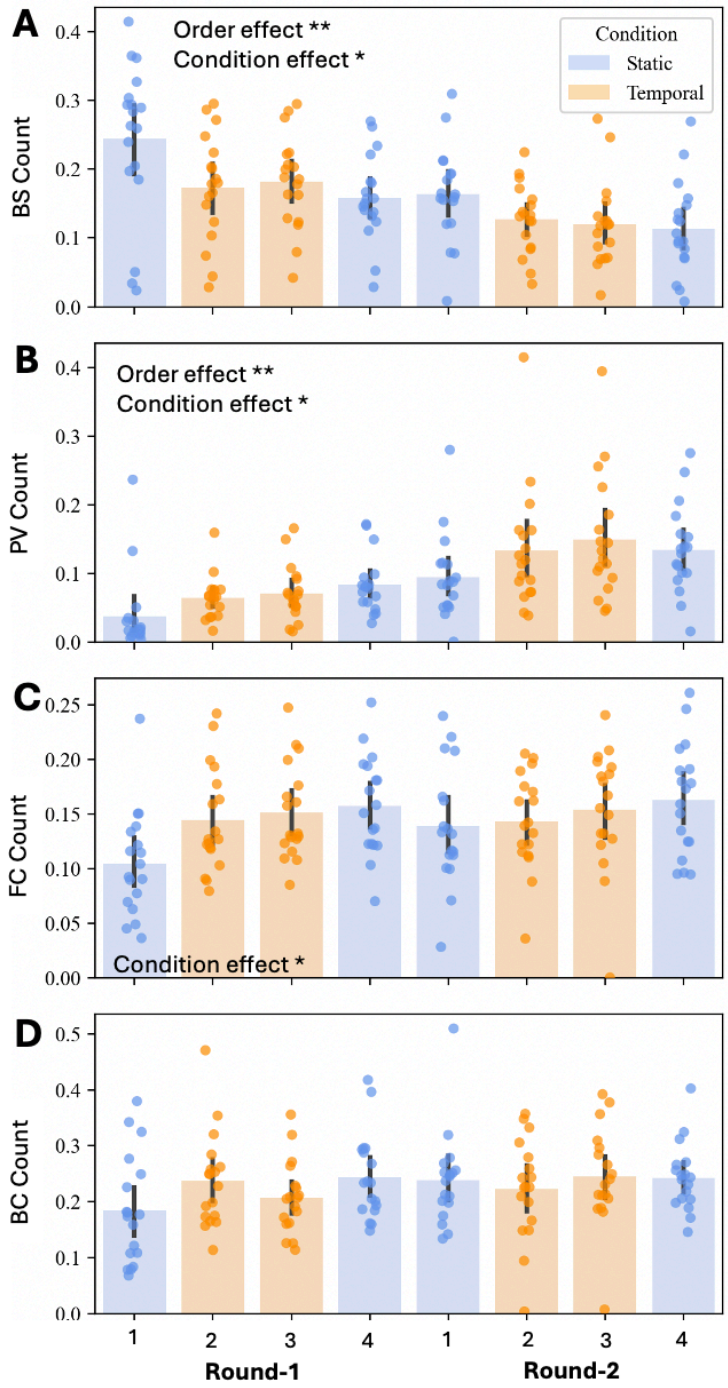

Figure 4.4 Time and condition effect present for BS and PV but not BC.

A) Frequency count of BS (ratio) over time for trials 1-4 in round 1 and 2. Order effect p=1.09x10-5; condition effect p=0.014. B) Same as A) for PV frequency count. Order effect p=4.23x10-6; condition effect p=0.037. C) Same as A) and B) for FC frequency count. Condition effect = 0.0065. D) BC frequency count. No significant order or condition effect. Bars show population average. Circles show raw data. Black bars show standard deviation.

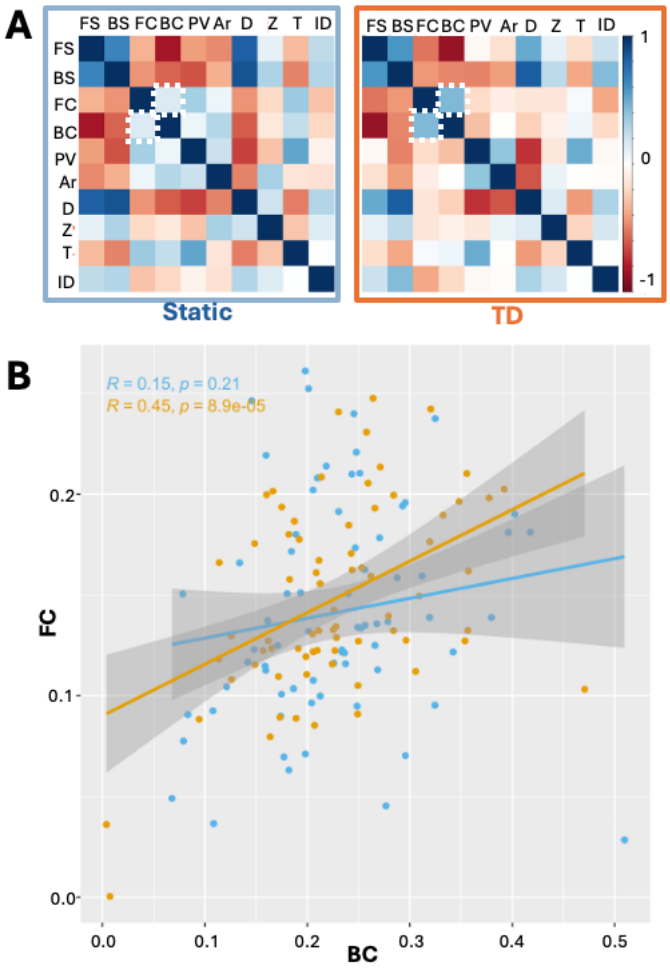

Figure 4.5 Syllable interactions suggest increased bending in TD conditions.

Top: Correlation matrices (R value) for all factors. Left = static condition correlations. Right = TD condition correlations. White dotted lines highlight FC-BC and BC-FC intersections. FS = forward straight, BS = backward straight, FC= forward C-shaped, BC = backward C-shaped, PV = pivot, Ar = area, D = distance, T = time, ID = individual identity. Bottom: Linear regression comparing static (blue) and TD (orange) showing correlation between FC and BC frequency count ratios for each individual (circles) with all time points included.

4.6 Supplemental

4.6.1 PV association with nose-probing

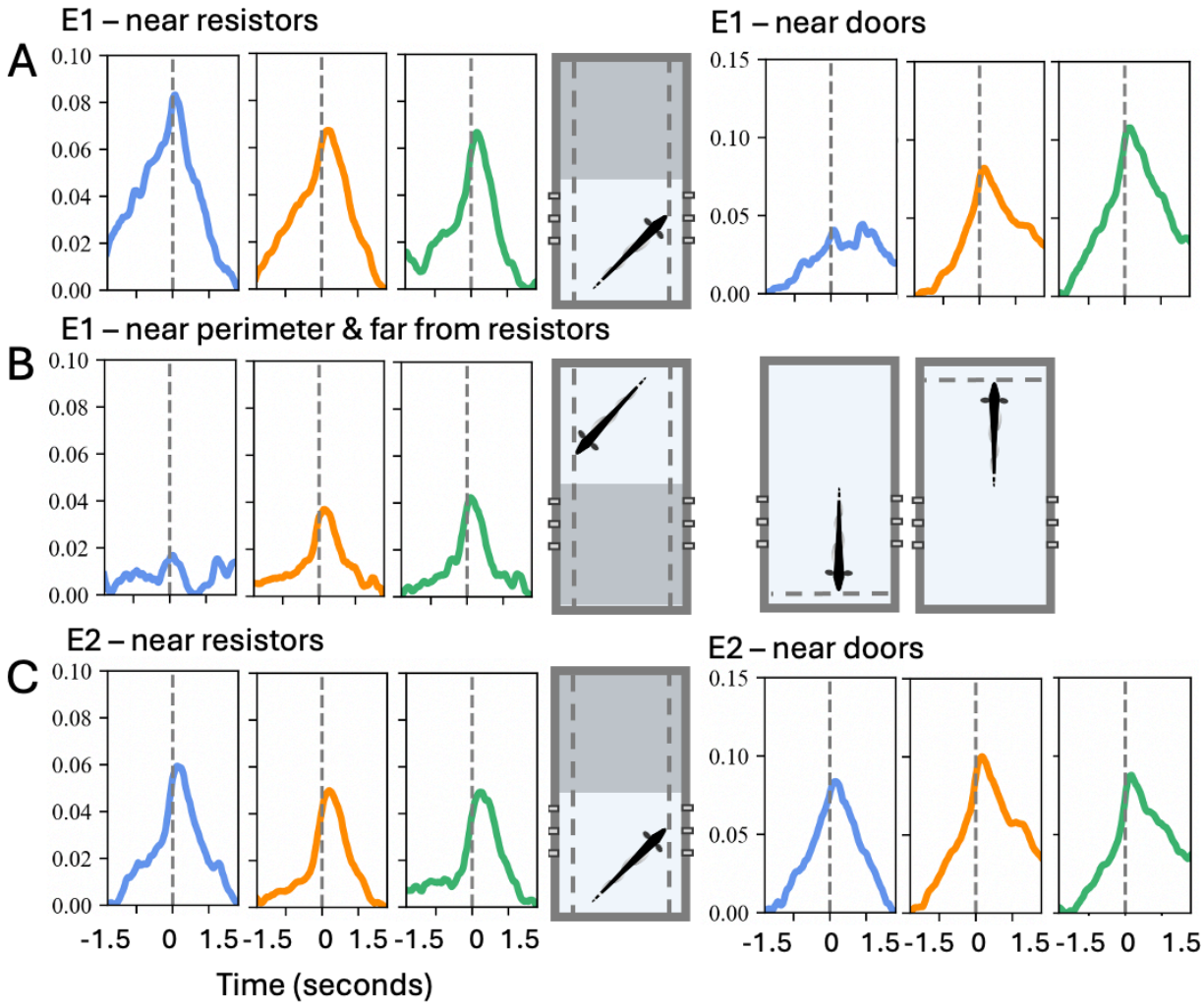

Supplemental Figure 4.1 Characterization of PV correlations with different areas of the tank.

PV correlation in three different environments. Vertical dashed line indicates time when fish passes distance threshold (1.5 cm) from target. Plots show 2-seconds before crossing threshold until 2-seconds after. PV has highest correlation almost immediately after crossing threshold. A-C) Left: correlation with threshold along longitudinal perimeter of refuge (see schematic). Right: correlation with threshold along horizontal perimeter of refuge (location of doors). A) Correlation when fish is in bottom half of the refuge containing resistors. B) Correlation when fish is in the top half of the refuge away from resistors. C) Repetition of A).

4.6.2 Linear Mixed Model Summary Statistics

4.6.2.1 Area Covered

```
> summary(model)
Linear mixed model fit by REML. t-tests use Satterthwaite's method ['lmerModLmerTest']
Formula: y ~ time + cond + (time | indiv)
   Data: df

REML criterion at convergence: 281.4

Scaled residuals:
     Min       1Q   Median       3Q      Max
-2.14455 -0.58321 -0.02761  0.53539  2.92936

Random effects:
 Groups   Name        Variance Std.Dev. Corr
 indiv    (Intercept) 0.853926 0.92408
          time        0.007754 0.08806  -0.35
 Residual             0.234681 0.48444
Number of obs: 144, groups:  indiv, 18

Fixed effects:
             Estimate Std. Error        df t value Pr(>|t|)
(Intercept)   0.45908    0.25989  27.39752   1.766  0.08846 .
time         -0.03367    0.02723  16.99672  -1.237  0.23301
cond         -0.22749    0.08074 107.00037  -2.818  0.00576 **
---
Signif. codes:  0 ‘***’ 0.001 ‘**’ 0.01 ‘*’ 0.05 ‘.’ 0.1 ‘ ’ 1

Correlation of Fixed Effects:
     (Intr) time
time -0.379
cond -0.466  0.000
> anova(model)
Type III Analysis of Variance Table with Satterthwaite's method
      Sum Sq Mean Sq NumDF   DenDF F value   Pr(>F)
time 0.35893 0.35893     1  16.997  1.5295 0.233010
cond 1.86304 1.86304     1 107.000  7.9386 0.005765 **
---
Signif. codes:  0 ‘***’ 0.001 ‘**’ 0.01 ‘*’ 0.05 ‘.’ 0.1 ‘ ’ 1
```

Supplemental Figure 4.2 Statistical summary output for LMM with Area covered as the dependent variable. Time = order of environmental exposure. Cond = environmental condition. Indiv = individual fish ID.

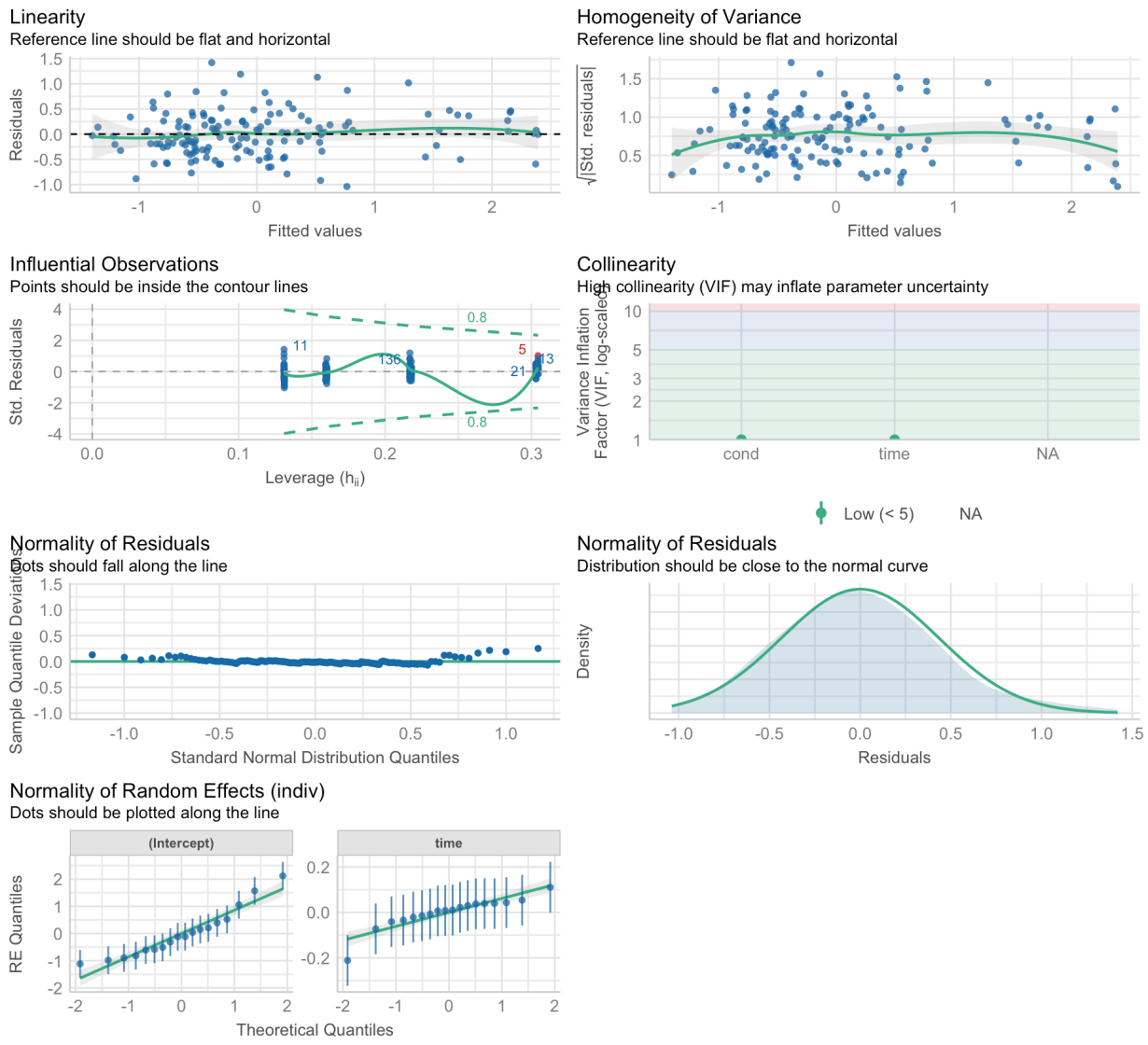

Supplemental Figure 4.3 Statistical summary output graphs for LMM with Area covered as the dependent variable.

Time = order of environmental exposure. Cond = environmental condition. Indiv = individual fish ID.

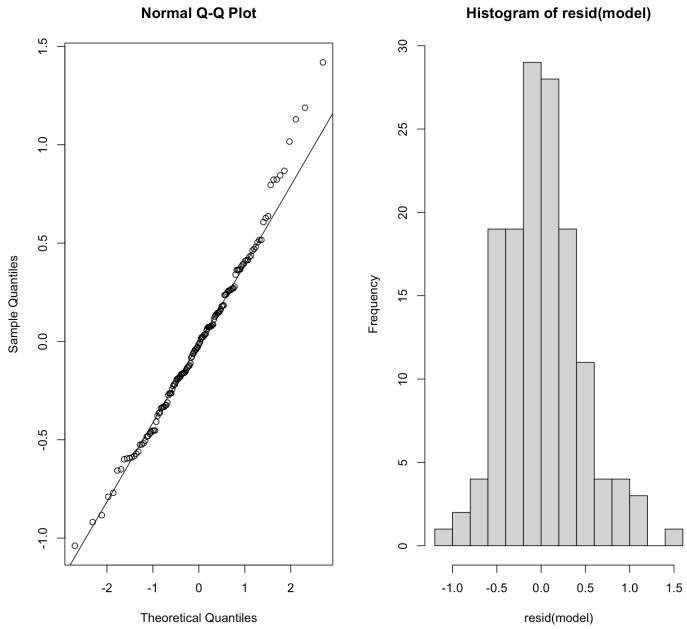

Supplemental Figure 4.4 Statistical summary output for normality of residuals for LMM with Area covered as the dependent variable.

4.6.2.2 Distance Travelled

```
> summary(model)
Linear mixed model fit by REML. t-tests use Satterthwaite's method ['lmerModLmerTest']
Formula: y ~ time + cond + (time | indiv)
   Data: df

REML criterion at convergence: 170.7

Scaled residuals:
     Min       1Q   Median       3Q      Max
-2.24791 -0.54355 -0.02006  0.52252  2.36646

Random effects:
 Groups   Name        Variance Std.Dev. Corr
 indiv    (Intercept) 0.82058  0.9059
          time        0.01339  0.1157   -0.75
 Residual             0.09120  0.3020
Number of obs: 144, groups:  indiv, 18

Fixed effects:
             Estimate Std. Error        df t value Pr(>|t|)
(Intercept)   0.83073    0.23108  21.25731   3.595  0.00168 **
time         -0.17538    0.02941  16.99977  -5.964 1.54e-05 ***
cond         -0.14949    0.05033 107.00010  -2.970  0.00368 **
---
Signif. codes:  0 ‘***’ 0.001 ‘**’ 0.01 ‘*’ 0.05 ‘.’ 0.1 ‘ ’ 1

Correlation of Fixed Effects:
     (Intr) time
time -0.707
cond -0.327  0.000
> anova(model)
Type III Analysis of Variance Table with Satterthwaite's method
     Sum Sq Mean Sq NumDF DenDF F value   Pr(>F)
time 3.2437  3.2437     1    17 35.5670 1.54e-05 ***
cond 0.8045  0.8045     1   107  8.8214 0.003676 **
---
Signif. codes:  0 ‘***’ 0.001 ‘**’ 0.01 ‘*’ 0.05 ‘.’ 0.1 ‘ ’ 1
```

Supplemental Figure 4.5 Statistical summary output for LMM with distance travelled as the dependent variable. Time = order of environmental exposure. Cond = environmental condition. Indiv = individual fish ID.

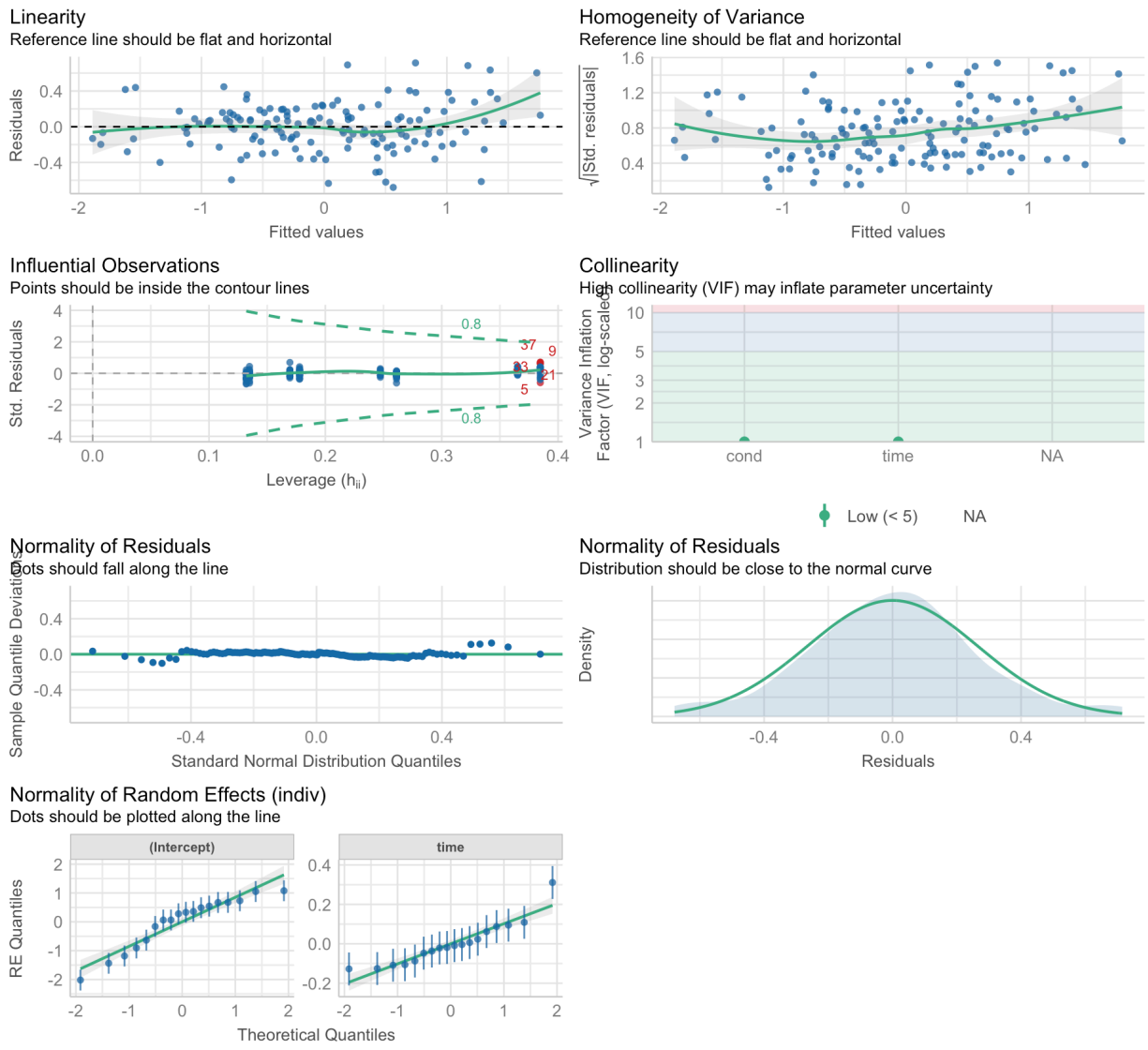

Supplemental Figure 4.6 Statistical summary output graphs for LMM with distance travelled as the dependent variable. Time = order of environmental exposure. Cond = environmental condition. Indiv = individual fish ID.

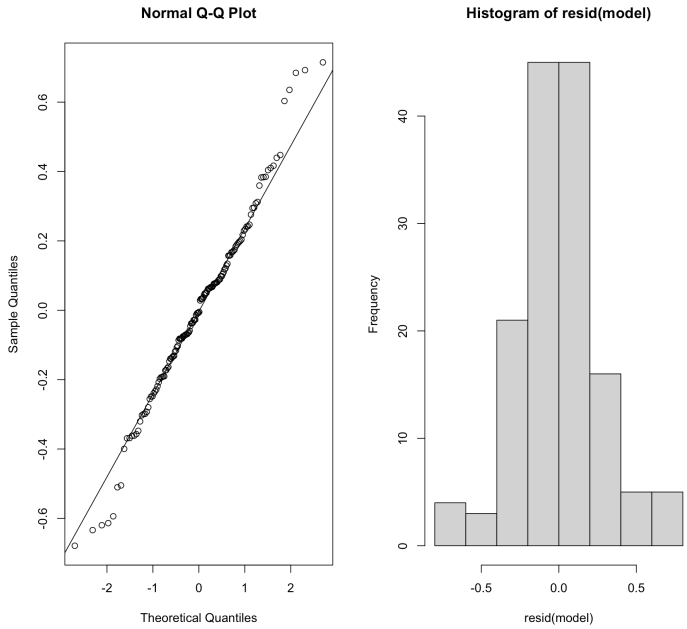

Supplemental Figure 4.7 Statistical summary output for normality of residuals for LMM with distance travelled as the dependent variable.

4.6.2.3 Time-spent near resistors

```
> summary(model)
Linear mixed model fit by REML. t-tests use Satterthwaite's method ['lmerModLmerTest']
Formula: y ~ time + cond + (time | indiv)
   Data: df

REML criterion at convergence: -162

Scaled residuals:
    Min      1Q  Median      3Q     Max
-3.2809 -0.5110  0.0518  0.4703  3.6600

Random effects:
 Groups   Name        Variance  Std.Dev. Corr
 indiv    (Intercept) 0.0120743 0.10988
          time        0.0003646 0.01909  -0.50
 Residual             0.0118951 0.10906
Number of obs: 144, groups:  indiv, 18

Fixed effects:
             Estimate Std. Error         df t value Pr(>|t|)
(Intercept)   0.703418   0.041105  49.367254  17.113   <2e-16 ***
time         -0.016692   0.005999  16.999663  -2.782   0.0128 *
cond         -0.044843   0.018177 107.000245  -2.467   0.0152 *
---
Signif. codes:  0 ‘***’ 0.001 ‘**’ 0.01 ‘*’ 0.05 ‘.’ 0.1 ‘ ’ 1

Correlation of Fixed Effects:
     (Intr) time
time -0.459
cond -0.663  0.000
> anova(model)
Type III Analysis of Variance Table with Satterthwaite's method
       Sum Sq  Mean Sq NumDF DenDF F value  Pr(>F)
time 0.092092 0.092092     1    17  7.7420 0.01277 *
cond 0.072392 0.072392     1   107  6.0859 0.01521 *
---
Signif. codes:  0 ‘***’ 0.001 ‘**’ 0.01 ‘*’ 0.05 ‘.’ 0.1 ‘ ’ 1
```

Supplemental Figure 4.8 Statistical summary output for LMM with time spent near the resistors as the dependent variable. Time = order of environmental exposure. Cond = environmental condition. Indiv = individual fish ID.

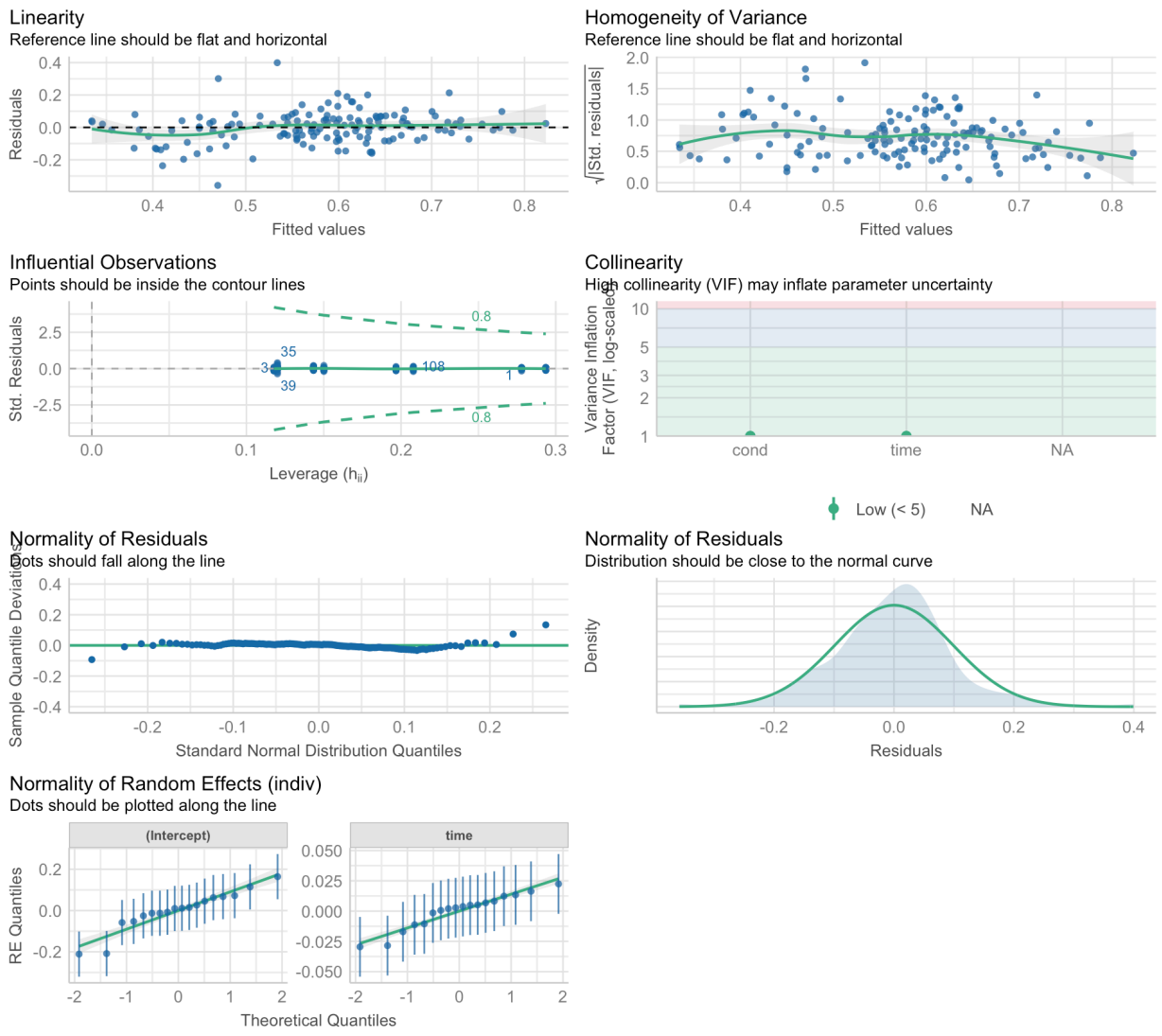

Supplemental Figure 4.9 Statistical summary output graphs for LMM with time spent near the resistors as the dependent variable. Time = order of environmental exposure. Cond = environmental condition. Indiv = individual fish ID.

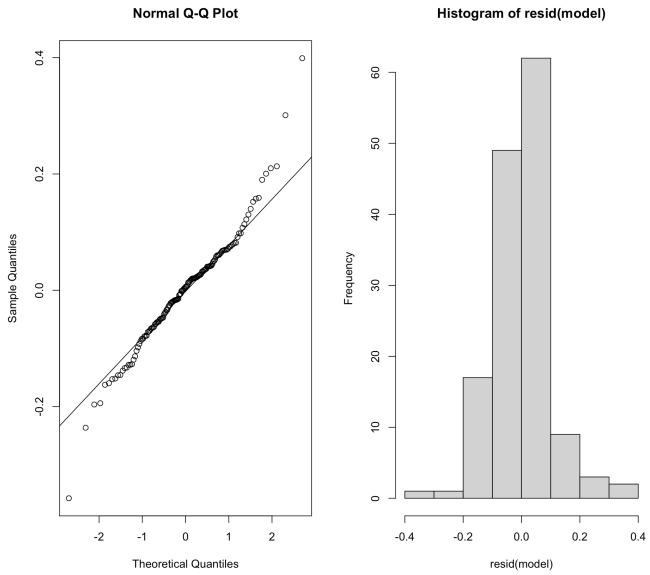

Supplemental Figure 4.10 Statistical summary output for normality of the residuals for LMM with time spent near the resistors as the dependent variable.

```
Linear mixed model fit by REML. t-tests use Satterthwaite's method ['lmerModLmerTest']
Formula: y ~ time + cond + sylbl4 + sylbl5 + (time | indiv)
   Data: df

REML criterion at convergence: 269.6

Scaled residuals:
    Min      1Q  Median      3Q     Max
-2.2061 -0.6363 -0.0162  0.5600  3.3140

Random effects:
 Groups   Name        Variance Std.Dev. Corr
 indiv    (Intercept) 1.135713 1.06570
          time        0.008661 0.09306  -0.59
 Residual             0.218541 0.46748
Number of obs: 144, groups:  indiv, 18

Fixed effects:
             Estimate Std. Error        df t value Pr(>|t|)
(Intercept)   1.00240    0.33619  39.64832   2.982  0.00488 **
time         -0.01370    0.02849  18.34733  -0.481  0.63641
cond         -0.20681    0.07845 105.76028  -2.636  0.00965 **
sylbl4       -2.78534    1.28400 127.21602  -2.169  0.03192 *
sylbl5       -1.05691    0.73729 128.31415  -1.433  0.15415
---
Signif. codes:  0 ‘***’ 0.001 ‘**’ 0.01 ‘*’ 0.05 ‘.’ 0.1 ‘ ’ 1

Correlation of Fixed Effects:
       (Intr) time   cond   sylbl4
time   -0.329
cond   -0.308  0.021
sylbl4 -0.303 -0.175 -0.117
sylbl5 -0.312 -0.081  0.032 -0.316
> anova(model)
Type III Analysis of Variance Table with Satterthwaite's method
        Sum Sq Mean Sq NumDF   DenDF F value   Pr(>F)
time   0.05050 0.05050     1  18.347  0.2311 0.636413
cond   1.51879 1.51879     1 105.760  6.9497 0.009645 **
sylbl4 1.02840 1.02840     1 127.216  4.7058 0.031921 *
sylbl5 0.44908 0.44908     1 128.314  2.0549 0.154147
---
Signif. codes:  0 ‘***’ 0.001 ‘**’ 0.01 ‘*’ 0.05 ‘.’ 0.1 ‘ ’ 1
```

Supplemental Figure 4.11 Statistical summary output for LMM with Area covered as the dependent variable. Time = order of environmental exposure. Cond = environmental condition. Indiv = individual fish ID. FC = forward C-shaped mean frequency counts. BC = backward C-shaped mean frequency counts.

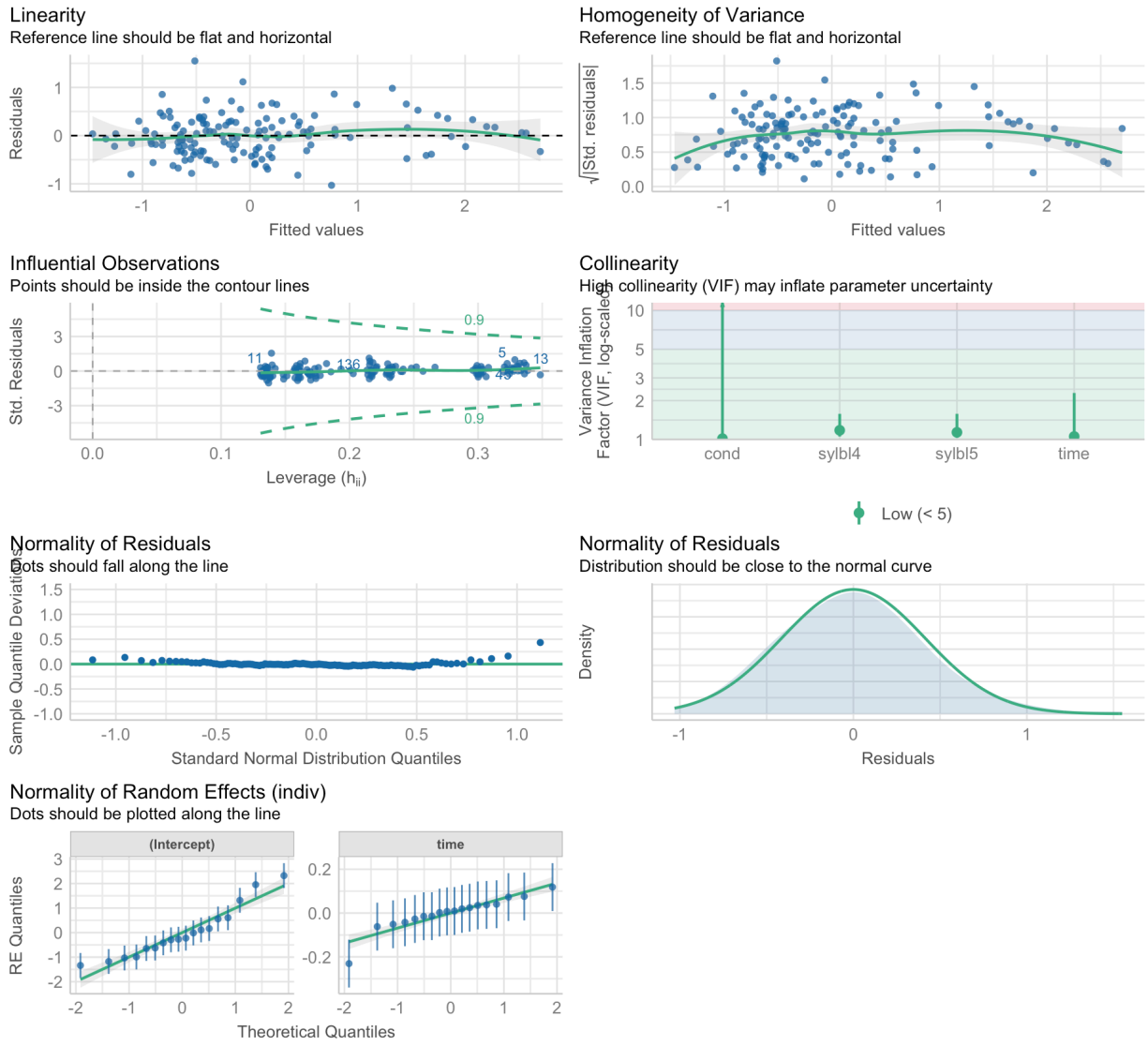

Supplemental Figure 4.12 Statistical summary output for LMM with Area covered as the dependent variable. Time = order of environmental exposure. Cond = environmental condition. Indiv = individual fish ID. FC = forward C-shaped mean frequency counts. BC = backward C-shaped mean frequency counts.

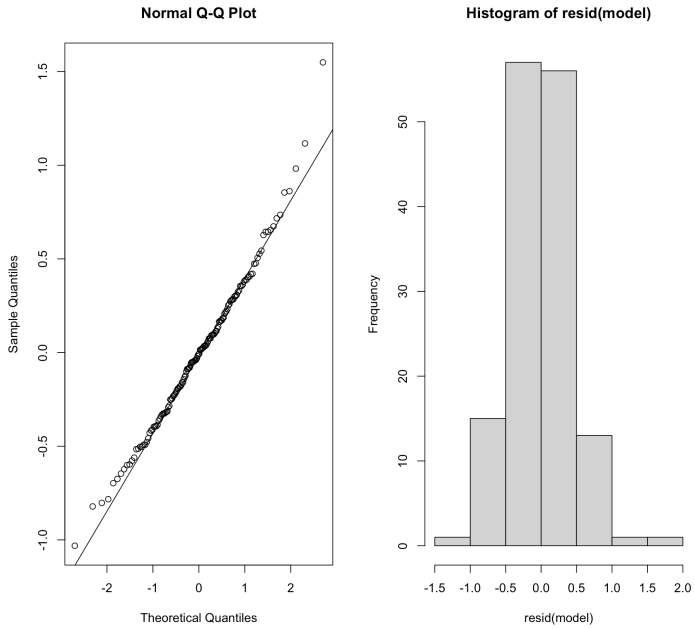

Supplemental Figure 4.13 Statistical summary output for normality of the residuals for LMM with Area covered as the dependent variable.

4.6.3 Correlation Matrices Over Time

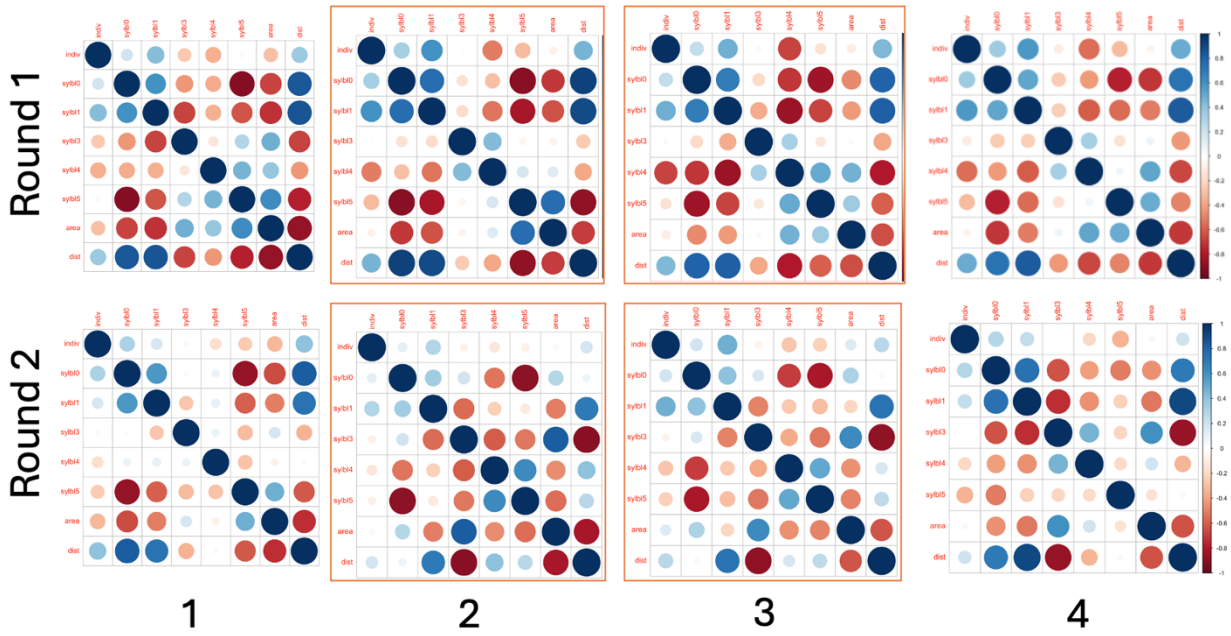

Supplemental Figure 4.14 Correlation matrices between fixed and random variables for each trial.

Top-to-bottom rows: Indiv = individual; sylbl0 = FS; sylbl1 = BS; Sylbl3 = PV; sylbl4 = FC; sylbl5 = BC; area = area covered; dist = distance travelled. Left-to-right columns same order as rows. Y-axis of entire figure shows round number; x-axis shows trial order. 1 & 4 = static, 2 & 3 = temporally dynamic.

4.6.4 FC-BC Linear Regression by trial

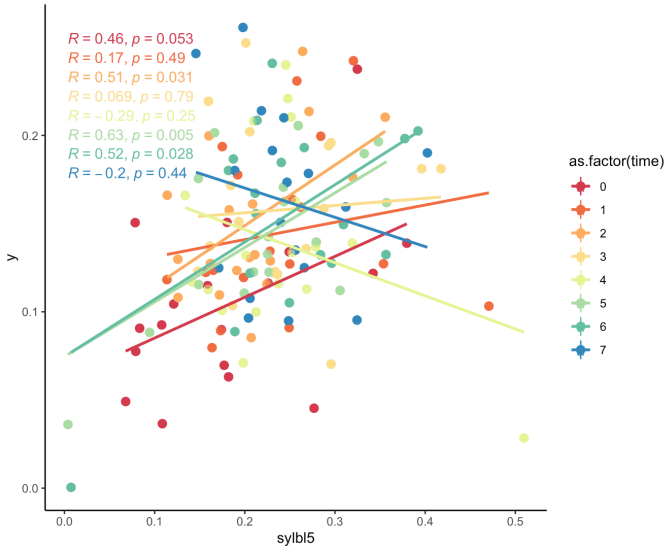

Supplemental Figure 4.15 Linear regression between FC and BC for each trial in order of time of exposure.

Y-axis = FC, x-axis = BC. 0-3 = Round-1 trials. 4-7 = Round-2 trials. 0, 3, 4, 7 = static environment. 1, 2, 5, 6 = temporally dynamic environment. R-values and p-values shown in top-left legend corresponding to colours in legend in middle-right.

Chapter 5: Scanning Increases Sensory Input Amplitude in Weakly Electric Fish

5.1 Introduction

Behavioural identification methods have made much progress in the last decade by making use of increased computational power, data storage solutions, and improved algorithms (Datta et al., 2019). We have recently used computational identification methods to examine components of behaviours which we used to investigate active sensing behaviours in weakly electric fish (see Chapters 3 and 4). I have supported the idea that active sensing improves electrosensory acquisition. The electrosensory array enabling electric sensing is distributed across the surface of the skin of the fish. Therefore, there is an added entanglement between electrosensory input and behavioural output. The mechanism of electrosensation arises from their self-generated electric field whereby external objects and locomotory behaviour influence the flow of current in the field and in turn the incoming electrosensory information.

Historically, active sensing movements have theoretical, neurophysiological, and recent behavioural evidence that they are likely deliberately involved in electrosensation in at least some contexts (Assad, 1997; Babineau et al., 2007; Bastian, 1981; Caputi,

2017; Heiligenberg, 1973; Jun et al., 2016; Jung & Engelmann, 2019; Knudsen, 1974; Sim & Kim, 2011; Stamper et al., 2012; Upshall, 2024; von der Emde, 1999). However, this has so far been without a direct link tying these movements to the incoming electrosensory information perceived by the electroreceptor array. To address this gap, we use a novel custom-made software (fish2EOD; Shifman, Upshall, and Lewis, in prep) to understand the true sensory inputs during simulated and true swimming behaviour. This is the first tool to show the causal effect of active sensing movements by directly modelling both the interaction of the external environment and fish dynamics on the electric field. With this we can investigate the electrosensory information available to the receptors at each body point along the length of the fish.

Traditionally, to understand inputs to the electrosensory system they are processed by subtracting the electrosensory scene without the object from the scene with the object assuming the perspective of a single electroreceptor. This produces the “electric image” (EI) that is the perturbation caused by the object alone. Without any modification, the direct input caused by the object that is computed across the skin, called the transdermal potential (TDP), is largely affected by the body shape. As shown in Figure 5.1A this is true even under stationary conditions where the fish and object are unchanging. However, under the same conditions, computing the EI creates a gaussian-like shape with a peak formed at the object location relative to the rostro-caudal position on the fish (see Figure 5.1B). If we consider that their self-generated electric field is on the order of 10s of millivolts, then the amplitude value in Figure 5.1E is roughly a difference of 2 orders of magnitude. Remarkably, tuberous electroreceptors encode

these miniscule perturbations with a sensitivity threshold near 0.1-1μVs (Nelson & Maciver, 1999a). While the fish may not be subtracting the background electrosensory scene per se, behavioural and electrophysiological studies show that they can clearly extract these small changes (Bastian, 1981; Chacron et al., 2001; Knudsen, 1974; Metzen & Chacron, 2023; Viancour, 1979).

The challenge instead arises with movement. For perspective, body-shape modifications such as tail-bending produce roughly 50-150μV amplitude modulations depending on angle and body location (Assad, 1997; Bastian, 1995). Furthermore, the fish's anatomy enables fine-tuned movements owed to a specialized ribbon fin which permits locomotion to be uncoupled from body-bending. Since the fish's precise behavioural outputs can influence the electric field with such impact, we wonder if the consequences are helpful or harmful to the fish's sensing abilities.

Here we focus on scanning which is an active sensing behaviour where the fish maintains a straight posture and involves swimming back and forth past an object of interest. In Chapters 3 and 4 we have shown behavioural evidence suggesting a role for scanning in novel conditions. We now aim to address the effects of scanning on the electrosensory inputs at the level of the electroreceptors. Using the custom-made software, we modelled the exact dimensions of the refuge used in Chapters 3 and 4 with the same water conductivity and resistor locations. We also had full control over the temporal dynamics, allowing us to modify the fish's position in time as well as the simulated contrasts of the resistors. Throughout this manuscript we build upon a model

with a stationary fish and environment followed by those including simulated scanning behaviour, then by the true locomotion produced by the fish. We also show that even with minimal linear transformations the relevant information for object detection is theoretically available at the receptor level and that the sensory input amplitudes are enhanced by scanning.

5.2 Methods

5.2.1 Behavioural Data Collection

Behavioural data were collected from experiments performed in Chapter 4 (see Chapter 4 for experimental method specifics).

5.2.2 Simulations with Fish2EOD

Fish2EOD uses nodes within a defined mesh to calculate the properties of the electrosensory scene within the simulated environment. We inputted the dimensions and electrical properties of the refuge and resistor elements defined in Chapter 4. The simulation was calibrated using the same species of fish, *Apteronontus albifrons*, as used in Chapters 3 and 4. Therefore the specifics of the model matched the electric organ discharge native to the fish. See docs https://fish2eod.readthedocs.io/en/latest/.

In the simulated experiments we set the fish to 15cm. We simulated the fish with a straight body when evaluating the effect of scanning with the fish positioned parallel to the refuge at a distance of 2cm. As is expected of the behaviour, we assumed a straight

and rigid body shape that was constant over time. When the fish was simulated to move, we simulated a speed of 1.5cm/s for visual clarity. Fish plotted at faster or slower speeds produced similar results but with narrower or broader gaussian-like waveforms from the effect of the resistors, respectively (not shown).

For the simulations of the freely swimming fish, we used a numpy function *np.random()* to choose a random video from a list of all experiments. From that video we visually identified a continuous section containing an event where the fish swam near the resistors.

5.2.3 Plotting and Analysis

We used DeepLabCut (Mathis et al., 2018) to label 6 body points along the spine of the fish as was done in Chapters 3 and 4. This positional data was used to extract the x,y position of each of the 6 points at 30 fps. These data were used to plot the data seen in Figure 5.5.

Heatmaps and other figures were generated using matplotlib.pyplot library see https://matplotlib.org.

5.3 Results and Discussion

5.3.1 Modelling Transdermal Potentials with Fish2EOD

To build a comprehensive picture of the components involved in influencing the transdermal potential of the fish, we began with a simple scenario to quantify the effects of resistor contrast on a non-moving fish. We simulated the stationary fish positioned 2cm from the refuge wall with a single embedded resistor (see Figures 5.1C and D) across three resistor contrasts (low = 75kΩ, medium = 20kΩ and high = 5kΩ). We observe a contrast-dependent change in transdermal potential (see Figure 5.1C) with each being influenced by body shape. These differences occur on such a small scale relative to the amplitude of the electric field that the qualitative comparison appears identical (see Figure 5.1D). However, when we show the effects of the object alone (see Figure 5.1F) by computing the electric image, the contrast differences can be observed more clearly. As expected, higher resistor contrasts exhibit higher amplitude electric images (see Figure 5.1E).

We then began to investigate the role of motion. For these we simulate scanning due to behavioural evidence suggesting its role in novel environments (see Chapter 3 and 4). We aimed to complement these findings by identifying the impact of scanning on the electrosensory input available to the electroreceptors. To mimic a scan, we added translational movement to our simulation with a fixed straight body-pose. We repeated the resistor stimuli three separate times again at low, medium, or high contrast (see Figure 5.2A). For simplicity, we observed the transdermal potential at a body point along the fish (the 20th body point or 20% from the rostral end; referred to as bp-20) assuming

the perspective of a single receptor. At time = 0 seconds (t=0) the fish was longitudinally furthest from the resistor while lateral distance was left constant (2cm). At this starting point (t=0) the transdermal potentials all had the same potential value (-0.057mV) at bp-20. This was because in each of the three conditions the effects of the resistor were too far to influence the field at this location. As the fish swam closer, the object induced an increased amplitude relative to the intensity of the stimulus. Each peaked when bp-20 was closest to the resistor then began to decrease as the fish continued swimming by.

We repeated this experiment, continuing to observe the TDP from the perspective of bp-20 with different combinations of movement parameters (see Figure 5.2B-D). First, we kept the fish stationary and fixed at 2cm lateral to the resistor (as in Figure 5.1) and applied an amplitude varying contrast within the mid-contrast range (max=18kΩ, min=32kΩ; see Figure 5.2E). Given that each body point (receptor) is at a different location within the electric field, the TDP is influenced according to its location. For bp-20 for example, the relative potential range observed at this location is negative (~0mV – -0.2mV). On this sub-millivolt scale the potential over time was relatively flat with some slight amplitude changes in the transdermal potential (see Figure 5.2B). However, to confirm that the resistor temporal dynamics were still being reflected in the TDP, we zoomed in at a much finer voltage scale (-0.135 to -0.131 mV). At this scale the maximum amplitude difference in the TDP was ~0.004mV, but the reflection of the changes in the resistor contrast were clearly observed (not shown). Therefore, the signal produced by the resistor was present but extremely small when the fish was stationary with a fixed distance of 2cm.

Next, we moved the fish as was done in Figure 5.2A and dynamically varied the contrast (same trace in Figure 5.2E). Here (Figure 5.2C), the temporal dynamics of the resistor contrast were washed out by the TDP magnitude induced by the mere presence of the resistor (R2). In other words, the contrast difference from the plexiglass relative to the resistor location was a much larger signal than that of the resistor contrast temporal dynamics. However, the shape of the TDP in Figure 5.2C (with resistor temporal dynamics) was not identical to the mid-contrast (orange) trace in Figure 5.2A (without resistor temporal dynamics). This is because there is a compounding interaction between the fish's translational movement and the changing contrast of the resistor. Therefore, the shape of the peak observed in Figure 5.2C is skewed to the left because as the fish approached the resistor, the contrast was also increasing. Likewise, the amplitude of the TDP decreases as the contrast decreases, even though the fish's relative position to the resistor was the same as in Figure 5.2A.

Lastly, we repeated the experiment in Figure 5.2C but included two more resistors (see Figure 5.2D) which all varied identically according to the trace in Figure 5.2E. The starting location was next to the refuge wall with the first resistor being 8 cm away longitudinally. The distance between bp-20 and each resistor was smallest at 5.0s for R1, 7.4s for R2, and 9.7s for R3. As with the compounding factors between the moving fish and single temporal dynamic resistor (Figure 5.2C) there are even more considerations with three temporally dynamic resistors. For example, at the location between R1 and R2 both resistors are influencing the TDP at bp-20 which is why the potential does not return to values observed at t=0. However, at this location between

R1 and R2, the effect of both resistors on the TDP is still less than the effect of being directly across from either of the active resistors. As such, as the distance between bp-20 from R1 increases and the distance to R2 decreases, the amplitude of the TDP begins to increase again. As observed in Figure 5.2C, there are again the temporal dynamics of the resistors to consider.

Overall, as the fish approaches the resistor while the contrast is also increasing, this will have a larger effect than if the fish were swimming away. Similarly, if the fish is approaching a resistor that is decreasing in contrast, the effects will combine as seen when the fish passes near the third resistor (R3; Figure 5.2D).

While informative for the single receptor perspective, the fish have approximately 200 tuberous receptors per cm^2 (Carr et al., 1982; Nelson & Maciver, 1999a). Regions of the body have electroreceptors with different receptive fields and densities, all of which converge to be received in the electrosensory lateral line lobe (ELL; Carr et al., 1982). Furthermore, these regions are conserved in the ELL via topographical mapping (Krahe & Maler, 2014).

We aimed to investigate the transdermal potential across a larger area along the body using a broader set of body points (10%-40% rostro caudally) for 10 seconds with and without resistor temporal dynamics (see Figure 5.3A). We visualized the side of the fish closest to the resistor (left side) creating a heatmap. As in Figure 5.2A, we simulated a scan at the three fixed contrasts from low (75kΩ) to high (5kΩ). Again, at 2cm the potential at these points along the body is negatively shifted as also seen with the transdermal potential data for bp-20. Expectedly, the intensity of the change in TDP

increases with increasing resistor contrast. As the fish approaches the resistor head-first the potential begins to increase rostrally. As the fish passes the resistor the amplitude of the caudal TDP also increases given sufficient object contrast (see Figure 5.3A).

Expanding on Figure 5.2B-D, we included the heatmaps for the temporally dynamic stimuli in a static and scanning fish with either 1 or 3 resistors (see Figure 5.3A bottom 3 panels). To quantify the amplitude of the observed TDP changes we again considered the perspective from a single receptor compared to a collection of receptors. For bp-20, scanning increased the amplitude by 2 orders of magnitude compared to the static fish (see Figure 5.3C). To quantify the amplitude across bp-10 to bp-40, we computed the difference for each receptor (maximum transdermal potential – minimum transdermal potential) and took the average. This resulted in a more modest difference between the static and scanning fish, though the absolute amplitudes were still greater with scanning by ~0.07mV with the fish 2cm from the object. For the amplitudes computed across all body points see Supplemental Figure 5.3.

The transdermal potentials between bp-10 and bp-40 are relatively consistent owing to the relative consistency of the electric field at this location. However, as previously mentioned, the body shape of the fish and the voltage vary rostro-caudally. We aimed to address how these challenges could be accounted for by investigating how the spatiotemporal signals are extracted by the electroreceptors. We consider two methods with which amplitude changes could be computed. The first was that the fish compute a constant temporal difference (temporal derivative), comparing the current

transdermal potentials along the body to those of a previous time point. The second followed a similar logic, but instead the comparisons are made across adjacent body points (spatial derivative). For simplicity we used two linear transformations to illustrate these ideas: a frame-to-frame temporal difference, and a body point-to-point spatial difference (see Figure 5.4). Here, the temporal difference especially, revealed stimulus-relevant modulations. Again, the TDP from the static fish produced smaller signals which were revealed on a smaller voltage scale (see 5.4B). We also saw the compounding effects of the stimulus temporal dynamics and scanning fish evidenced by the irregularity in Figure 5.4C which was not present in Figure 5.4A (without resistor temporal dynamics).

5.3.2 The Effect of True Swimming Behaviour on Transdermal Potential

Finally, we aimed to address all the complexities of fish movement (translational and body-shape) and environmental motion on the electrosensory input. A freely-swimming fish would constantly be changing relative distance while its environment could vary unpredictably as well. To account for the complexities of spatiotemporal changes we observed the TDP of an example fish from an experiment in Chapter 4. We chose this time series segment since the fish swam with a relatively straight body-pose past all 3 resistors. When we investigated the true TDP we observed a large effect of the fish engaging with the refuge. For example, in the time traces in Figure 5.5D, the fish approaches the wall of the refuge which creates a large positive potential. When the fish later passes by the resistors, the effects are much smaller than the effect of the fish approaching the wall at this scale.

Using the findings generated with our simulated fish, we again investigated the impact of taking the temporal and spatial difference. If the temporal differences were a true strategy, then this would mean the fish is in some way storing recent memory of the electrosensory scene with which it can subtract the current scene.

The spatial difference subtracts each receptor TDP from an adjacent receptor. In both cases (temporal and spatial differences), we observe the qualitative effects of the fish swimming past all three resistors which was not present in the raw TDP.

Both temporal and spatial differences are common strategies employed by neural systems. Spatial computations are relevant in systems such as those displaying centre-surround receptive fields (visual system), which have been found to facilitate novel object detection (Gaynes et al., 2022). Temporal computations are important in many systems including tactile adaptations resulting in desensitization to repetitive stimuli (Chung et al., 2015). In the case of weakly electric fish these neural computations are likely given that receptive fields of electroreceptors have a centre-surround organization, and their electroreceptors are known to undergo adaptation (Caputi, 2017; Chacron et al., 2003; Clarke et al., 2014, 2015; Clarke & Maler, 2017; Krahe et al., 2008). This suggests that even with simple linear transformations more stimulus-specific signals can be extracted from the raw TDP using true freely-swimming fish potentials and behaviour.

To understand the effects of true-swimming compared to a fish lacking body-pose dynamics, we simulated a straight fish with translational movement preserved (see Figure 5.5D) and computed the same raw TDP and difference plots as done for the true fish (see Figure 5.5B). We observed the TDP to be qualitatively less informative at the

location of the resistors. We used bp-20 to quantify this effect and found that the transdermal potential amplitude in the true fish was 59.4% larger (see Figure 5.6). These findings imply that the adjustments in body-pose over the observed time segment greatly improve the signal amplitude compared to a purely straight-posed fish.

5.4 Conclusion

In the present study we use a novel custom-made model to demonstrate the effects of scanning at the receptor level. We observe the electrosensory inputs in simple, static conditions and gradually introduce motion to build a picture of the electrosensory scene. We found that when the fish is not moving, the effects of the object intensity are small but possibly within detectable ranges (Nelson & Maciver, 1999a). However, when we simulate a scan past the object, the relative amplitude changes over time increased by two orders of magnitude from the perspective of a single receptor and by ~0.07mV (from 2cm distance) when considering a larger section of the body (bp-10 to bp-40). We propose two methods demonstrating that even with a simple linear transformation the fish could account for the large effects of the environment and body-shape on the TDP by performing these amplitude calculations; permitting sensory information that could be used for object detection in the least.

5.5 Figures

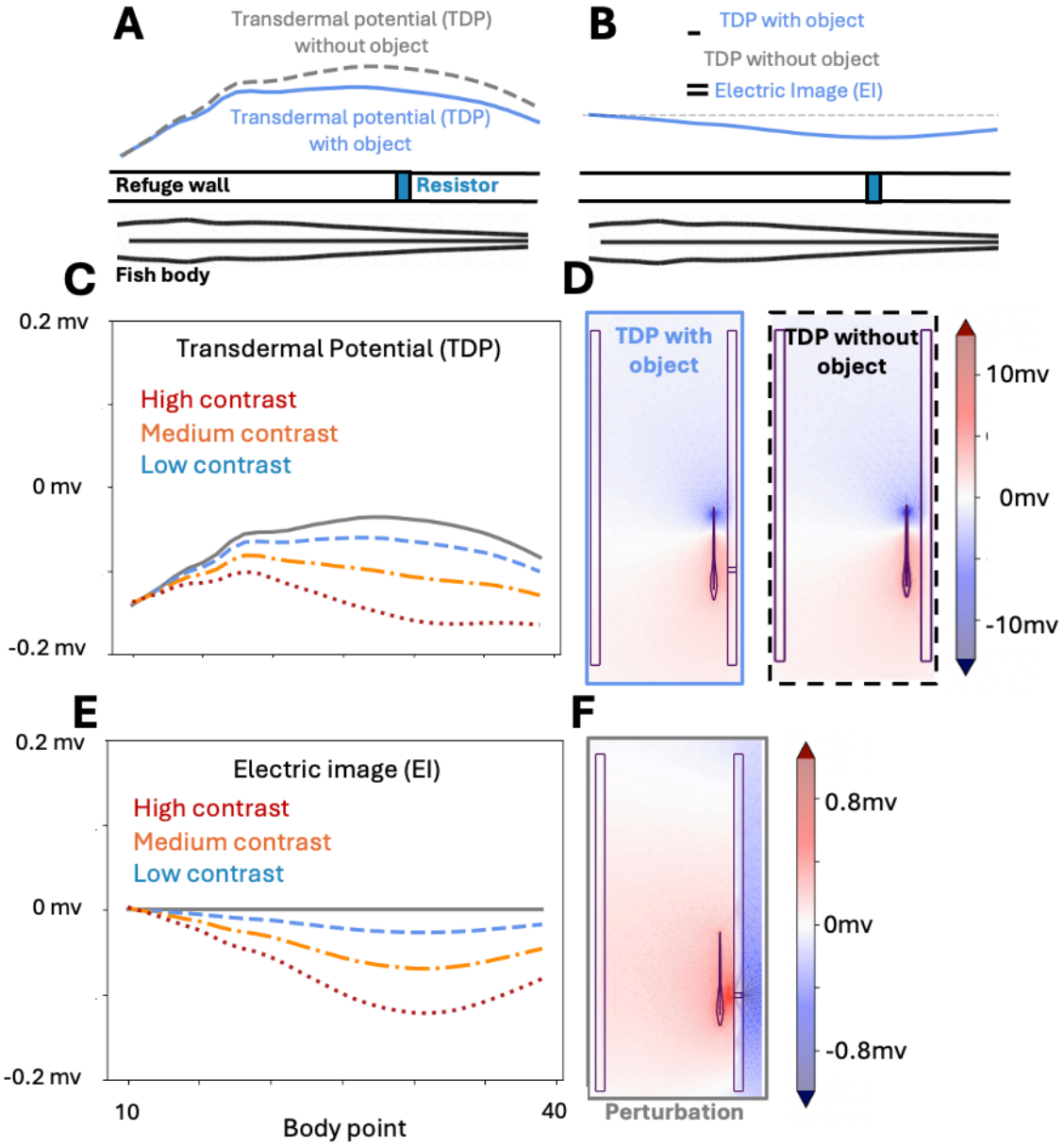

Figure 5.1 *Electric images (transdermal potential (TDP) with object – TDP without object) are often used to illustrate the perturbation caused by an object in the environment.*

A) Bottom shows a zoomed in (10-40%) schematic of the fish body near the resistor wall. The object is simulated using the resistor (blue). Transdermal potential without the object (grey dashed line) and with the object (blue solid line). B) Same as A) but plotting electric image (TDP with object – TDP without object). C) Transdermal potentials of three simulated objects of different contrasts relative to the refuge wall (low: blue, medium: orange, high: red, none: grey). D) Schematic of fish in refuge (used to create plot C) where the impact of the object (rectangle embedded in right wall) on the electric field is visually indistinguishable. E) Same as C) but for the electric image. F) Perturbation produced due to the object alone. Result is obtained by taking D) (left) – D) (right).

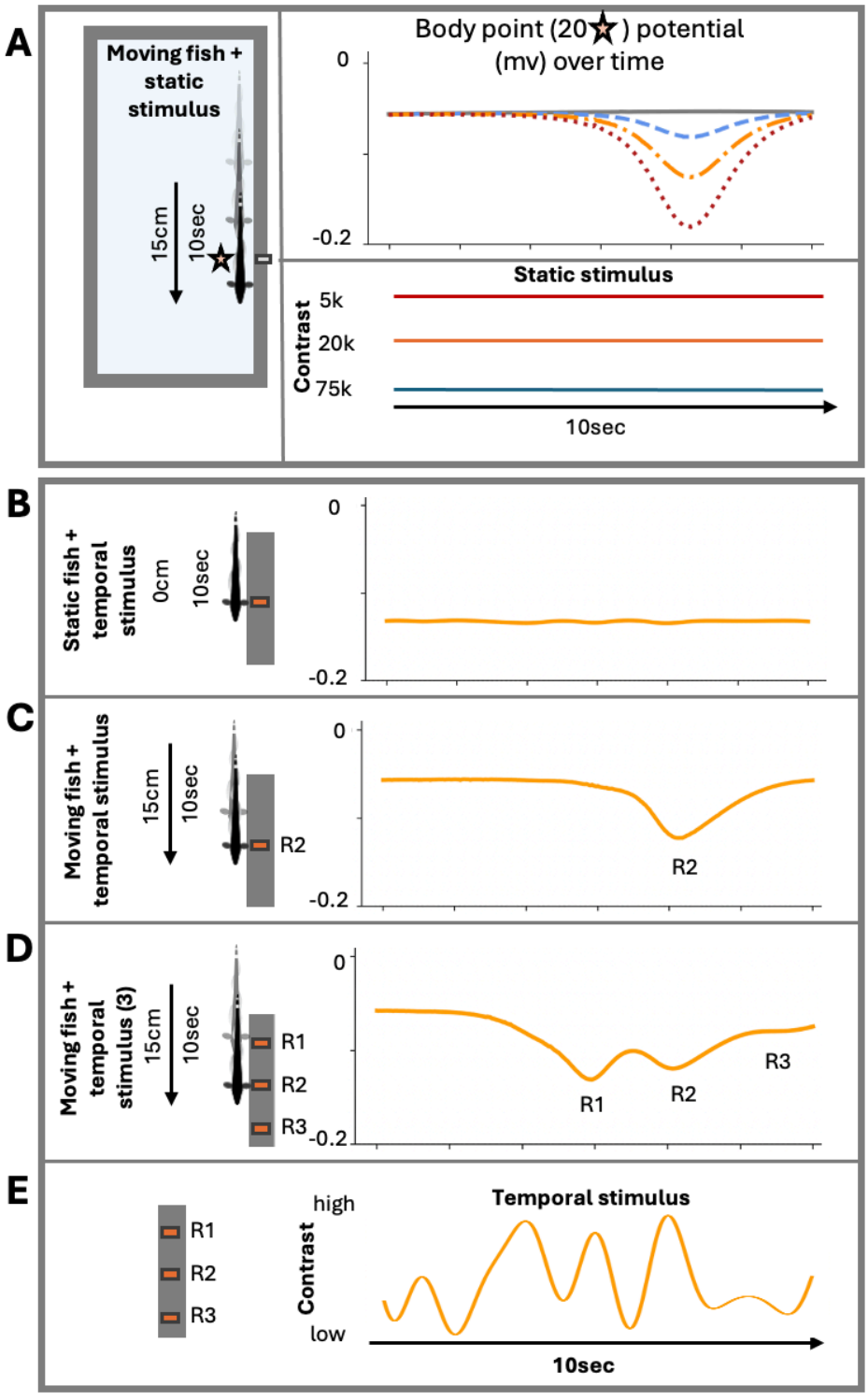

Figure 5. 2 Scanning impacts object detection.

A) Left: Star indicates the location which the subsequent time plots are generated. Schematic illustrates a simulated fish travelling 1.5cm/sec for 10sec in a straight line. Resistor embedded in the refuge wall was set to resistance 5k (high; red), 20k (medium; orange), and 75k (low; blue) ohms. Top: resulting transdermal potential (mv) over 10 seconds for each contrast value. B) Same as A) but fish remained static while the temporal stimulus (E) was applied. C) Combination of A) and B) where the fish travelled 1.5cm/sec for 10 seconds and the temporal stimulus was applied. Number 2 indicates second resistor location (rectangle; orange). D) Same as C) but all 3 resistors were activated according to the time series in E). E) Time series of the temporal stimulus used for R1-R3.

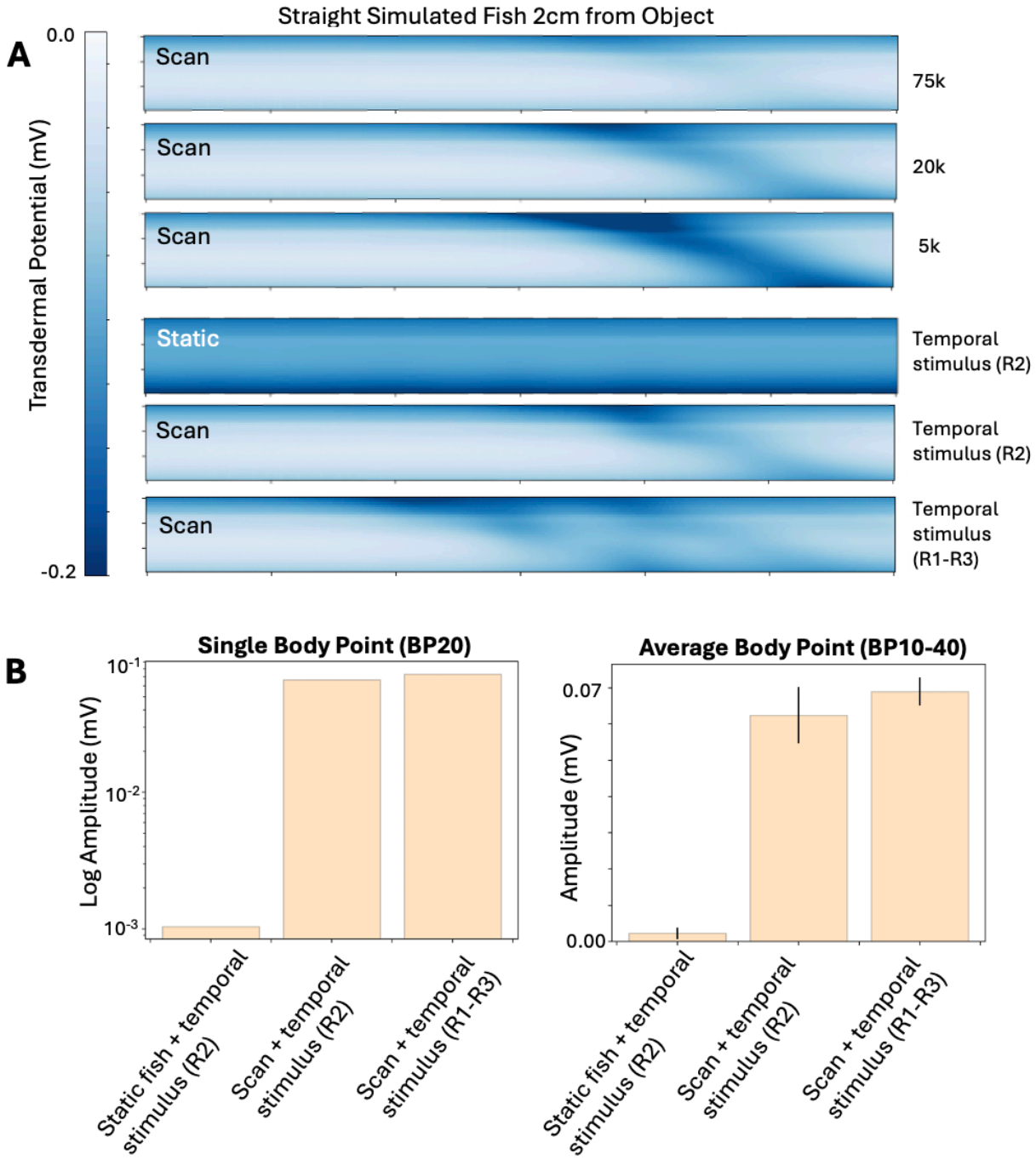

Figure 5.3 Temporal and spatial differences show scanning increases the transdermal potential amplitude compared to a static fish.

A) Effects of scanning on transdermal potential of straight fish with objects of varying contrasts. Top 3 panels = heatmaps of fish scanning by 1 resistor (R2) at low (75k), medium (20k), and high (5k) stimulus contrast. Bottom 3 panels = dynamic stimulus either for a single resistor (R2) or all three resistors (R1-R3). In the static fish example, the fish was simulated 2cm adjacent to R2. Scanning fish were 2cm from plexiglass wall and simulated to swim straight at 1.5cm/s. B) Left: log amplitude of the $TDP_{max} – TDP_{min}$ for body point 20 over 10 seconds. Right: amplitude of the average $TDP_{max} – TDP_{min}$ for each body point over 10 seconds.

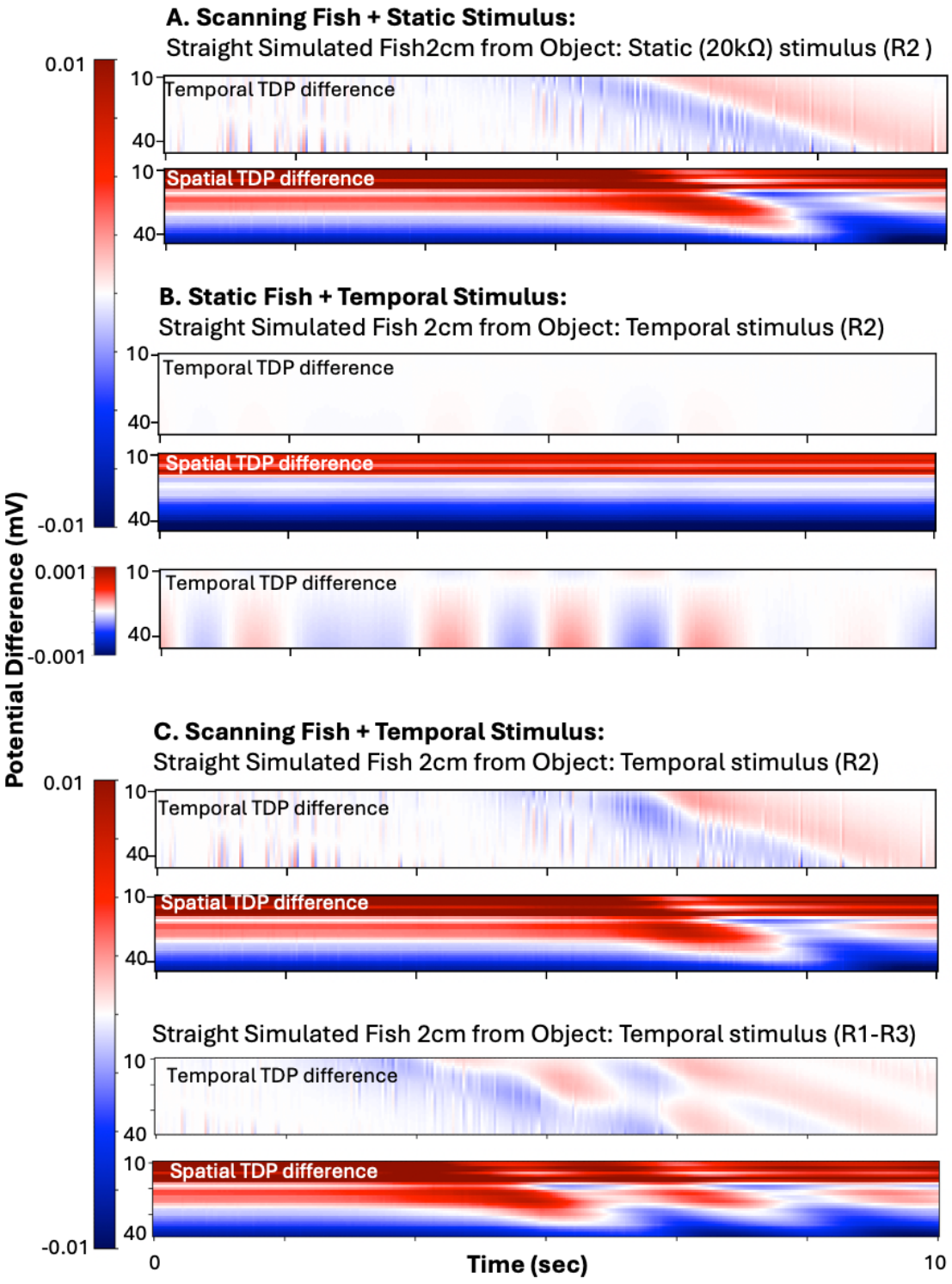

Figure 5.4 Temporal and spatial differences show effects of relative fish distance and resistor contrast on transdermal potential.

Temporal (TDP-t_n – TDP-t_{n-1}) and spatial (TDP-bp_n – TDP-bp_{n-1}) differences over time across body points (y-axis) 10-40. A) Straight fish scanning by a static stimulus at resistor 2 (R2) set to medium contrast (20kΩ). B) Static fish positioned directly across from R2 with a temporally dynamic stimulus (seen in Figure 5.1E). Top temporal difference is plotted on the same color bar scale as the spatial TDP difference plot (-0.01mV – 0.01 mV). Bottom temporal difference is same as above but plotted on a narrower potential difference scale (-0.001mV – 0.001 mV). C) Top: Temporal and spatial TDP for straight fish scanning by R2 which has a temporal stimulus (same as in B). Bottom: Same as top but R1, R2, and R3 all temporally varying contrast.

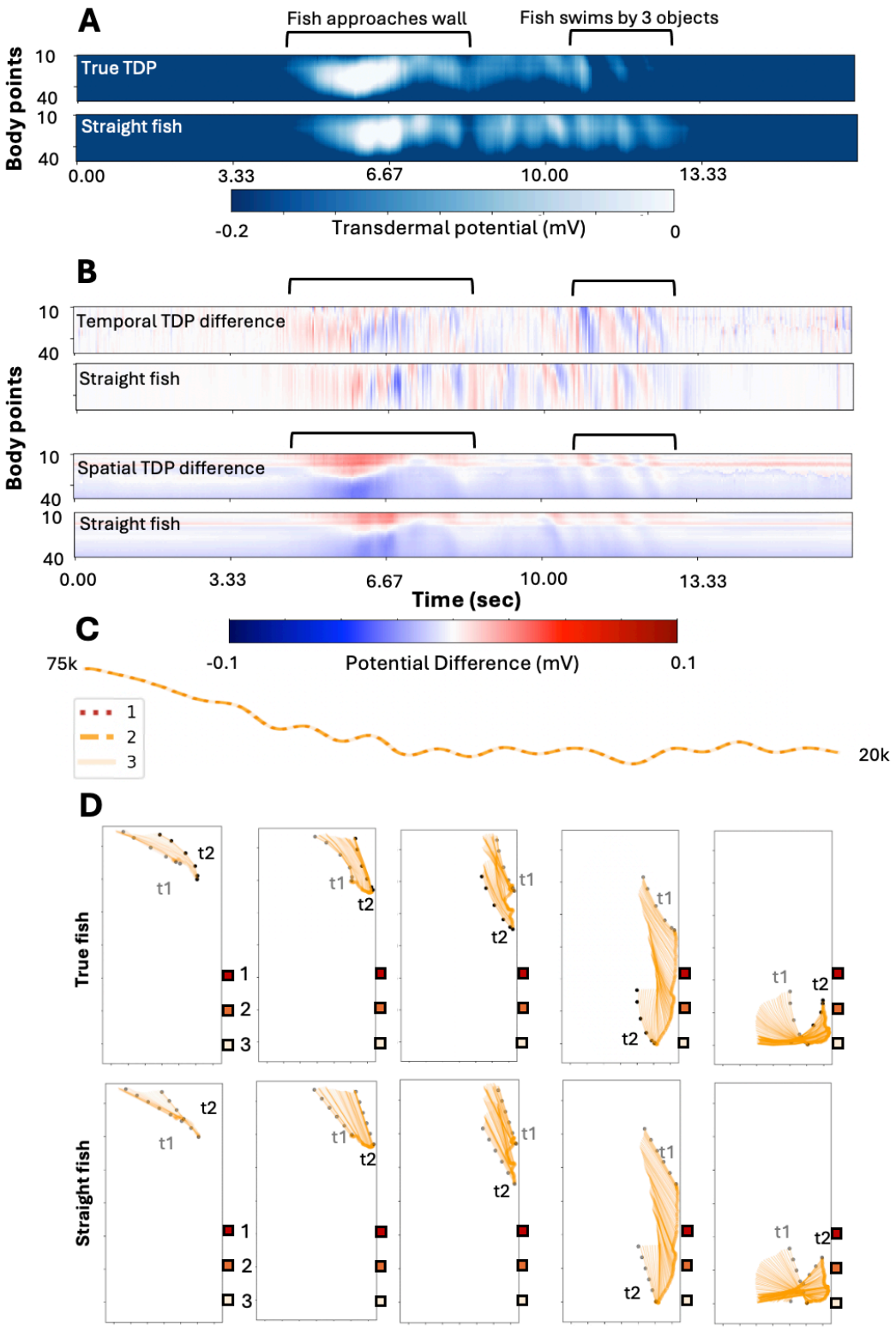

Figure 5.5 Scanning behaviour observed from data shows increased transdermal potential amplitude at object location compared to straight fish.

A) Heatmap of the transdermal potential for raw data (top) and straight fish (bottom) at equivalent locations over time. B) Temporal (top; TDP-t_n – TDP-t_{n-1}) and spatial (bottom; TDP-bp_n – TDP-bp_{n-1}) consecutive transdermal potential differences corresponding to the heatmaps in A) for both the raw data and simulated straight fish. C) Resistor contrast values corresponding to the time trace in heatmaps of A) and B). 75K (low contrast), 20K (medium contrast). Numbers in legend correspond to resistors (small coloured boxes) in D). D) Time series of the fish location in the refuge for the true fish (raw data) and the straight fish (simulated). Fish plotted as line with orange circles denoting head location. Light grey circles correspond to positional data at the beginning (t1) of the time trace for 6 points along the midline of the fish. Black circles correspond to end of time trace (t2). Time traces correspond to 3.33 second bins for each plot from left to right. Example: left most plot t1=0, t2=3.33; right most plot t1=13.33, t2=16.67.

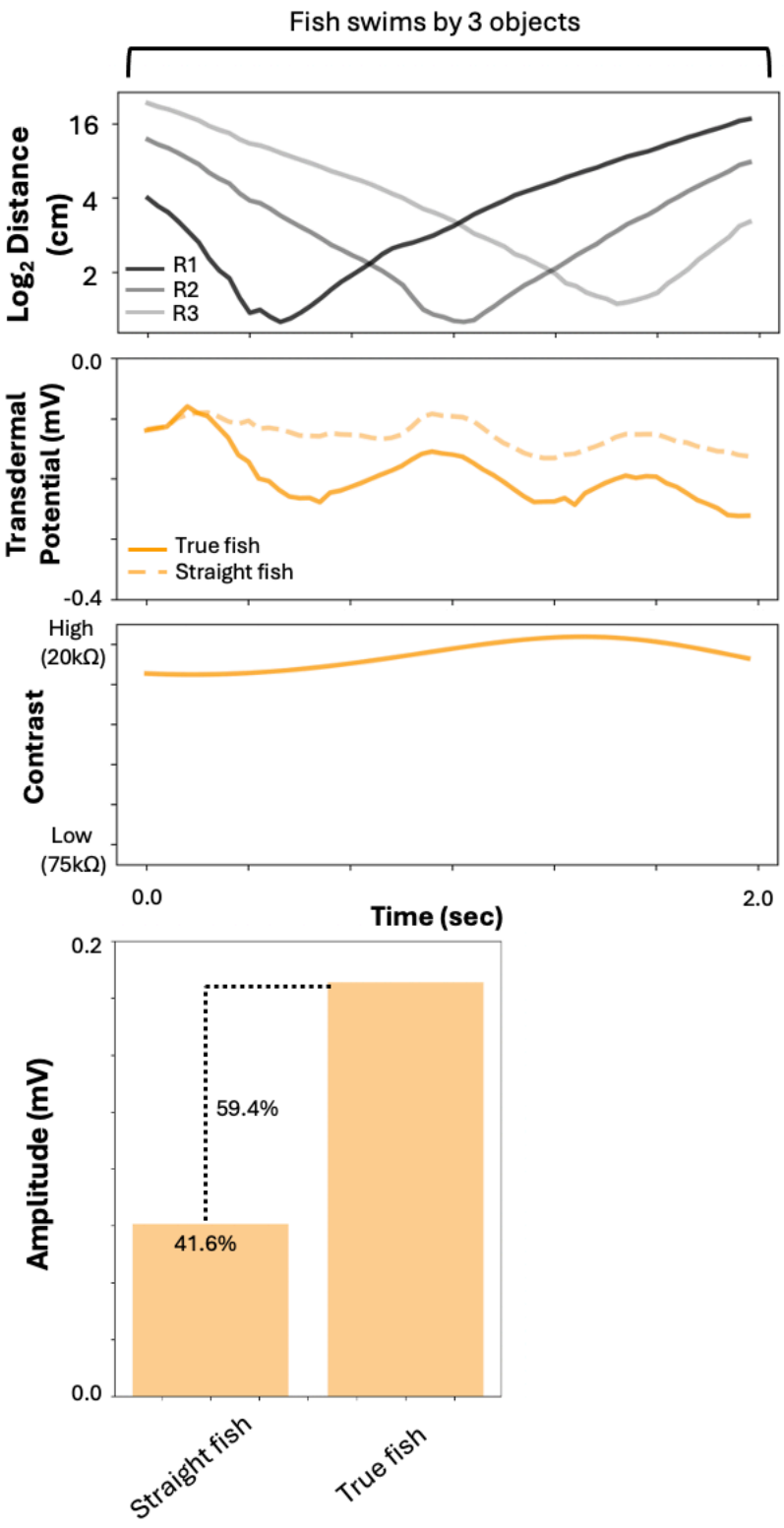

Figure 5.6 Quantification of the transdermal potential at the resistor locations confirms larger signal in scanning behaviour with true body-shape compared to straight body-shape.

Corresponds to the time at which the fish swims by three resistors (R1-R3) from Figure 5.5. Top panel: Distance between the fish's nose point and each resistor. Middle panel: Transdermal potential for the true fish and straight fish. Bottom panel: Stimulus contrast over time. Bottom: Amplitude (max-min) of the transdermal potential for the straight fish and true fish as it passes by R1-R3.

5.6 Supplemental

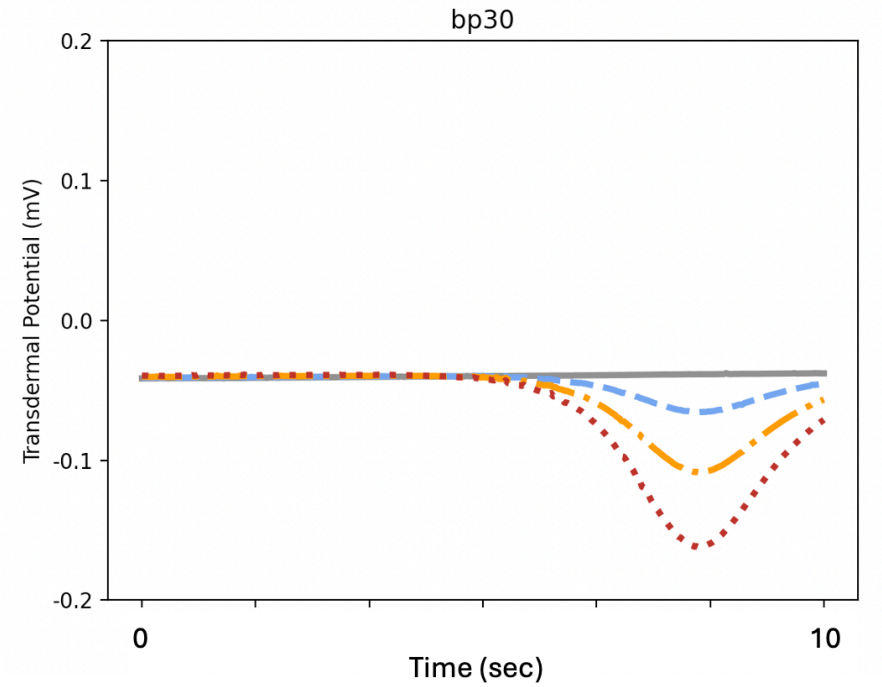

Supplemental Figure 5.1 Body point 30 plotted over time for a straight simulated fish scanning by object (R2).

All parameters are equivalent to Figure 5.2A . Grey = no object, blue = low contrast, orange = medium contrast, red = high contrast.

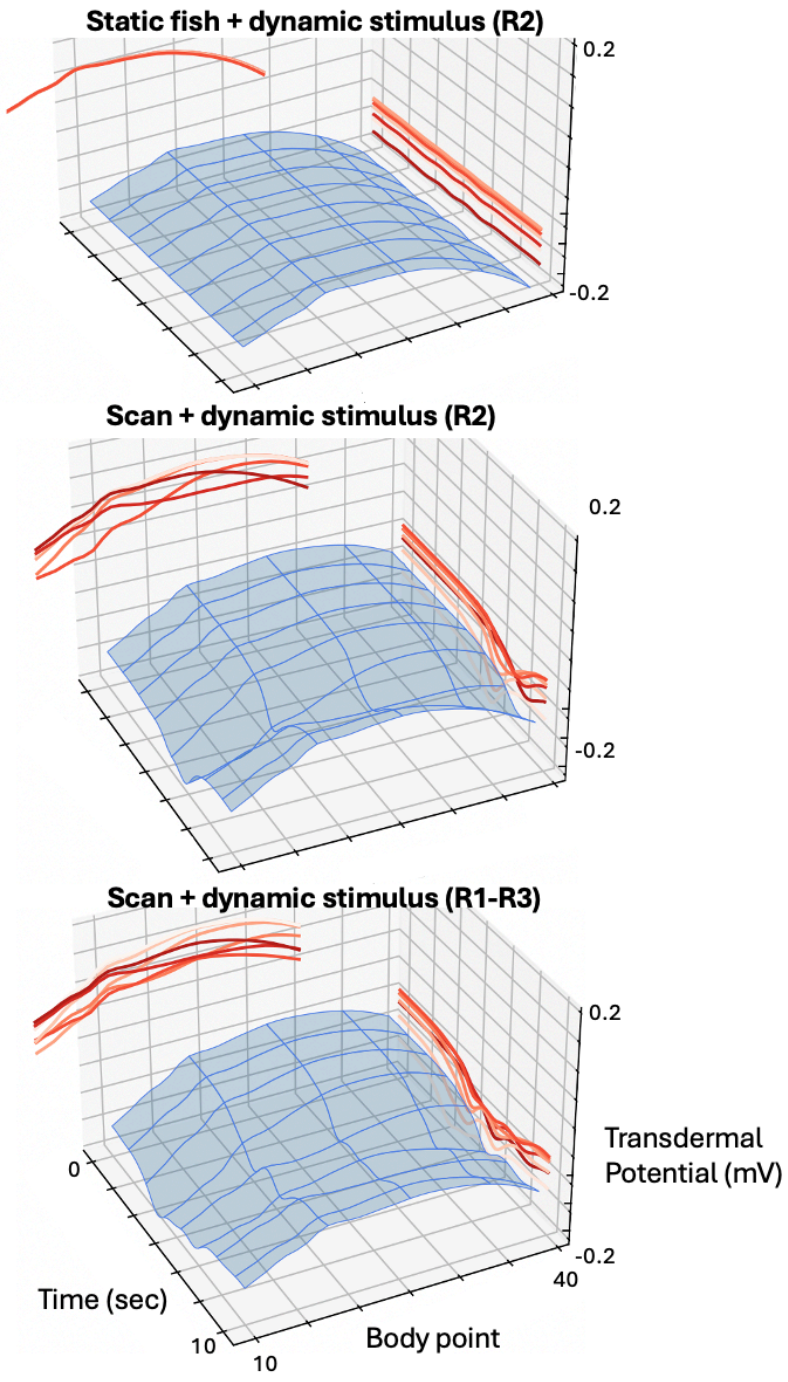

Supplemental Figure 5.2 Mesh plots showing transdermal potential from fish left-side body plane from body points 10-40 for 10 seconds.

Transdermal potential pertaining to x and y axis are projected respectively (pink-red lines). Correspond to heat maps in Figure 5.3A.

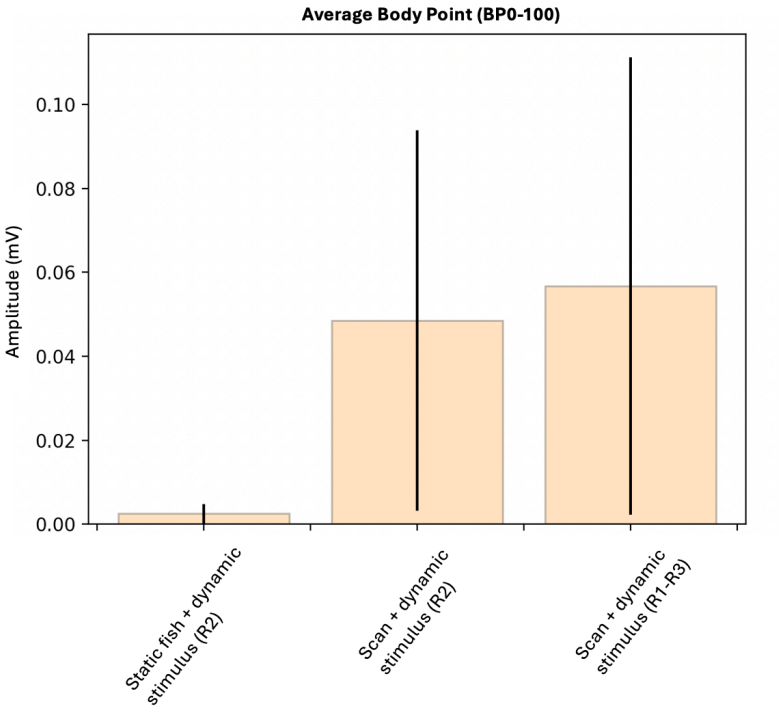

Supplemental Figure 5.3 Average transdermal potential amplitude across all body points.

Chapter 6: General Discussion

Sensory-motor integration is a persistent topic in neurophysiology. In the case of weakly electric fish, their body-movement is directly tied to their electrosensory system. As we have discussed, this interplay is likely to their advantage. Using computational techniques, we established 6 behavioural syllables which described the behaviour of the fish. We described the fish's baseline behavioural syllable repertoire and further showed different combinations of syllables to be consistent with previously hypothesized active sensing behaviours. We demonstrate that scanning (FS-BS) increases in the presence of novel objects and that this behaviour enhances the information pertaining to object detection. Using behavioural data, we simulated a scanning event and showed that a simple linear transformation could provide increased electrosensory information via increased stimulus-specific amplitudes.

We also looked at the evolution of behaviours over time and suggest roles for tail-bending (FC/BC) and nose-probing (PV). Here we elaborate on some of these ideas further and discuss other future directions.

Different paradigms are used to describe behavioural decisions. A recently proposed theory addresses risk-assessment and proposes that weakly electric fish among other animals use a cost-benefit analysis (Chen et al., 2020). In chapters 3 and 4 we noted increased scanning when the environmental conditions were most novel. We proposed that this repetitive back-and-forth could be evidence of such risk assessment. C-bending and nose-probing behaviours became more prevalent as time

passed. As evidenced in convergently related species, it is likely that C-bending or tail-bending is cancelled out in familiar environments. However, as the fish gathers information and explores there could be an advantage to the increased area coverage that comes with bending behaviours. Increased bending creates a contrast between the left and right sensory arrays on either side of the fish (Assad, 1997; Sim & Kim, 2011). It also modifies the amplitude of incoming sensory information. These movements come with both cost and risk. Following a similar paradigm as that of the cost-benefit analysis, as time passes the fish becomes less risk averse and is willing to expose itself by covering more area for the possible benefit of gaining information. Of course, this assumes that bending is beneficial to electric sensing. Future studies investigating the role of bending in risk-assessment may provide a behavioural baseline with which to settle if it has a role in exploration. Ideally, these studies would model after recent work (Wallach & Sawtell, 2023) using electrophysiological techniques in tandem with behavioural analysis to address these possibilities. However, studies which account for the receptor-level sensory input could at least provide indication of whether the information is accessible (Assad, 1997).

Similarly, I would assume nose-probing to be the riskiest behaviour. The fish exposes the head region, though the motivation behind it is less clear compared to bending. Depending on the velocity, nose-probing can be quite forceful and could be considered a form of attack (personal observation). These fish are generally known to be aggressive and territorial (Moller, 1995). Attacks involve whipping their bodies against the offender and biting. On the other hand, when done with less force the fish

could be employing the high-density area of receptors in the perioral region (the “electrosensory fovea”) for improved sensory input (Caputi, 2017). In either case, as time passes the increase in nose-probing suggests an increase in risk-taking behaviour. Given the short-range of the electroreceptive sensing capacities, for the fish to update its environmental awareness it needs to constantly be sampling (Chen et al., 2020). With movement the fish can continue to update its external understanding, though this exploration would likely only arise with familiarity. Otherwise, needless exploration could subject the animal to increased predation.

The 2-D nature of our electrosensory input model could be used to address the tail-bending aspect of exploration. Simulations similar to those in Chapter 5 could focus on building a picture of the inputs available during bending. This builds upon past work by using real behavioural data to simulate the sensory inputs rather than estimations. Addressing nose-probing, however, would require improvements to the model which account for the geometry of the front of the fish where 3-D implementations would be necessary.

It is often easy to forget about the other senses available to these fish, even in the dark. While they have evolved to allocate more resources to active sensing via tuberous receptors, they still possess ampullary (passive) sensing abilities. Furthermore, the detection of mechanosensation via the lateral line is also available (Moller, 1995). I chose to try to isolate the electric sense using virtual objects, but future studies could subject the fish to more integrative conditions and investigate the role of the interplay of

these systems. This has previously been done using visual and electrosensory cues which provided evidence of active sensing in the first place (Stamper et al., 2012).

With the continued development of electrophysiological and computational techniques the study of weakly electric fish will continue to provide a unique and elegant demonstration of sensorimotor harmony with which we can continue to learn from and apply more broadly.

References

Angiulli, E., Pagliara, V., Cioni, C., Frabetti, F., Pizzetti, F., Alleva, E., & Toni, M. (2020). Increase in environmental temperature affects exploratory behaviour, anxiety and social preference in Danio rerio. *Scientific Reports*, *10*(1), 5385. https://doi.org/10.1038/s41598-020-62331-1

Assad, C. (1997). *Electric field maps and boundary element simulations of electrolocation in weakly electric fish*. https://api.semanticscholar.org/CorpusID:86023139

Assad, C., Rasnow, B., & Stoddard, P. K. (1999a). Electric organ discharges and electric images during electrolocation. *Journal of Experimental Biology*, *202*(10), 1185–1193. https://doi.org/10.1242/JEB.202.10.1185

Assad, C., Rasnow, B., & Stoddard, P. K. (1999b). Electric organ discharges and electric images during electrolocation. *The Journal of Experimental Biology*, *202*(Pt 10), 1185–1193. http://www.ncbi.nlm.nih.gov/pubmed/10210660

Babineau, D., Lewis, J. E., & Longtin, A. (2007). Spatial Acuity and Prey Detection in Weakly Electric Fish. *PLOS Computational Biology*, *3*(3), e38. https://doi.org/10.1371/JOURNAL.PCBI.0030038

Babineau, D., Longtin, A., & Lewis, J. E. (2006). Modeling the electric field of weakly electric fish. *Journal of Experimental Biology*, *209*(18), 3636–3651. https://doi.org/10.1242/jeb.02403

Bastian, J. (1975). Receptive fields of cerebellar cells receiving exteroceptive input in a Gymnotid fish. *Journal of Neurophysiology*, *38*(2), 285–300. https://doi.org/10.1152/JN.1975.38.2.285

Bastian, J. (1981). Electrolocation. *Journal of Comparative Physiology*, *144*(4), 465–479. https://doi.org/10.1007/BF01326832

Bastian, J. (1995). Pyramidal-cell plasticity in weakly electric fish: a mechanism for attenuating responses to reafferent electrosensory inputs. *J Comp Physiol A*, *176*, 63–78.

Bastian, J. (1999). Plasticity of feedback inputs in the apteronotid electrosensory system. *Journal of Experimental Biology*, *202*(10), 1327–1337. https://doi.org/10.1242/JEB.202.10.1327

Bastian, J., Chacron, M. J., & Maler, L. (2004). Plastic and Nonplastic Pyramidal Cells Perform Unique Roles in a Network Capable of Adaptive Redundancy Reduction. *Neuron*, *41*(5), 767–779. https://doi.org/10.1016/S0896-6273(04)00071-6

Benda, J. (2020). *The Physics of Electrosensory Worlds*. *7*, 228–254.

Bennett, M. V. L. (1970). *COMPARATIVE PHYSIOLOGY: ELECTRIC ORGANS1 1052*. www.annualreviews.org

Bennett, M. V. L. (1971). Electric Organs. *Fish Physiology*, *5*(C), 347–491. https://doi.org/10.1016/S1546-5098(08)60051-5

Berman, G. J., Choi, D. M., Bialek, W., & Shaevitz, J. W. (2014). Mapping the stereotyped behaviour of freely moving fruit flies. *Journal of The Royal Society Interface*, *11*(99), 20140672. https://doi.org/10.1098/rsif.2014.0672

Bernt, M. J., Tagliacollo, V. A., & Albert, J. S. (2019). Molecular phylogeny of the ghost knifefishes (Gymnotiformes: Apteronotidae). *Molecular Phylogenetics and Evolution*, *135*, 297–307. https://doi.org/10.1016/J.YMPEV.2019.02.019

Biswas, D., Arend, L. A., Stamper, S. A., Vágvölgyi, B. P., Fortune, E. S., & Cowan, N. J. (2018). Closed-Loop Control of Active Sensing Movements Regulates Sensory Slip. *Current Biology*, *28*(24), 4029-4036.e4. https://doi.org/10.1016/J.CUB.2018.11.002

Blake, R. W. (1983). Swimming in the electric eels and knifefishes. *Https://Doi.Org/10.1139/Z83-192*, *61*(6), 1432–1441. https://doi.org/10.1139/Z83-192

Bratton, B., & Bastian, J. (1990). Descending control of electroreception. II. Properties of nucleus praeeminentialis neurons projecting directly to the electrosensory lateral line lobe. *Journal of Neuroscience*, *10*(4), 1241–1253. https://doi.org/10.1523/JNEUROSCI.10-04-01241.1990

Campello Ricardo J. G. B. and Moulavi, D. and S. J. (2013). Density-Based Clustering Based on Hierarchical Density Estimates. In V. S. and C. L. and M. H. and X. G. Pei Jian and Tseng (Ed.), *Advances in Knowledge Discovery and Data Mining* (pp. 160–172). Springer Berlin Heidelberg.

Caputi, A. A. (2017). Active Electroreception in Weakly Electric Fish. *Oxford Research Encyclopedia of Neuroscience*. https://doi.org/10.1093/ACREFORE/9780190264086.013.106

Carlson, B. A., Sisneros, J. A., Carlson, B. A., & Sisneros, J. A. (2019). A Brief History of Electrogenesis and Electroreception in Fishes. *Nature*, *70*, 1–23. https://doi.org/10.1007/978-3-030-29105-1_1

Carr, C. E., Maler, L., & Sas, E. (1982). Peripheral organization and central projections of the electrosensory nerves in gymnotiform fish. *Journal of Comparative Neurology*, *211*(2), 139–153. https://doi.org/10.1002/CNE.902110204

Cazelles, B., Chavez, M., Berteaux, D., Ménard, F., Vik, J. O., Jenouvrier, S., & Stenseth, N. C. (2008). Wavelet analysis of ecological time series. *Oecologia*, *156*(2), 287–304. https://doi.org/10.1007/S00442-008-0993-2/METRICS

Chacron, M. J., Doiron, B., Maler, L., Longtin, A., & Bastian, J. (2003). Non-classical receptive field mediates switch in a sensory neuron's frequency tuning. *Nature 2003 423:6935*, *423*(6935), 77–81. https://doi.org/10.1038/nature01590

Chacron, M. J., Longtin, A., & Maler, L. (2001). Simple models of bursting and non-bursting P-type electroreceptors. *Neurocomputing*, *38–40*, 129–139. https://doi.org/10.1016/S0925-2312(01)00549-5

Chacron, M. J., Maler, L., & Bastian, J. (2005). Electroreceptor neuron dynamics shape information transmission. *Nature Neuroscience 2005 8:5*, *8*(5), 673–678. https://doi.org/10.1038/nn1433

Chen, C., Murphey, T. D., & MacIver, M. A. (2020). Tuning movement for sensing in an uncertain world. *ELife*, *9*, e52371. https://doi.org/10.7554/eLife.52371

Chung, Y. G., Han, S. W., Kim, H.-S., Chung, S.-C., Park, J.-Y., Wallraven, C., & Kim, S.-P. (2015). Adaptation of cortical activity to sustained pressure stimulation on the fingertip. *BMC Neuroscience*, *16*(1), 71. https://doi.org/10.1186/s12868-015-0207-x

Clarke, S. E., Longtin, A., & Maler, L. (2014). A Neural Code for Looming and Receding Motion Is Distributed over a Population of Electrosensory ON and OFF Contrast Cells. *Journal of Neuroscience*, *34*(16), 5583–5594. https://doi.org/10.1523/JNEUROSCI.4988-13.2014

Clarke, S. E., Longtin, A., & Maler, L. (2015). Contrast coding in the electrosensory system: parallels with visual computation. *Nature Reviews Neuroscience 2015 16:12*, *16*(12), 733–744. https://doi.org/10.1038/nrn4037

Clarke, S. E., & Maler, L. (2017). Feedback Synthesizes Neural Codes for Motion. *Current Biology*, *27*(9), 1356–1361. https://doi.org/10.1016/J.CUB.2017.03.068

Crampton, W. G. R. (2019). Electroreception, electrogenesis and electric signal evolution. In *Journal of Fish Biology* (Vol. 95, Issue 1, pp. 92–134). Blackwell Publishing Ltd. https://doi.org/10.1111/jfb.13922

Crampton, W. G. R., & Albert, J. S. (2006). Evolution of Electric Signal Diversity in Gymnotiform Fishes. *Fish Communication*.

Crampton, W., Sébert, P., Onyango, D., & Kapoor, B. (2007). *Diversity and adaptation in deepchannel neotropical electric fishes*. http://erepository.uonbi.ac.ke/handle/11295/51308

Curet, O. M., Patankar, N. A., Lauder, G. V., & MacIver, M. A. (2011). Aquatic manoeuvering with counter-propagating waves: a novel locomotive strategy. *Journal of The Royal Society Interface*, *8*(60), 1041–1050. https://doi.org/10.1098/RSIF.2010.0493

Datta, S. R., Anderson, D. J., Branson, K., Perona, P., & Leifer, A. (2019). Computational Neuroethology: A Call to Action. *Neuron*, *104*(1), 11–24. https://doi.org/10.1016/J.NEURON.2019.09.038

Davis, R. W. (2019). Sensory Systems. In *Marine Mammals: Adaptations for an Aquatic Life* (pp. 177–217). Springer International Publishing. https://doi.org/10.1007/978-3-319-98280-9_7

de Santana, C. D., Crampton, W. G. R., Dillman, C. B., Frederico, R. G., Sabaj, M. H., Covain, R., Ready, J., Zuanon, J., de Oliveira, R. R., Mendes-Júnior, R. N., Bastos, D. A., Teixeira, T. F., Mol, J., Ohara, W., Castro, N. C. e., Peixoto, L. A., Nagamachi, C., Sousa, L., Montag, L. F. A., … Wosiacki, W. B. (2019). Unexpected species diversity in electric eels with a description of the strongest living bioelectricity generator. *Nature Communications 2019 10:1*, *10*(1), 1–10. https://doi.org/10.1038/s41467-019-11690-z

dos Santos, C. P., de Oliveira, M. N., Silva, P. F., & Luchiari, A. C. (2023). Relationship between boldness and exploratory behavior in adult zebrafish. *Behavioural Processes*, *209*, 104885. https://doi.org/https://doi.org/10.1016/j.beproc.2023.104885

Engelmann, J., Wallach, A., & Maler, L. (2021a). Linking active sensing and spatial learning in weakly electric fish. In *Current Opinion in Neurobiology* (Vol. 71). https://doi.org/10.1016/j.conb.2021.07.002

Engelmann, J., Wallach, A., & Maler, L. (2021b). Linking active sensing and spatial learning in weakly electric fish. In *Current Opinion in Neurobiology* (Vol. 71, pp. 1–10). Elsevier Ltd. https://doi.org/10.1016/j.conb.2021.07.002

Fotowat, H., Lee, C., Jun, J. J., & Maler, L. (2019). Neural activity in a hippocampus-like region of the teleost pallium is associated with active sensing and navigation. *ELife*, *8*. https://doi.org/10.7554/ELIFE.44119

Franchina, C. R., & Hopkins, C. D. (1996). The Dorsal Filament of the Weakly Electric Apteronotidae (Gymnotiformes; Teleostei) Is Specialized for Electroreception. *Brain, Behavior and Evolution*, *47*(4), 165–178. https://doi.org/10.1159/000113236

Gaynes, J. A., Budoff, S. A., Grybko, M. J., Hunt, J. B., & Poleg-Polsky, A. (2022). Classical center-surround receptive fields facilitate novel object detection in retinal bipolar cells. *Nature Communications*, *13*(1), 5575. https://doi.org/10.1038/s41467-022-32761-8

Geva-Sagiv, M., Las, L., Yovel, Y., & Ulanovsky, N. (2015). Spatial cognition in bats and rats: from sensory acquisition to multiscale maps and navigation. *Nature Reviews Neuroscience 2015 16:2*, *16*(2), 94–108. https://doi.org/10.1038/nrn3888

Gómez-Sena, L., Pedraja, F., Sanguinetti-Scheck, J. I., & Budelli, R. (2014). Computational modeling of electric imaging in weakly electric fish: Insights for physiology, behavior and evolution. *Journal of Physiology-Paris*, *108*(2), 112–128. https://doi.org/https://doi.org/10.1016/j.jphysparis.2014.08.009

Hagiwara, S., Szabu, T., Enger, P. S., Angeles, L., & Puraense Emilio Goeldi, M. (1965). Electroreceptor mechanisms in a high-frequency weakly electric fish, sternarchus albifrons. *Journal of Neurophysiology*, 784–799.

Heiligenberg, W. (1973). Electrolocation of objects in the electric fish Eigenmannia (Rhamphichthyidae, Gymnotoidei). *Journal of Comparative Physiology*, *87*(2), 137–164. https://doi.org/10.1007/BF01352158/METRICS

Heiligenberg, W. (1975). Theoretical and experimental approaches to spatial aspects of electrolocation. *Journal of Comparative Physiology ■ A*, *103*(3), 247–272. https://doi.org/10.1007/BF00612021/METRICS

Heyser, C. J., & Chemero, A. (2012). Novel object exploration in mice: Not all objects are created equal. *Behavioural Processes*, *89*(3), 232–238. https://doi.org/https://doi.org/10.1016/j.beproc.2011.12.004

Hofmann, V., Geurten, B. R. H., Sanguinetti-Scheck, J. I., Gómez-Sena, L., & Engelmann, J. (2014a). Motor patterns during active electrosensory acquisition. *Frontiers in Behavioral Neuroscience*, *8*(MAY), 186. https://doi.org/10.3389/FNBEH.2014.00186/ABSTRACT

Hofmann, V., Geurten, B. R. H., Sanguinetti-Scheck, J. I., Gómez-Sena, L., & Engelmann, J. (2014b). Motor patterns during active electrosensory acquisition. *Frontiers in Behavioral Neuroscience*, *8*(MAY), 186. https://doi.org/10.3389/FNBEH.2014.00186/ABSTRACT

Hopkins, C. D. (1976). Stimulus filtering and electroreception: Tuberous electroreceptors in three species of Gymnotoid fish. *Journal of Comparative Physiology ■ A*, *111*(2), 171–207. https://doi.org/10.1007/BF00605531

Hossain, A., Uddin, S., Rahman, P., Anee, M. J., Rifat, M. M. H., & Uddin, M. M. (2022). Wavelet and Spectral Analysis of Normal and Abnormal Heart Sound for Diagnosing Cardiac Disorders. *BioMed Research International*, *2022*. https://doi.org/10.1155/2022/9092346

Hsu, A. I., & Yttri, E. A. (2021). B-SOiD, an open-source unsupervised algorithm for identification and fast prediction of behaviors. *Nature Communications*, *12*(1), 5188. https://doi.org/10.1038/s41467-021-25420-x

Jørgensen, J. M. (2005). Morphology of Electroreceptive Sensory Organs. *Electroreception*, 47–67. https://doi.org/10.1007/0-387-28275-0_3

Jun, J. J., Longtin, A., & Maler, L. (2016). Active sensing associated with spatial learning reveals memory-based attention in an electric fish. *Journal of Neurophysiology*,

115(5), 2577–2592. https://doi.org/10.1152/JN.00979.2015/SUPPL_FILE/SUPPLEMENTAL_VIDEO_1.MP4

Jung, S. N., & Engelmann, J. (2019). Active Electrolocation and Spatial Learning. *Electroreception: Fundamental Insights from Comparative Approaches*. https://api.semanticscholar.org/CorpusID:214370190

Kalmijn, A. J. (1971). The Electric Sense of Sharks and Rays. *Journal of Experimental Biology*, *55*(2), 371–383. https://doi.org/10.1242/JEB.55.2.371

Kappeler Peter and Kraus, C. (2010). Levels and mechanisms of behavioural variability. In P. Kappeler (Ed.), *Animal Behaviour: Evolution and Mechanisms* (pp. 655–684). Springer Berlin Heidelberg. https://doi.org/10.1007/978-3-642-02624-9_21

Keogh, E., & Mueen, A. (2017). Curse of Dimensionality. *Encyclopedia of Machine Learning and Data Mining*, 314–315. https://doi.org/10.1007/978-1-4899-7687-1_192

Knudsen, E. I. (1974). Behavioral thresholds to electric signals in high frequency electric fish. *Journal of Comparative Physiology*, *91*(4), 333–353. https://doi.org/10.1007/BF00694465

Krahe, R., Bastian, J., & Chacron, M. J. (2008). Temporal processing across multiple topographic maps in the electrosensory system. *Journal of Neurophysiology*, *100*(2), 852–867. https://doi.org/10.1152/JN.90300.2008/ASSET/IMAGES/LARGE/Z9K00808896900 11.JPEG

Krahe, R., & Maler, L. (2014). Neural maps in the electrosensory system of weakly electric fish. *Current Opinion in Neurobiology*, *24*(1), 13–21. https://doi.org/10.1016/J.CONB.2013.08.013

Kramer, L. B. (2019). Harmonic and temporal structure of electric organ discharges of the wave-type in Amazonian knifefishes (Gymnotiformes). *Journal of Ethology*, *37*(1), 1–11. https://doi.org/10.1007/S10164-018-0560-1/FIGURES/4

Kuznetsova, A., Brockhoff, P. B., & Christensen, R. H. B. (2017). lmerTest Package: Tests in Linear Mixed Effects Models. *Journal of Statistical Software*, *82*(13), 1–26. https://doi.org/10.18637/jss.v082.i13

Lannoo, M. J., & Lannoo, S. J. (1993). Why do electric fishes swim backwards? An hypothesis based on gymnotiform foraging behavior interpreted through sensory constraints. *Environmental Biology of Fishes 1993 36:2*, *36*(2), 157–165. https://doi.org/10.1007/BF00002795

Lannoo, M. J., & Maler, L. (1990). Interspecific variation in the projection of primary afferents onto the electrosensory lateral line lobe of weakly electric teleosts: Different solutions to the same mapping problem. *Journal of Comparative Neurology*, *294*(1), 153–160. https://doi.org/10.1002/CNE.902940112

Lee, G., Gommers, R., Waselewski, F., Wohlfahrt, K., & O'Leary, A. (2019). PyWavelets: A Python package for wavelet analysis. *Journal of Open Source Software*, *4*(36), 1237. https://doi.org/10.21105/JOSS.01237

Lewis, J. E. (2014). Active Electroreception Signals, Sensing, and Behavior. *The Physiology of Fishes*, *4th Edition*, 373–388.

Lilly, J. M. (2017). Element analysis: a wavelet-based method for analysing time-localized events in noisy time series. *Proceedings of the Royal Society A: Mathematical, Physical and Engineering Sciences*, *473*(2200). https://doi.org/10.1098/RSPA.2016.0776

Lissmann, H. W., & Machin, K. E. (1958). The Mechanism of Object Location in Gymnarchus Niloticus and Similar Fish. *Journal of Experimental Biology*, *35*(2), 451–486. https://doi.org/10.1242/JEB.35.2.451

MacIver, M. A., Fontaine, E., & Burdick, J. W. (2004). Designing future underwater vehicles: Principles and mechanisms of the weakly electric fish. *IEEE Journal of Oceanic Engineering*, *29*(3), 651–659. https://doi.org/10.1109/JOE.2004.833210

MacIver, M. A., Sharabash, N. M., & Nelson, M. E. (2001). Prey-capture behavior in gymnotid electric fish: motion analysis and effects of water conductivity. *Journal of Experimental Biology*, *204*(3), 543–557. https://doi.org/10.1242/JEB.204.3.543

Magnhagen, C., Hellström, G., Borcherding, J., & Heynen, M. (2012). Boldness in two perch populations – long-term differences and the effect of predation pressure. *Journal of Animal Ecology*, *81*(6), 1311–1318. https://doi.org/https://doi.org/10.1111/j.1365-2656.2012.02007.x

Markham, M. R. (2019). Biophysical Basis of Electric Signal Diversity. *Nature*, *70*, 125–161. https://doi.org/10.1007/978-3-030-29105-1_5

Martins, C. I. M., Schaedelin, F. C., Mann, M., Blum, C., Mandl, I., Urban, D., Grill, J., Schößwender, J., & Wagner, R. H. (2012). Exploring novelty: a component trait of behavioural syndromes in a colonial fish. *Behaviour*, *149*(2), 215–231. https://doi.org/https://doi.org/10.1163/156853912X634430

Mathis, A., Mamidanna, P., Cury, K. M., Abe, T., Murthy, V. N., Mathis, M. W., & Bethge, M. (2018). DeepLabCut: markerless pose estimation of user-defined body parts with deep learning. *Nature Neuroscience*, *21*(9), 1281–1289. https://doi.org/10.1038/s41593-018-0209-y

McInnes, L., & Healy, J. (2018). *UMAP: Uniform Manifold Approximation and Projection for Dimension Reduction*.

Metzen, M. G., & Chacron, M. J. (2023). Descending pathways increase sensory neural response heterogeneity to facilitate decoding and behavior. *IScience*, *26*(7). https://doi.org/10.1016/j.isci.2023.107139

Mitchinson, B., Martin, C. J., Grant, R. A., & Prescott, T. J. (2007). Feedback control in active sensing: rat exploratory whisking is modulated by environmental contact. *Proceedings of the Royal Society B: Biological Sciences*, *274*(1613), 1035–1041. https://doi.org/10.1098/RSPB.2006.0347

Moller, P. (1995). *Electric Fishes: History and Behavior* (illustrated, Vol. 17). Springer Netherlands, 1995.

Nelson, M. E., & Maciver, M. A. (1999a). Prey capture in the weakly electric fish Apteronotus albifrons: sensory acquisition strategies and electrosensory consequences. *Journal of Experimental Biology*, *202*(10), 1195–1203. https://doi.org/10.1242/JEB.202.10.1195

Nelson, M. E., & Maciver, M. A. (1999b). Prey capture in the weakly electric fish Apteronotus albifrons: sensory acquisition strategies and electrosensory consequences. *Journal of Experimental Biology*, *202*(10), 1195 LP – 1203. http://jeb.biologists.org/content/202/10/1195.abstract

Nelson, M. E., & MacIver, M. A. (2006). Sensory acquisition in active sensing systems. *Journal of Comparative Physiology A: Neuroethology, Sensory, Neural, and*

Behavioral Physiology, *192*(6), 573–586. https://doi.org/10.1007/S00359-006-0099-4/FIGURES/3

Nelson, M. E., Xu, Z., & Payne, J. R. (1997). Characterization and modeling of P-type electrosensory afferent responses to amplitude modulations in a wave-type electric fish. *Journal of Comparative Physiology A*, 532–544.

Noer, C. L., Needham, E. K., Wiese, A.-S., Balsby, T. J. S., & Dabelsteen, T. (2015). Context Matters: Multiple Novelty Tests Reveal Different Aspects of Shyness-Boldness in Farmed American Mink (Neovison vison). *PLOS ONE*, *10*(6), e0130474-. https://doi.org/10.1371/journal.pone.0130474

Ortega-Jiménez, V. M., & Sanford, C. P. (2021). Beyond the Kármán gait: Knifefish swimming in periodic and irregular vortex streets. *Journal of Experimental Biology*, *224*(10). https://doi.org/10.1242/JEB.238808/VIDEO-1

Pedraja, F., Hofmann, V., Goulet, J., & Engelmann, J. (2020). Task-related sensorimotor adjustments increase the sensory range in electrolocation. *Journal of Neuroscience*, *40*(5). https://doi.org/10.1523/JNEUROSCI.1024-19.2019

Peixoto, L. A. W., Dutra, G. M., & Wosiacki, W. B. (2015). The Electric Glass Knifefishes of the Eigenmannia trilineata species-group (Gymnotiformes: Sternopygidae): monophyly and description of seven new species. *Zoological Journal of the Linnean Society*, *175*(2), 384–414. https://doi.org/10.1111/ZOJ.12274

Peixoto, L. A. W., & Ohara, W. M. (2019). A new species of Eigenmannia Jordan & Evermann (Gymnotiformes: Sternopygidae) from rio Tapajós, Brazil, with discussion on its species group and the myology within Eigenmanniinae. *PLOS ONE*, *14*(8), e0220287. https://doi.org/10.1371/JOURNAL.PONE.0220287

Peixoto, L. A. W., Pastana, M. N. L., & Ballen, G. A. (2021). New species of glass knifefish genus Eigenmannia (Gymnotiformes: Sternopygidae) with comments on the morphology and function of the enlarged cephalic lateral-line canals of Sternopygidae. *Journal of Fish Biology*, *98*(1), 142–153. https://doi.org/10.1111/JFB.14564

Postlethwaite, C. M., Psemeneki, T. M., Selimkhanov, J., Silber, M., & MacIver, M. A. (2008). Optimal movement in the prey strikes of weakly electric fish: a case study of

the interplay of body plan and movement capability. *Journal of The Royal Society Interface*, *6*(34), 417–433. https://doi.org/10.1098/RSIF.2008.0286

Pourziaei, B., Lewis, G. M., & Lewis, J. E. (2022). Minimal sensor arrays for localizing objects using an electric sense. *Physical Biology*, *19*(4), 046007. https://doi.org/10.1088/1478-3975/AC75A5

Rasnow, B. (1996). The effects of simple objects on the electric field of Apteronotus. *Journal of Comparative Physiology A: Sensory, Neural, and Behavioral Physiology*, *178*(3), 397–411. https://doi.org/10.1007/BF00193977/METRICS

Ruiz-Torres, R., Curet, O. M., Lauder, G. V., & MacIver, M. A. (2013). Kinematics of the ribbon fin in hovering and swimming of the electric ghost knifefish. *Journal of Experimental Biology*, *216*(5), 823–834. https://doi.org/10.1242/JEB.076471/258018/AM/KINEMATICS-OF-THE-RIBBON-FIN-IN-HOVERING-AND

Scheich, H., & Bullock, T. H. (1974). *The Detection of Electric Fields from Electric Organs*. 201–256. https://doi.org/10.1007/978-3-642-65926-3_6

Schroeder, C. E., Wilson, D. A., Radman, T., Scharfman, H., & Lakatos, P. (2010). Dynamics of Active Sensing and perceptual selection. *Current Opinion in Neurobiology*, *20*(2), 172–176. https://doi.org/10.1016/J.CONB.2010.02.010

Sefati, S., Neveln, I., MacIver, M. A., Fortune, E. S., & Cowan, N. J. (2012). Counter-propagating waves enhance maneuverability and stability: A bio-inspired strategy for robotic ribbon-fin propulsion. *Proceedings of the IEEE RAS and EMBS International Conference on Biomedical Robotics and Biomechatronics*, 1620–1625. https://doi.org/10.1109/BIOROB.2012.6290909

Sfakiotakis, M., Lane, D. M., & Davies, J. B. C. (1999). Review of fish swimming modes for aquatic locomotion. *IEEE Journal of Oceanic Engineering*, *24*(2), 237–252. https://doi.org/10.1109/48.757275

Shirgaonkar, A. A., Curet, O. M., Patankarm, N. A., & MacIver, A. A. (2008). The hydrodynamics of ribbon-fin propulsion during impulsive motion. *Journal of Experimental Biology*, *211*(21), 3490–3503. https://doi.org/10.1242/JEB.019224

Sim, M., & Kim, D. E. (2011). Electrolocation based on tail-bending movements in weakly electric fish. *Journal of Experimental Biology*, *214*(14), 2443–2450. https://doi.org/10.1242/JEB.052308

Sîrbulescu, R. F., Ilieş, I., & Zupanc, G. K. H. (2009). Structural and functional regeneration after spinal cord injury in the weakly electric teleost fish, Apteronotusleptorhynchus. *Journal of Comparative Physiology A*, *195*(7), 699–714. https://doi.org/10.1007/s00359-009-0445-4

Snyder, J. B., Nelson, M. E., Burdick, J. W., & MacIver, M. A. (2007). Omnidirectional Sensory and Motor Volumes in Electric Fish. *PLOS Biology*, *5*(11), e301. https://doi.org/10.1371/JOURNAL.PBIO.0050301

Sontag, E. D., Biswas, D., & Cowan, N. J. (2022). *An observability result related to active sensing*.

Stamper, S. A., Roth, E., Cowan, N. J., & Fortune, E. S. (2012). Active sensing via movement shapes spatiotemporal patterns of sensory feedback. *Journal of Experimental Biology*, *215*(9), 1567–1574. https://doi.org/10.1242/JEB.068007

Stephens, G. J., Johnson-Kerner, B., Bialek, W., & Ryu, W. S. (2008). Dimensionality and Dynamics in the Behavior of C. elegans. *PLOS Computational Biology*, *4*(4), e1000028. https://doi.org/10.1371/JOURNAL.PCBI.1000028

Stoddard, P. K. (2009). *Electric Signals & Electric Fish*.

Todd, J. G., Kain, J. S., & de Bivort, B. L. (2017). Systematic exploration of unsupervised methods for mapping behavior. *Physical Biology*, *14*(1), 015002. https://doi.org/10.1088/1478-3975/14/1/015002

Turner, C. R., Derylo, M., De David Santana, C., Alves-Gomes, J. A., & Troy Smith, G. (2007). Phylogenetic comparative analysis of electric communication signals in ghost knifefishes (Gymnotiformes: Apteronotidae). *Journal of Experimental Biology*, *210*(23), 4104–4122. https://doi.org/10.1242/JEB.007930

Upshall, M. (2024). Weakly electric fishes. In S. L. Alderman & T. E. Gillis (Eds.), *Encyclopedia of Fish Physiology (Second Edition)* (Second Edition, pp. 537–546). Academic Press. https://doi.org/https://doi.org/10.1016/B978-0-323-90801-6.00121-X

Uyanik, I., Sefati, S., Stamper, S. A., Cho, K. A., Ankarali, M. M., Fortune, E. S., & Cowan, N. J. (2020). Variability in locomotor dynamics reveals the critical role of feedback in task control. *ELife*, *9*. https://doi.org/10.7554/ELIFE.51219

Valletta, J. J., Torney, C., Kings, M., Thornton, A., & Madden, J. (2017). Applications of machine learning in animal behaviour studies. *Animal Behaviour*, *124*, 203–220. https://doi.org/10.1016/J.ANBEHAV.2016.12.005

Veenstra, F., Jørgensen, J., Risi, S., Sartor, J. B., & De, W. (2018). *Evolution of Fin Undulation on a Physical Knifefish-inspired Soft Robot*. https://doi.org/10.1145/3205455

Viancour, T. A. (1979). Electroreceptors of a weakly electric fish. *Journal of Comparative Physiology*, *133*(4), 317–325. https://doi.org/10.1007/BF00661134

von der Emde, G. (1990). Discrimination of objects through electrolocation in the weakly electric fish, Gnathonemus petersii. *Journal of Comparative Physiology A*, *167*(3), 413–421. https://doi.org/10.1007/BF00192576

von der Emde, G. (1999). Active electrolocation of objects in weakly electric fish. *Journal of Experimental Biology*, *202*(10), 1205–1215. https://doi.org/10.1242/jeb.202.10.1205

Von Der Emde, G., Schwarz, S., Gomez, L., Budelli, R., & Grant, K. (1998). Electric fish measure distance in the dark. *Nature 1998 395:6705*, *395*(6705), 890–894. https://doi.org/10.1038/27655

Wallach, A., & Sawtell, N. B. (2022). An Internal Model of Sensorimotor Context in Freely Swimming Electric Fish. *BioRxiv*, 2022.06.08.495343. https://doi.org/10.1101/2022.06.08.495343

Wallach, A., & Sawtell, N. B. (2023). An internal model for canceling self-generated sensory input in freely behaving electric fish. *Neuron*, *111*(16), 2570-2582.e5. https://doi.org/10.1016/j.neuron.2023.05.019

Weinreb, C., Pearl, J. E., Lin, S., Osman, M. A. M., Zhang, L., Annapragada, S., Conlin, E., Hoffmann, R., Makowska, S., Gillis, W. F., Jay, M., Ye, S., Mathis, A., Mathis, M. W., Pereira, T., Linderman, S. W., & Datta, S. R. (2024). Keypoint-MoSeq: parsing behavior by linking point tracking to pose dynamics. *Nature Methods*, *21*(7), 1329–1339. https://doi.org/10.1038/s41592-024-02318-2

Wiltschko, A. B., Johnson, M. J., Iurilli, G., Peterson, R. E., Katon, J. M., Pashkovski, S. L., Abraira, V. E., Adams, R. P., & Datta, S. R. (2015). Mapping Sub-Second Structure in Mouse Behavior. *Neuron*, *88*(6), 1121–1135. https://doi.org/10.1016/J.NEURON.2015.11.031

Zakon, H. H. (1986). The emergence of tuning in newly generated tuberous electroreceptors. *Journal of Neuroscience*, *6*(11), 3297–3308. https://doi.org/10.1523/JNEUROSCI.06-11-03297.1986